Signal-Level Relaying Strategies for Broadband MIMO ARQ Communications

Hatim Chergui

THÈSE / Télécom Bretagne
sous le sceau de l'Université européenne de Bretagne
pour obtenir le grade de Docteur de Télécom Bretagne
En accréditation conjointe avec l'Ecole Doctorale Sicma
Mention : Sciences de l'ingénieur

présentée par
Hatim Chergui
préparée dans le département Signal et Communications
Laboratoire Labsticc

Signal-Level Relaying Strategies for Broadband MIMO ARQ Communications

Thèse soutenue le 14 décembre 2015
Devant le jury composé de :

Gilles Burel
Professeur, Université de Bretagne Occidentale / président

Jean-Pierre Cances
Professeur, Ensil - Limoges / rapporteur

Ghais El Zein
Professeur, Insa - Rennes / rapporteur

Mohamed-Slim Alouini
Professeur, KAUST, KSA - Arabie Saoudite / examinateur

Mustapha Benjillali
Professeur habilité, INPT-RABAT - Maroc / examinateur

Samir Saoudi
Professeur, Télécom Bretagne / directeur de thèse

N° d'ordre: 2015telb0386

Sous le sceau de l'Université Européenne de Bretagne

Télécom Bretagne

en accréditation conjointe avec l'Ecole Doctorale SICMA

Signal-Level Relaying Strategies for Broadband MIMO ARQ Communications

---

Thèse de Doctorat

Mention: *Sciences pour l'ingénieur*

Présentée par **Hatim CHERGUI**

Département: Signal & Communications

Directeur de thèse: Prof. Samir SAOUDI

Soutenue le 14 Décembre 2015

Jury:

M. Gilles Burel, Professeur, UBO (Président)

M. Jean-Pierre Cances, Professeur, ENSIL (Rapporteur)

M. Ghais El Zein, Professeur, INSA-Rennes (Rapporteur)

M. Mohamed-Slim Alouini, Professeur, KAUST, KSA (Examinateur)

M. Mustapha Benjillali, Professeur Habilité, INPT, Maroc (Encadrant)

M. Samir Saoudi, Professeur, Telecom Bretagne (Directeur de thèse)

To my parents: Amina and Mohammed,
To Ommi,
To Oumama and Nouamane,
To all my family.

Acknowledgments

First of all, I am deeply thankful to my thesis advisor, Prof. Samir Saoudi, for giving me the opportunity to conduct this PhD in parallel to my engineering work. It has been a painstaking yet fruitful journey, where Samir's confidence, patience and care have been an inextinguishable flame of motivation inside me. My sincere gratitude goes to my supervisor, Prof. Mustapha Benjillali from INPT Rabat for his incredible support and availability; his strong research works, his modesty and friendship have been always a source of inspiration for me. I am also grateful to Dr. Tarik Ait-Idir for all his valuable help and coordination that paved the way to this research career. I am aware that saying "tank you" to all of them is too little, but dwelling on their virtues and deeds is an approach they would not have appreciated.

Many thanks are due to the members of my doctoral committee, Prof. Jean Pierre Cances, Prof. Ghais El Zein, Prof. Gilles Burel—from France—and Prof. Mohamed-Slim Alouini—from KAUST, KSA—for their interest in this thesis, in spite of all the efforts and long-haul flights that it requires. I am truly honored to have such a great examining committee.

I wish also to thank Prof. Houda Chafnaji from INPT Rabat for her support, especially by providing me with the dissertation LyX template. My thanks go in turn to my former managers at INWI, M. Ali Iraqi and M. Hicham Hatim —for their comprehension, support, and flexibility that have eased my research activities—and to my friends Zakaria El-Moutaouakkil and Anas Fedoul, with whom I have had nice catch-ups on advanced wireless communications topics.

Last, but not least, I am deeply grateful to my parents Amina El Moussaed and Mohammed Chergui, my gran Fattouma Boutaibi, my oncle Ahmed El Moussaed and his family, my brother Nouamane and my sister Oumama, for their boundless care, incredible love, endless support, and encouragement.

Abstract

Cooperative relaying, multiple-input multiple-output (MIMO), and hybrid-automatic repeat request (ARQ) are paramount techniques to enhance the transmission throughput and quality over the wireless broadband channel. The performance analysis reveals their gain, but also unveils the practical trade-offs they encompass: the spatial diversity of relays comes at the expense of the spectral-efficiency due to the half-duplex constraint; the multi-antenna channel rank deficiency at cell-edge—where a relay is supposed to be deployed—does not allow for the space-time multiplexing mode; the temporal diversity of a pure hybrid-ARQ process is quickly degraded by the long-term quasi-static nature of slow fading environments. The present thesis attempts to overcome these inherent challenges by proposing a joint design of the three techniques for communications over the MIMO-intersymbol interference (ISI) ARQ channel. In a pure signal-level approach, we exploit the rank-deficiency of the source-relay channel—stemming from either the scatterers distribution or the number of antennas at both sides—by adopting project-and-forward (PF)-type relaying. The projection concept is first validated by analyzing its performance over the realistic mixed MIMO-pinhole and Rayleigh flat fading relay channel—using a wide set of generalized mathematical functions. Invoking the residue theory, we study the system asymptotic behavior and infer practical design recommendations. We then apply the orthogonal projection concept to the MIMO-ISI relay channel to alleviate the half-duplex constraint. Hence, we introduce a PF-based signal-level cooperative spatial multiplexing (CM) architecture that allows for the shortening of the relaying phase without resorting to any symbol detection or re-mapping at the relay side. The end-to-end communication model is derived in a seamless fashion; as though the destination is receiving multiple transmissions from the source, which maintains the possibility to use advanced joint detection and combining algorithms at the destination side. The final step of this thesis consists on introducing a cross-layer design, where the projection is performed jointly over multiple MIMO-ARQ transmissions to increase both the diversity gain and the spectral efficiency.

Keywords: ARQ, asymptotic behavior, broadband MIMO, cooperative relaying, cross-layer design, degrees of freedom, generalized functions, joint processing, performance analysis, project-and-forward, rank-deficiency, residue theory.

Résumé

Le relayage coopératif, multiple-input multiple-output (MIMO) et hybrid-ARQ sont des techniques primordiales pour améliorer le débit et la qualité des transmissions sans-fil sur les canaux large-bande. L'analyse de performance permet d'en évaluer les gains conséquents, mais également dévoile les compromis qu'elles impliquent: la diversité spatiale des relais est obtenue aux dépens de la capacité suite à la contrainte half-duplex; la déficience de rang du canal multi-antennes aux bordures de la cellule, où les relais sont généralement déployés, entrave l'activation du multiplexage spatio-temporel; la diversité temporelle du hybrid-ARQ se trouve rapidement dégradée par la nature quasi-statique et long-terme des environnements à évanouissement lent. Cette thèse essaie de surmonter ces enjeux inhérents en proposant une conception conjointe des trois techniques pour les communications sur les canaux MIMO-ARQ limités par les interférences entre symboles (IES). Dans une approche niveau-signal, nous exploitons la déficience de rang du canal source-relai—découlant de la distribution des réflecteurs et/ou du nombre d'antennes—en s'appuyant sur un relayage de type project-and-forward (PF). Le concept de projection est premièrement validé à travers l'analyse de sa performance sur un canal mixte MIMO-pinhole/Rayleigh à évanouissement plat, et ce en utilisant des fonctions mathématiques généralisées. En invoquant la théorie des résidus, nous étudions le comportement asymptotique du système, ce qui mène à des recommandations sur la conception des schémas de relayage basés sur PF. Nous appliquons ensuite le concept de projection orthogonale aux canaux MIMO à IES pour alléger la contrainte half-duplex. Ainsi, nous introduisons une architecture de multiplexage spatial coopératif à base de PF pour réduire la durée de la phase de relayage, sans toutefois recourir à la détection ou la remodulation au niveau du relais. Le modèle de communication mis en place permet d'assimiler le système de relayage à une transmission point à point MIMO, ce qui permet d'adopter les techniques de détection et de combinaison conjointes côté destination. Finalement, nous introduisons une conception inter-couches, où la projection est effectuée conjointement sur des transmissions MIMO-ARQ multiples, augmentant ainsi le gain de diversité et l'efficacité spectrale.

Mots-clefs: Analyse de performance, ARQ, comportement asymptotique, conception inter-couches, déficience de rang, degrés de liberté, MIMO large-bande, fonctions généralisées, project-and-forward, relayage coopératif, théorie des résidus, traitement conjoint.

List of Acronyms

ACK	positive acknowledgment
AF	amplify-and-forward
ARQ	automatic repeat request
AWGN	additive white Gaussian noise
BICM	bit-interleaved coded modulation
BH	busy hour
BLER	block error rate
BS	base station
CAPEX	capital expenditure
CCDF	complementary cumulative distribution function
CDF	cumulative distribution function
CF	compress-and-forward
CFR	channel frequency response
CP	cyclic prefix
CSI	channel state information
c.u.	channel use
DeNB	donor eNodeB
DetF	detect-and-forward
DF	decode-and-forward
DFT	discrete Fourier transform
DMT	diversity-multiplexing trade-off
DoF	degree of freedom
HetNet	heterogeneous network
IDFT	inverse discrete Fourier transform
i.i.d.	independent and identically distributed
ISI	inter-symbol interference
LT	long-term
LTE	long-term evolution
MAP	maximum a posteriori
MIMO	multiple-input–multiple-output
ML	maximum likelihood
MMSE	minimum mean square error

MRC	maximum ratio combining
NACK	negative acknowledgment
NE	network element
OPEX	operational expenditure
PDF	probability density function
PF	project-and-forward
QoS	quality of service
QRD	QR decomposition
RF	radio frequency
RN	relay node
RV	random variable
SC	single carrier
SNR	signal-to-noise ratio
ST	space-time
STC	space–time code
TS	time slot
UE	user equipment

List of Notations

$^{\mathrm{T}}$, and $^{\mathrm{H}}$	transpose and Hermitian transpose, respectively
$\lvert . \rvert$	absolute value of a variable or cardinal of a set
$\lVert \cdot \rVert_{\mathrm{F}}$	Frobenius norm
$\lceil x \rceil$	ceiling of x, i.e., the smallest integer greater than or equal to x
$\otimes$	Kronecker product
$\delta_{tt'}$	Kronecker symbol, i.e., $\delta_{tt'} = 1$ for $t = t'$ and $\delta_{tt'} = 0$ for $t \neq t'$
$\mathbf{0}_{N \times M}$	all zero $N \times M$ matrix
$\mathbf{I}_N$	$N \times N$ identity matrix
$\det(\mathbf{X})$	determinant of matrix $\mathbf{X}$
$\mathrm{diag}\{\mathbf{X}_1, \cdots, \mathbf{X}_M\}$	block diagonal matrix composed of matrices $\mathbf{X}_1, \cdots, \mathbf{X}_M$
$\mathrm{E}[\cdot]$	mathematical expectation of the argument $[\cdot]$
$\mathrm{E}[\cdot \mid \mathbf{H}]$	conditional expectation with respect to $\mathbf{H}$
$\Pr[\cdot]$	probability of the argument $[\cdot]$
$\Gamma(\cdot)$	Gamma function of the argument $(\cdot)$
$\mathrm{G}^{\cdot,\cdot}_{\cdot,\cdot}(\cdot \mid \cdot)$	Meijer G-function
$\mathrm{G}^{\cdot,\cdot:\cdot,\cdot:\cdot,\cdot}_{\cdot,\cdot:\cdot,\cdot:\cdot,\cdot}(\cdot,\cdot \mid \cdot \mid \cdot \mid \cdot)$	bivariate Meijer G-function
$K_\nu(\cdot)$	ν^{th}-order modified Bessel function of the second kind of the argument $(\cdot)$
$\psi^{(0)}(\cdot)$	digamma function
$\mathrm{Res}[g(s), s_0]$	residue of function g at pole s_0
$\mathcal{N}(m, v)$	normal distribution with mean m and variance v
$\mathcal{X}_n^2$	Chi-square distribution of n degrees of freedom
$\mathbb{C}$	set of complex number
$\mathcal{A}$	constellation alphabet
$\alpha_{\epsilon\epsilon'}$	average propagation loss of link $\epsilon - \epsilon'$
α_{r}	relay normalization factor
$\overline{C}$	ergodic capacity
$\mathbf{C}_{\mathrm{sr},t}$	channel frequency response matrix for subcarrier t
$\mathbf{C}_{\mathrm{sr}}$	channel frequency response
$\mathbf{C}_{\mathrm{sr}}^{(k)}$	block diagonal matrix limping channel frequency responses of rounds $1, \ldots, k$
$\mathbf{C}_{\mathrm{sr},t}^{(k)}$	block diagonal matrix limping channel frequency responses of rounds $1, \ldots, k$ at channel use t

$d_{\epsilon\epsilon'}$	distance between nodes ϵ and ϵ'
$\mathbf{\Xi}_{\mid\mathbf{H}}$	conditional covariance matrix with respect to $\mathbf{H}$
$\mathbf{\Xi}^{(k)}_{\mid\mathbf{H}}$	multi-transmission conditional covariance matrix with respect to $\mathbf{H}$
$F_{\gamma_{\epsilon\epsilon'}}$	CDF of SNR $\gamma_{\epsilon\epsilon'}$
$\widetilde{F}_{\gamma_{\epsilon\epsilon'}}$	complementary CDF of SNR $\gamma_{\epsilon\epsilon'}$
γ	instantaneous end-to-end SNR
$\gamma_{\epsilon\epsilon'}$	instantaneous SNR of link $\epsilon - \epsilon'$
$\overline{\gamma}_{\epsilon\epsilon'}$	average SNR of link $\epsilon - \epsilon'$
γ_{th}	SNR threshold
$\mathbf{h}_{\mathrm{r}}$	first row of matrix $\mathbf{R}$
$\mathbf{H}_{\epsilon\epsilon'}$	channel matrix of MIMO flat fading link $\epsilon - \epsilon'$
$\mathbf{H}_{\epsilon\epsilon',l}$	MIMO channel of path l corresponding to the $\epsilon - \epsilon'$ link
$\mathbf{H}^{(k)}_{l}$	multi-slot MIMO channel block matrix for path l at round k
$\widetilde{\mathbf{H}}_{\mathrm{sr},l}$	l^{th} path matrix corresponding to the equivalent $\mathrm{s} - \mathrm{r}$ MIMO multipath channel after relay processing
$\mathbf{H}^{(k)}_{\epsilon\epsilon',l}$	MIMO channel of path l corresponding to the $\epsilon - \epsilon'$ link at ARQ round k
$\underline{\mathbf{H}}^{(k)}_{l}$	multi-slot multi-transmission MIMO channel block matrix for path l
$\underline{\mathbf{H}}^{(k)}_{\mathrm{sr}}$	multi-transmission MIMO multipath channel block matrix
$\underline{\mathbf{H}}^{(k)}_{\mathrm{sr},l}$	multi-transmission MIMO channel block matrix for path l
$\mathbf{H}^{(k)}_{\mathrm{srd},l}$	equivalent $\mathrm{s} - \mathrm{r} - \mathrm{d}$ MIMO channel for path l at round k
I	mutual information
κ	path loss exponent
l	MIMO tap index
$L_{\epsilon\epsilon'}$	number of taps in the MIMO multipath channel corresponding to the $\epsilon - \epsilon'$ link
$\mathbf{\Lambda}_{\mid\mathbf{H}}$	colored noise conditional covariance matrix with respect to $\mathbf{H}$
$\mathbf{\Lambda}^{(k)}_{\mid\mathbf{H}}$	multi-transmission colored noise conditional covariance matrix with respect to $\mathbf{H}$
n_{ϵ}	number of antennas at node ϵ
$\mathbf{P}$	antenna mapping matrix at the relay
P_{out}	outage probability
$P^{\mathrm{AF}}_{\mathrm{out}}$	outage probability for AF scheme
$\mathbf{Q}$	unitary matrix of the QR decomposition
$\mathbf{Q}_{t}$	unitary matrix of the QR decomposition corresponding to channel use t
$\mathbf{Q}^{(k)}_{t}$	unitary matrix of the QR decomposition corresponding to channel use t and round k
$\mathbf{q}$	first column vector of $\mathbf{Q}$

ρ	channel rank
$\mathbf{R}$	upper triangular matrix of the QR decomposition
$\mathbf{R}_t$	upper triangular matrix of the QR decomposition corresponding to channel use t
$\mathbf{R}^{(k)}$	block diagonal matrix gathering matrices $\mathbf{R}_0^{(k)}, \ldots, \mathbf{R}_{T-1}^{(k)}$
$\mathbf{R}_t^{(k)}$	upper triangular matrix of the QR decomposition corresponding to channel use t and round k
$\mathbf{s}$	precoded transmitted symbol vector
$\mathbf{S}$	transmitted symbol matrix
$\mathcal{S}$	modulation spectral efficiency
σ^2	AWGN noise variance
$\mathbf{s}_t$	transmitted symbol vector at channel use t
T	number of channel use
$\mathcal{T}$	average throughput
T_c	channel coherence time
$\mathbf{x}'$	block discrete Fourier transform (DFT) of $\mathbf{x}$ defined as $\mathbf{x}' \triangleq \mathbf{U}_{T,N}\mathbf{x}$.
$\widetilde{\mathbf{x}}$	projected version of $\mathbf{x}$
$\underline{\mathbf{x}}$	column vector composed of several channel uses
$\mathbf{y}_{\mathrm{d}}$	received signal vector at node d
$\mathbf{y}_{\mathrm{d},t,i}$	received signal vector corresponding to node d at channel use t and during slot $i \in \{1,2\}$
$\mathbf{y}_{\mathrm{r}}$	received signal vector at node r
y_{r}	received signal at relay node
$\widetilde{y}_{\mathrm{r}}$	DoF resulting from signal projection
$\mathbf{y}_{\mathrm{r},t,}$	received signal vector corresponding to node r at channel use t
$\underline{\mathbf{y}}_{\mathrm{r},t}^{(k)}$	multi-transmission received stacked vector at the relay at channel use t
$\mathbf{y}_{\mathrm{d},t,i}^{(k)}$	received signal corresponding to destination node at channel use t and ARQ round k and during slot $i \in \{1,2\}$
$\mathbf{y}_{\mathrm{r},t}^{(k)}$	received signal at the relay at channel use t and ARQ round k
$\underline{\mathbf{y}}'^{(k)}_{\mathrm{r}}$	frequency domain multi-transmission received signal at the relay
$\underline{\mathbf{y}}'^{(k)}_{\mathrm{r},t}$	frequency domain multi-transmsssion received signal at the relay at channel use t
$\widetilde{\mathbf{y}}'^{(k)}_{\mathrm{r}}$	frequency domain DoF vector resulting from signal projection at round k
$\widetilde{\mathbf{y}}'^{(k)}_{\mathrm{r},t}$	frequency domain DoF vector resulting from signal projection at channel use t and round k
$\mathbf{y}_{\mathrm{d},t}^{(k)}$	multi-slot stacked received signal at the destination at channel use t and round k
$\underline{\mathbf{y}}_{\mathrm{d},t}^{(k)}$	multi-slot multi-transmission stacked received signal at the destination at channel use t

$\mathbf{U}_T$	$T \times T$ unitary Fourier matrix whose (m,n)-th element is $\mathbf{U}_T[m,n] = \frac{1}{\sqrt{T}} e^{-j2\pi mn/T}$, and $j = \sqrt{-1}$.
$\mathbf{U}_{T,N}$	$TN \times TN$ matrix defined as $\mathbf{U}_{T,N} \triangleq \mathbf{U}_T \otimes \mathbf{I}_N$
$\mathrm{vec}_T\left\{\mathbf{x}_t\right\}$	stacked column vector limping sub-vectors $\mathbf{x}_t$ $(t = 0, \ldots, T-1)$ as $\mathrm{vec}_T\left\{\mathbf{x}_t\right\} \triangleq \left[\mathbf{x}_0^{\mathrm{T}}, \ldots, \mathbf{x}_{T-1}^{\mathrm{T}}\right]^{\mathrm{T}}$
$\mathbf{w}_{\mathrm{d},t,i}$	AWGN noise corresponding to node d at channel use t and during slot $i \in \{1,2\}$
$\mathbf{w}_\epsilon$	additive white Gaussian noise (AWGN) vector at node ϵ
$\mathbf{w}_{\mathrm{r},t}$	AWGN noise corresponding to node r at channel use t
$\mathbf{w}_{\mathrm{d},t,i}^{(k)}$	AWGN noise corresponding to destination node at channel use t and ARQ round k and during slot $i \in \{1,2\}$
$\mathbf{w}_{\mathrm{d},t}^{(k)}$	multi-slot AWGN noise stacked vector at the destination at channel use t and round k
$\underline{\mathbf{w}}_{\mathrm{d},t}^{(k)}$	multi-transmission multi-slot AWGN noise stacked vector at the destination at channel use t
$\mathbf{w}_{\mathrm{r},t}^{(k)}$	AWGN noise at the relay at c.u. t and ARQ round k
$\underline{\mathbf{w}}_{\mathrm{r},t}^{(k)}$	AWGN noise multi-transmission stacked vector at channel use t
$\underline{\mathbf{w}'}_{\mathrm{r}}^{(k)}$	frequency domain multi-transmission AWGN noise at the relay
$\underline{\mathbf{w}'}_{\mathrm{r},t}^{(k)}$	frequency domain multi-transmission AWGN noise at the relay at channel use t

Contents

List of Figures

List of Tables

Chapter 1

Introduction

1.1 Context

In the quest for the gigabit wireless, cellular systems have undergone a metamorphosis over the last few years. From the classical network densification driven by cells shrinking, higher carrier frequencies, and larger bandwidth; to the exploitation of the space-time (ST) dimension through the spatial multiplexing oriented multiple-input-multiple-output (MIMO) and the frame error rate reduction via the temporal diversity of hybrid-automatic repeat request (ARQ) protocols: Signal transmission and reception techniques have been sharpened to leverage all the wireless channel capacity degrees of freedom (DoF) [1]. The dawn of the smartphone era, however, announced the reinvention of users' behavior, and instead of measuring traffic busy hours (BH) in almost deterministic areas and time frames; data traffic has become non-uniformly distributed in both space and time, with an accentuated concentration in indoors [2]. It has been a complete paradigm shift; a new trend that has prompted the adoption of the heterogeneous networks (HetNet) concept, where a mix of small-cells and relays are deployed in the macro-cell area to cope with punctual quality of service (QoS) degradations in a customized fashion [2, 3], whence palpable CAPEX and OPEX[1] savings are achieved.

In practice, while relays are intended to enhance coverage and throughput at the cell-edge [4] by breaking the low signal-to-noise-ratio (SNR) source-destination link into two independent high SNR hops; they also act as packet retransmitters in slow fading environments, where the performance of ARQ mechanisms is usually limited by the long-term (LT) quasi-static nature of the channel, wherein multiple ARQ rounds experience the same channel realization [5].

Since the work of Sendonaris *et al.* [6, 7] that introduced the notion of cooperative diversity, several relaying protocols have emerged [8–11], among which amplify-and-forward (AF) and decode-and-forward (DF) are the prevalent ones. In the AF mode, the signal packet received from the source is merely amplified and retransmitted towards the destination. The DF mode however consists on decoding then re-encoding the received data frame before forwarding it

[1] For CAPital EXpenditures and OPerational EXpense, respectively.

to the destination. While the first approach suffers from noise amplification, the second one endures error propagation when the relay forwards an erroneously decoded data packet [10]. Alternatively, a selective DF protocol, where the relay only transmits when it can correctly decode the data packet, has been introduced as an efficient method to reduce error propagation [12]. On the other hand, detect-and-forward (DetF) (see 2.4.2) becomes an interesting relaying strategy in resource-limited networks, because the relay only demodulates—instead of decoding—the received signals and sends the detected symbol block to the destination [13, 14]. In their draft paper [15], the authors have introduced project-and-forward (PF) (see 2.4.3) as a new relaying scheme functioning over MIMO flat fading multihop relay channels. By operating at signal-level, a PF multi-antenna relay extracts and forwards only the degrees of freedom (DoF) contained in received signals, reducing hence the number of relay active antennas during the relaying phase and therefore the noise propagation effect at the destination. This approach leads to an SNR gain compared to the AF mode as well as a similar diversity gain while presenting a lower complexity than DF and DetF that operate at the bit and symbol levels, respectively.

From a radio frequency (RF) design viewpoint, a relay may operate in either *half-duplex* or *full-duplex* modes. In the former, the relay transmission and reception alternate in time which makes the conveyance of one symbol from the source to the destination span two channel uses, leading thereby to a throughput loss represented by the $1/2$ pre-log factor in the corresponding capacity expressions. By contrast, in full-duplex schemes, relay transmission and reception are concurrent which mitigates the aforementioned distortion factor [16]. Yet, the capacity can be significantly degraded from another angle. Indeed, when a relay simultaneously transmits and receives over the same frequency channel, an interference link, dubbed loopback or echo interference link, is introduced from the relay transmitter to its receiver. Existing isolation and cancellation techniques [17, 18] cannot perfectly prevent the relay transmit signal from leaking into its receiver. Consequently, a residual self-interference persists and adversely affects the effective SNR inside the capacity logarithm [19], especially in high transmit power regimes. Altogether then, these practical considerations have urged the community to resort to the half-duplex scheme while trying to optimize the resulting throughput loss through new protocols. Hence, from interference cancellation-aided multi-relay architectures [20–22] and the use of extra frequency or spreading code resources to orthogonalize relay transmission and reception [23, 24]; to the two-way relaying [25], the increase of modulation order at the relay [26], and the joint design of hybrid-ARQ and relaying functions [27–30]: a panoply of approaches have been addressed in the literature.

That said, performance analysis is also required for an accurate benchmark of the outlined relaying schemes. In its relentless advance, the wireless communications community has developed an extensive set of mathematical tools to characterize the MIMO relay channel. Hence, Hasna and Alouini have presented in [31] a useful and semi analytical framework for the evaluation of the end-to-end outage probability of multihop wireless systems with AF channel state information (CSI)-assisted relays over Nakagami-m fading channels. Moreover, the same authors have characterized the performance of both CSI-assisted and fixed gain dual-hop AF and DF relays over Rayleigh [32, 33], and Nakagami-m [34] fading channels. Karagiannidis *et al.* have studied in [35] the performance bounds for multihop wireless communications with blind (fixed gain) relays over Rice, Hoyt, and Nakagami-m fading channels, using the moments-based approach [36]. In [37, 38], Suraweera *et al.* have investigated the end-to-end performance of dual-hop AF fixed gain relaying systems when the source-relay and the relay-destination channels experience asymmetric fading conditions, namely Rayleigh/Rician and Rician/Rayleigh fading scenarios. In [39–41], the authors have attempted to investigate the effects of keyhole[2] (a.k.a. pinhole) radio conditions on MIMO AF relaying networks, by considering a downlink scenario in which the source-relay channel enjoys a rich-scattering environment while the source-destination and relay-destination channels suffer from the keyhole phenomenon. The studies have shown—via the derivation of either diversity or multiplexing gains—that cooperative diversity can mitigate or at least reduce the keyhole effect provided that certain conditions on the relay transmit power and/or the number of antennas are respected. Based on practical coding schemes, Benjillali *et al.* have invoked in [26, 42] the bit-interleaved coded modulation (BICM) [43] capacity and throughput metrics to demonstrate the efficiency of DetF scheme. In [15], the diversity gain of PF relaying over the Rayleigh product channel has been derived—using the joint distribution of the Wishart matrix eigenvalues—and has been shown to be equivalent to the AF case.

1.2 Thesis Objective

Zooming out from the aforementioned plethora of relaying techniques, the insistent question that arises is: how one can design relaying architectures, overcoming the half-duplex constraint, enabling the joint detection of source and relay signals at the destination, yet presenting a low-complexity?

In our endeavor to answer the question, we use the projection concept—adopted in PF scheme—as a key ingredient to devise new throughput-efficient signal-level relaying functions, operating over MIMO-ARQ broadband channels. In the introduced designs, we leverage the rank-deficiency nature of the source-relay MIMO channel that stems from either the scattering properties or the number of antennas at each side. Through a set of new mathematical analysis tools, we first unveil the interesting performance of the projection component in such scenarios. We then use it to optimize the relay multi-antenna transmission by operating on the degrees of freedom of received signals in a seamless way that maintains also the possibility of joint signal-level source-relay detection algorithms at the destination. The approach is extended afterward to MIMO broadband Chase-type hybrid-ARQ systems, where the signal DoFs are extracted via a joint projection over the source-relay multi-transmission MIMO channel.

[2] In the MIMO-keyhole—also known as pinhole—channel, the scatterers are too close to each other that the fading energy travels over a very thin air-pipe just like a "keyhole"; the MIMO channel matrix is unit rank in that case.

1.3 Thesis Contributions

Besides the MIMO relaying literature review invoked every now and then, this research journey has been marked with numerous new contributions.

- Except the introductory paper [15], to the best of our knowledge, no works else had addressed the PF scheme. In contrast, this thesis has presented, for the first time, a complete analysis and design framework for PF-based relaying systems over practical MIMO broadband channels. Hence, our initial paper [44] has become a reference in the realm of PF relaying with citations in renowned journal articles (see [45, 46]) and thesis (see [47]).
- Unprecedented performance analysis of PF relaying has been conducted by deriving both the outage probability and the ergodic capacity in the realistic scenario of mixed MIMO-pinhole and Rayleigh dual-hop channel.
- Applying the residue theory on Mellin-Barnes integrals, it has been shown how asymptotic expressions can be easily derived for the most complicated generalized functions. The asymptotic behavior of PF scheme has been accordingly inferred, which has yielded recommendations on the design of PF-based systems.
- The QR-based orthogonal projection involved in PF scheme has been extended to the MIMO-ISI channel through a frequency domain processing. Moreover, the adopted communication models have been devised in such a way to mask the cooperation and virtually transform the relaying system into a point-to-point augmented size source-destination MIMO link, enabling thereby the researchers to use existing efficient MIMO joint detection algorithms at the destination side.
- The half-duplex throughput loss has been dramatically reduced by the introduced PF-based signal-level spatial multiplexing strategy which, unlike AF scheme, delivers higher throughput as the relay draws nearer to the destination.
- The diversity gain and throughput in MIMO half-duplex constrained relaying systems have been notably enhanced—compared to AF—by jointly designing PF relaying and hybrid-ARQ functions; an architecture that translates the temporal ARQ diversity into a spatial one via the orthogonal projection concept.

1.4 Thesis Outline

This thesis is organized as follows. As a preliminary review, we revisit in chapter 2 the main MIMO-ARQ relaying concepts mentioned throughout the thesis. In chapter 3, we invoke a wide set of mathematical generalized functions to analyze the performance of project-and-forward relaying in a realistic scenario, where the source-relay and relay-destination channels experience

MIMO-pinhole and Rayleigh flat fading conditions, respectively. Applying the residue theory on Mellin-Barnes integrals [48], we derive the asymptotic behavior of the system and show how it depends on the different channel parameters, and provide practical recommendations regarding PF-based relaying design. In chapter 4, we extend the relay projection concept to the MIMO-ISI channel via a frequency-domain (FD) processing, and use it to build a PF-based signal-level cooperative spatial multiplexing strategy for rate enhancement in half-duplex-limited relaying systems. We hence derive the communication model in such a way that the destination views the relayed signal as a direct retransmission from the source over an equivalent end-to-end MIMO channel. In chapter 5, a relay cross-layer design is introduced by conducting the FD projection jointly over multiple ARQ transmissions in the MIMO broadband block fading channel. This processing is masked to the destination that may jointly combine source and relay signals.

Chapter 2

Concepts on MIMO-ARQ Relay Communications

2.1 Introduction

The performance of a point-to-point wireless communication in a specific channel bandwidth setup is measured by the ability to achieve the highest spectral-efficiency with the lowest error rate. While the first metric is about the capability to simultaneously transmit, several bits per channel use, the second is closely related to the available natural (e.g., multipath) and/or artificial diversity, where several corrupt copies of a packet—with errors at different positions—might result in an error-free version after combining. For a pretty long time, adaptive modulation and coding (AMC) schemes had played the crucial role to enhance the multiplexing and diversity performance, by designing more robust coding/decoding architectures—such as *turbo codes* [49] and iterative equalization and decoding [50]—independently or jointly with higher order modulations like in the *bit interleaved coded modulation* (BICM) concept [43]; It had been a painstaking journey; one was relieved to approach the single-link AWGN channel capacity: a single winding road...

2.2 MIMO

Yes. There are more unexplored roads in a radio channel than we thought. One can create them by endowing both the transmitter and receiver with multiple antennas elements; physically separated with at least half of the carrier wavelength to decorrelate the wireless paths connecting each pair of transmit and receive antennas. It is, indeed, one of the conditions to fully exploit the multiplexing and diversity capabilities of this multiple-input multiple-output (MIMO) system. The transmitted signal at channel use t is now a symbol vector $\mathbf{s}_t \in \mathbb{C}^{n_\mathrm{s}}$—drawn from any constellation alphabet $\mathcal{A}$—for which corresponds a received signal $\mathbf{y}_t \in \mathbb{C}^{n_\mathrm{d}}$;

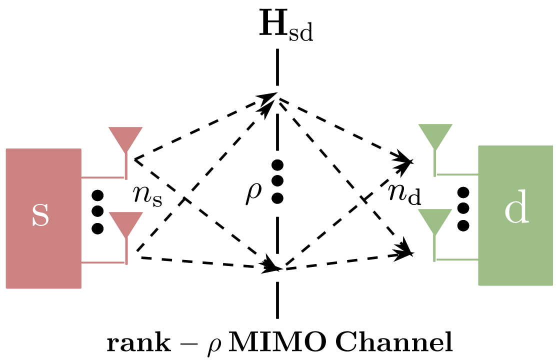

Figure 2.1: MIMO channel with arbitrary rank ρ, modeled as a multi-pinhole link; each pinhole is a cluster of scatterers very close to each other.

together linked by a linear relationship,

$$\mathbf{y}_t = \mathbf{H}_{\mathrm{sd}} \mathbf{s}_t + \mathbf{w}_t, \tag{2.1}$$

where matrix $\mathbf{H}_{\mathrm{sd}} \in \mathbb{C}^{n_{\mathrm{d}} \times n_{\mathrm{s}}}$—gathering fading coefficients between each couple of transmit and receive antennas—stands for the MIMO flat fading channel between the n_{s}-antennas transmitter and the n_{d}-antennas receiver, and vector $\mathbf{w}_t$ captures the effect of receiver thermal noise.

The number of parallel streams to be multiplexed over a MIMO link—known as ***degrees of freedom*** (DoF)—corresponds to the rank of the channel matrix thereof, i.e., $\rho = \mathrm{rank}\left(\mathbf{H}_{\mathrm{sd}}\right) \leq \min\left(n_{\mathrm{s}}, n_{\mathrm{d}}\right)$ [51]. In a rich scattering environment, the entries of $\mathbf{H}_{\mathrm{sd}}$ are independent with magnitudes being Rayleigh distributed; and one can see that the channel is full-rank, providing exactly $\min\left(n_{\mathrm{s}}, n_{\mathrm{d}}\right)$ spatial degrees of freedom. In contrast, when either the scatterers are very close to each other or the transmit-receive range is large, the MIMO channel becomes unit-rank and is thus dubbed a ***keyhole*** or ***pinhole*** channel, having therefore a single DoF. The corresponding matrix $\mathbf{H}_{\mathrm{sd}}$ is rather modeled as the outer product of two Rayleigh vectors $\mathbf{g}_{\mathrm{s}} \in \mathbb{C}^{n_{\mathrm{s}}}, \mathbf{g}_{\mathrm{d}} \in \mathbb{C}^{n_{\mathrm{d}}}$ [52],

$$\mathbf{H}_{\mathrm{sd}} = \mathbf{g}_{\mathrm{d}} \mathbf{g}_{\mathrm{s}}^{\mathrm{H}}. \tag{2.2}$$

A more general model for arbitrary rank ρ MIMO channels can be similarly written in terms of Gaussian matrices $\mathbf{G}_{\mathrm{s}} \in \mathbb{C}^{n_{\mathrm{s}} \times \rho}, \mathbf{G}_{\mathrm{d}} \in \mathbb{C}^{n_{\mathrm{d}} \times \rho}$ as

$$\mathbf{H}_{\mathrm{sd}} = \mathbf{G}_{\mathrm{d}} \mathbf{G}_{\mathrm{s}}^{\mathrm{H}}. \tag{2.3}$$

Having said that, linear dependencies might also exist between the elements of a signal vector; and thus it can be perfectly known by only determining its free components, i.e., its degrees of freedom. In case of a rank ρ channel for instance, the received signal $\mathbf{y}_t$ has ρ degrees of freedom; a fact that can be revealed by transforming the MIMO channel into a set of ρ parallel single-input single-output (SISO) subchannels using linear algebra methods, such as the QR

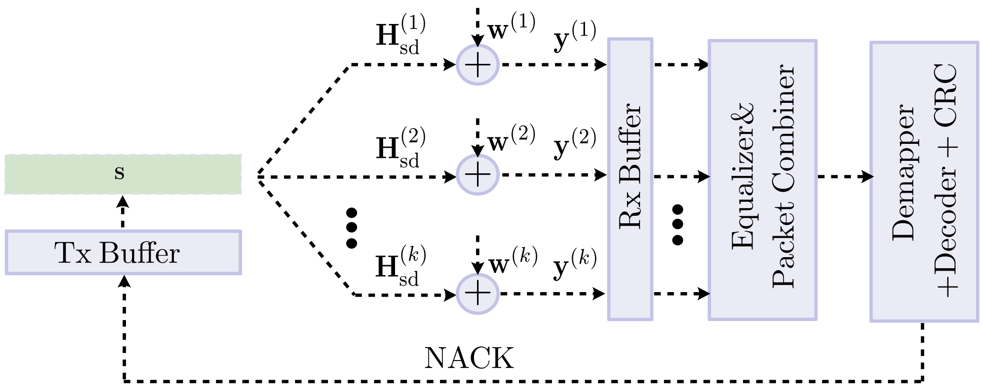

Figure 2.2: Chase-type ARQ and packet combining.

and SVD decompositions [53]: a free version of $\mathbf{y}_t$ is obtained for example as

$$\widetilde{\mathbf{y}}_t = \mathbf{R}\mathbf{s}_t + \mathbf{Q}^{\mathrm{H}}\mathbf{w}_t \in \mathbb{C}^{\rho\times 1}, \tag{2.4}$$

where $\mathbf{H}_{\mathrm{sd}} = \mathbf{QR}$, $\mathbf{Q} \in \mathbb{C}^{n_{\mathrm{d}}\times\rho}$ is a unitary matrix such that $\mathbf{Q}^{\mathrm{H}}\mathbf{Q} = \mathbf{I}_\rho$, and $\mathbf{R} \in \mathbb{C}^{\rho\times n_{\mathrm{s}}}$ is an upper triangular matrix.

Spatial multiplexing, however, comes at the expense of the multi-antenna diversity, as no MIMO algorithm can maximize them simultaneously [54]; it is an inherent trade-off, and while in a $n_{\mathrm{d}} \times n_{\mathrm{s}}$ MIMO full-rank channel there are initially $n_{\mathrm{s}}n_{\mathrm{d}}$ ***diversity branches***, the multiplexing of $0 \leq m \leq \min(n_{\mathrm{s}}, n_{\mathrm{d}})$ streams reduces the diversity order to only $(n_{\mathrm{s}} - m)(n_{\mathrm{d}} - m)$.

2.3 Hybrid-ARQ

Yet, the diversity can be sought in the time dimension as well: [55] states that packet retransmission can be exploited to significantly improve diversity, especially and fortunately at high multiplexing order—exactly where the multi-antenna diversity becomes low. This is justified by the fact that most packets are decoded successfully in the first round and ARQ retransmissions serve only to correct the rare error events, and hence, dramatically decreasing the probability of error with a negligible cost on the transmission rate. If we assume a block fading channel for example, the diversity order is shown to be $K\left(n_{\mathrm{s}} - \frac{m}{K}\right)\left(n_{\mathrm{d}} - \frac{m}{K}\right)$ for a maximum number of rounds, i.e., ***ARQ delay*** K [55, Theorem 2].

With the activation of an ARQ protocol at the upper layer, the reception of a NACK feedback from the receiver instigates the retransmission of the same packet over a block fading [1] MIMO channel, providing therefore an additional diversity branch that the receiver may combine with the previous copies of the packet—kept in a buffer—to yield a more reliable version for decision: it is the concept of ***Chase-type hybrid-ARQ*** (HARQ).

[1] A channel is termed *block fading* if it is quasi-static within a data packet interval, and independently varies from one packet interval to another.

The most efficient combining algorithms are those operating at the signal-level; they jointly perform equalization and packet combining by translating temporal ARQ diversity into a spatial one; as though at ARQ round k, the communication is virtually taking place over a $kn_\mathrm{d} \times n_\mathrm{s}$ MIMO channel constructed as [56, 57]

$$\underline{\mathbf{y}}_t^{(k)} = \underline{\mathbf{H}}_\mathrm{sd}^{(k)} \mathbf{s}_t + \underline{\mathbf{w}}_t^{(k)}, \tag{2.5}$$

where $\underline{\mathbf{y}}_t^{(k)} = \left[\mathbf{y}_t^{(1)^\mathrm{T}}, \cdots, \mathbf{y}_t^{(k)^\mathrm{T}}\right]^\mathrm{T}$, $\underline{\mathbf{H}}_\mathrm{sd}^{(k)} = \left[\mathbf{H}_\mathrm{sd}^{(1)^\mathrm{T}}, \cdots, \mathbf{H}_\mathrm{sd}^{(k)^\mathrm{T}}\right]^\mathrm{T}$, $\underline{\mathbf{w}}_t^{(k)} = \left[\mathbf{w}_t^{(1)^\mathrm{T}}, \cdots, \mathbf{w}_t^{(k)^\mathrm{T}}\right]^\mathrm{T}$, and $\mathbf{H}_\mathrm{sd}^{(k)}$ and $\mathbf{w}_t^{(k)}$ stand for the k-th round channel realization and noise, respectively. Optimal (e.g., MAP) and suboptimal (e.g., MMSE) detection strategies may be applied then to the received multi-transmission signal $\underline{\mathbf{y}}_t^{(k)}$ to yield accurate symbols' estimates. From an information theoretic point of view, this receive combining corresponds to an accumulation of the ***mutual information*** which—assuming a Gaussian input alphabet for tractability and given (2.5)—can be expressed as

$$\mathcal{I}_k = \log_2 \left(\det \left(\mathbf{I}_{kn_\mathrm{d}} + \frac{\overline{\gamma}}{n_\mathrm{s}} \underline{\mathbf{H}}_\mathrm{sd}^{(k)} \underline{\mathbf{H}}_\mathrm{sd}^{(k)^\mathrm{H}} \right) \right), \tag{2.6}$$

where $\overline{\gamma}$ is the average ***signal-to-noise ratio*** (SNR) per receive antenna. This means that for a fixed spectral-efficiency $\mathcal{S}$, the outage probability $P_\mathrm{out}(k) = \Pr[\mathcal{I}_k < \mathcal{S}]$ decrease is accelerated with higher k.

To reflect the above diversity-delay trade-off, we often resort to the ***average throughput*** metric, defined as the average number of correctly received information bits per channel use (bit/cu),

$$\overline{\mathcal{T}} = \frac{\mathrm{E}[s]}{\mathrm{E}[k]}, \tag{2.7}$$

where $\mathrm{E}[s]$ is the mean rate of the the MIMO link at SNR $\overline{\gamma}$, formalized as

$$\mathrm{E}[s] = \mathcal{S}\left(1 - P_\mathrm{out}(K)\right), \tag{2.8}$$

and $\mathrm{E}[k]$ is the average number of HARQ rounds spent transmitting an arbitrary packet, and which can be computed using the renewal-reward theory. Let $q(k) = \Pr\{\mathrm{NACK}_1, \ldots, \mathrm{NACK}_{k-1}, \mathrm{ACK}_k\}$ denote the probability of decoding success at round k, we have [58]

$$\mathrm{E}[k] = \sum_{k=1}^{K-1} kq(k), \tag{2.9}$$

which finally yields

$$\overline{\mathcal{T}} = \frac{\mathcal{S}\left(1 - P_\mathrm{out}(K)\right)}{\sum_{k=1}^{K-1} kq(k)}. \tag{2.10}$$

This result corroborates the fact that the average throughput is maximized when the transmit spectral-efficiency $\mathcal{S}$ is high (high multiplexing gain), and the majority of the packets are successfully decoded at the first round so that to optimize the ARQ delay.

A closer look at (2.6), however, reveals that the mutual information will not increase properly if correlations exist between ARQ channel realizations $\mathbf{H}_{\mathrm{sd}}^{(k)}$ $(k = 1, \ldots, K)$; a behavior driven by the fact that the matrix determinant drops with linear dependencies. Hence, in the so-called long-term (LT) quasi-static ARQ channels, where the fading slowly varies from one round to another, the ARQ diversity becomes limited and therefore impractical given the delay it costs.

2.4 Cooperative Relaying

Channel realizations of sufficiently spaced transmitters, however, remain decorrelated even in slow fading conditions; a key remark that induces the incorporation of a new type of nodes called ***relays*** into the point-to-point MIMO system depicted in Fig. 2.1. Given the broadcast nature of the wireless channel, the relaying node is able to overhear all the transmitter or ***source*** signals; to process them and finally forward them to the receiver or ***destination***, creating thereby additional diversity branches. This new ***cooperative relaying*** setup can be expressed using a set of communication models, corresponding to the direct source-destination, the source-relay and the relay-destination links, respectively:

$$\begin{cases} \mathbf{y}_{\mathrm{d},t,1} & = \mathbf{H}_{\mathrm{sd}}\mathbf{s}_t + \mathbf{w}_{\mathrm{d},t,1}, \\ \mathbf{y}_{\mathrm{r},t} & = \mathbf{H}_{\mathrm{sr}}\mathbf{s}_t + \mathbf{w}_{\mathrm{r},t}, \\ \mathbf{y}_{\mathrm{d},t,2} & = \mathbf{H}_{\mathrm{rd}}\widetilde{\mathbf{y}}_{\mathrm{r},t} + \mathbf{w}_{\mathrm{d},t,2}, \end{cases} \tag{2.11}$$

where $\widetilde{\mathbf{y}}_{\mathrm{r},t}$ is a processed version of the relay received signal $\mathbf{y}_{\mathrm{r},t}$; conveyed to the destination through channel $\mathbf{H}_{\mathrm{rd}}$. Signals $\mathbf{y}_{\mathrm{d},t,1}$ and $\mathbf{y}_{\mathrm{d},t,2}$, are combined at the destination, which enhances the diversity gain of the system.

2.4.1 Cooperation Protocols

A relay node operates generally in the ***half-duplex*** mode—in which packet reception and retransmission alternate in time—since the full-duplex one is not viable given the severe residual interference it induces, as detailed in 4.1. As such, relay-assisted cooperative communications are organized in two orthogonal phases (in the sens of time); which typically leads to three protocols:

- **Direct link with active source:** the source broadcasts a first data packet to both the relay and the destination during phase 1; then the relay forwards a processed version of packet 1 during phase 2, while the source sends a second packet to the destination,
- **Direct link with silent source during phase 2:** the source broadcasts a packet to the relay and destination nodes during the first phase; the relay forwards then the overheard

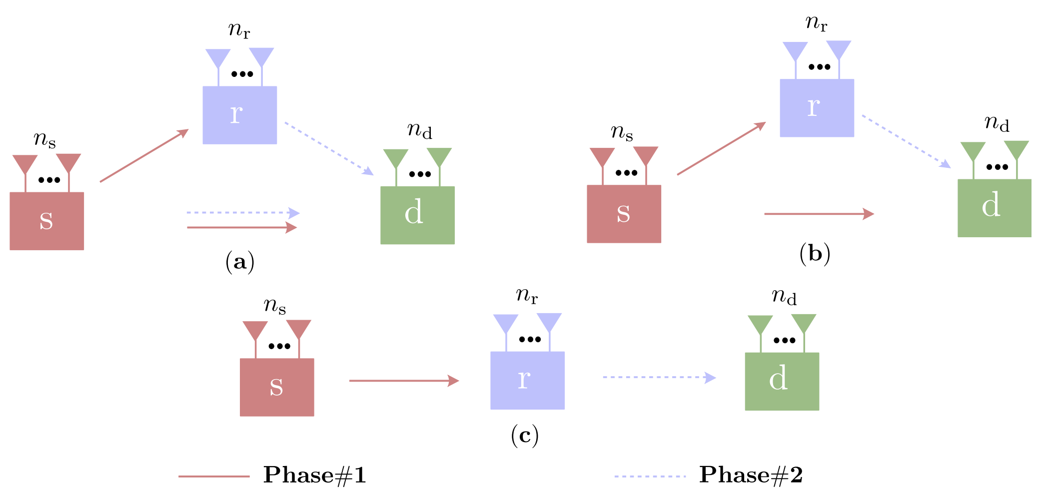

Figure 2.3: Cooperation protocols: (a) Direct link with active source, (b) Direct link with silent source during phase 2, (c) Dual-hop.

packet—after processing it—to the destination during phase 2, while the source remains silent,

- **Dual-hop:** in this case, there is no visibility between the source and the destination. The relay captures the packet transmitted by the source during the first phase, processes it, and retransmits it toward the destination during the second phase.

2.4.2 Classical Relaying Schemes

Several relaying classes exist and differ in processing level and performance. The prevalent ones are:

Amplify-and-forward (AF) The relay amplifies the source signal and forwards it to the destination; the resulting output signal at the nth relay antenna ($n = 1, \ldots, n_\mathrm{r}$) is given by

$$\widetilde{\mathbf{y}}_{\mathrm{r},t,n} = \alpha_{\mathrm{r},n} \mathbf{y}_{\mathrm{r},t,n}, \tag{2.12}$$

where the amplification factor $\alpha_{\mathrm{r},n}$ can be either fixed—in case of blind relaying—or channel state information (CSI)-dependent, i.e.,

$$\alpha_{\mathrm{r},n} = \frac{1}{\sqrt{\alpha_{\mathrm{sr}}^2 \left\| \mathbf{h}_{\mathrm{sr},n} \right\|_\mathrm{F}^2 + \sigma^2}}; \tag{2.13}$$

α_{sr} is the path-loss of the $\mathrm{s}-\mathrm{r}$ link, $\mathbf{h}_{\mathrm{sr},n}$ is the nth relay antenna $1 \times n_\mathrm{s}$ MISO channel, and σ^2 stands for the noise variance. AF scheme is of low complexity, but it suffers—on the other hand—from ***noise amplification***, that becomes even worse with the accumulation of the n_r relayed noises at each destination antenna.

Detect-and-Forward (DetF) In this strategy, the relay detects the transmitted symbols —using one of the algorithms (e.g., ML, MMSE...)—and forwards them to the destination. Although noise amplification and accumulation are completely mitigated, ***error propagation*** might still occur at the destination. The relayed signal $\widetilde{\mathbf{y}}_{\mathrm{r},t,n}$ in case of a MMSE filtering is obtained as

$$\begin{cases} \widehat{\mathbf{s}}_t & = \mathbf{F}\mathbf{y}_{\mathrm{r},t}, \\ \mathbf{F} & = \left(\mathbf{H}_{\mathrm{sr}}^{\mathrm{H}}\mathbf{H}_{\mathrm{sr}} + \sigma^2\mathbf{I}\right)^{-1}\mathbf{H}_{\mathrm{sr}}^{\mathrm{H}}, \\ \widetilde{\mathbf{y}}_{\mathrm{r},t,n} & = \arg\min_{s\in\mathcal{A}} \left\| s - \widehat{\mathbf{s}}_{t,n} \right\|^2. \end{cases} \tag{2.14}$$

Decode-and-forward (DF) DF relay detects and decodes the source signal, and regardless of the decoding outcome, re-encodes and modulates the resulting bit stream, then forwards it to the destination. While this strategy cancels noise accumulation, it does not prevent error propagation since erroneous packets are also conveyed to the destination. Alternatively, a variant termed ***selective DF*** (S-DF) fixes this problem by allowing the relay to retransmit only correctly decoded data packets. These two schemes present, however, a high complexity as they are operating at the bit level.

2.4.3 Project-and-Forward Relaying

To alleviate the effect of relayed noise amplification and accumulation arising in AF systems, one should optimize the number of the relay active antennas during the relaying phase. A key idea is to forward only the degrees of freedom of the received signal $\mathbf{y}_{\mathrm{r},t}$, that would occupy—as shown in 2.2—as few antennas as the s − r MIMO channel rank ρ. By recalling (2.4), the forwarded signal can be inferred from $\mathbf{y}_{\mathrm{r},t}$ through orthogonal projection as

$$\widetilde{\mathbf{y}}_{\mathrm{r},t} = \mathbf{A}\mathbf{Q}^{\mathrm{H}}\mathbf{y}_{\mathrm{r},t} = \mathbf{A}\left(\mathbf{R}\mathbf{s}_t + \mathbf{Q}^{\mathrm{H}}\mathbf{w}_{\mathrm{r},t}\right) \in \mathbb{C}^{\rho\times 1}, \tag{2.15}$$

where the QR decomposition [53] yields $\mathbf{H}_{\mathrm{sr}} = \mathbf{Q}\mathbf{R}$; $\mathbf{Q} \in \mathbb{C}^{n_\mathrm{r}\times\rho}$ is a unitary matrix such that $\mathbf{Q}^{\mathrm{H}}\mathbf{Q} = \mathbf{I}_\rho$, and $\mathbf{R} \in \mathbb{C}^{\rho\times n_\mathrm{s}}$ is an upper triangular matrix. $\mathbf{A} = \mathrm{diag}\left\{\alpha_{\mathrm{r},1}, \ldots, \alpha_{\mathrm{r},\rho}\right\}$ is the amplification matrix whose elements $\alpha_{\mathrm{r},n}$ $(n = 1, \ldots, \rho)$ are given by

$$\alpha_{\mathrm{r},n} = \frac{1}{\sqrt{\alpha_{\mathrm{sr}}^2 \left\|\mathbf{h}_{\mathrm{r},n}\right\|_{\mathrm{F}}^2 + \sigma^2}}, \tag{2.16}$$

where $\mathbf{h}_{\mathrm{r},n}$ represents the nth row of matrix $\mathbf{R}$.

The average noise power will therefore be reduced by a factor ρ/n_r, which turns out to be interesting in the scenario of unit-rank source-relay MIMO channel.

2.4.4 Complexity Benchmark

Relaying strategies present different computational complexity levels. Without accounting for channel estimation operations and based on [53], Table 2.1 provides a short benchmark of the floating point operations required by some classes of relays in the scenario of a $n_\mathrm{r} \times n_\mathrm{s}$ MIMO block fading relay channel with T symbols packet length. In this context, PF relaying presents an interesting trade-off between performance and complexity.

Relaying Scheme	Type	Complexity
AF (blind)	Signal-level	$n_\mathrm{r}T$
AF (CSI-assisted)	Signal-level	$(4n_\mathrm{s}+3)+n_\mathrm{r}T$
PF	Signal-level	$3n_\mathrm{s}^2(n_\mathrm{r}-n_\mathrm{s}/3)+(2n_\mathrm{r}^2-n_\mathrm{r})$ $+\rho(4n_\mathrm{s}-2\rho+3)+n_\mathrm{r}T$
DetF (MMSE-based)	Symbol-level	$12n_\mathrm{s}^3+n_\mathrm{s}^2(8n_\mathrm{r}+2)+3n_\mathrm{s}n_\mathrm{r}-n_\mathrm{r}+\lvert\mathcal{A}\rvert\, n_\mathrm{r}T$

Table 2.1: Computational complexity of relaying schemes.

2.5 Performance Metrics

To analytically characterize the diversity and multiplexing capabilities of any communication system, we resort to the outage probability and the ergodic capacity metrics.

2.5.1 Outage Probability

In noise-limited transmissions, quality of service (QoS)[2] is ensured by keeping the instantaneous end-to-end SNR above a certain threshold γ_th. Otherwise, the QoS is not respected and the service is said to be in outage. The probability of such an event is given by

$$P_\mathrm{out} \triangleq \Pr\left[\gamma < \gamma_\mathrm{th}\right], \tag{2.17}$$

which is actually the cumulative distribution function (CDF) of SNR γ.

2.5.2 Ergodic Capacity

A wireless channel is referred to as *ergodic* if the transmitted data packet (or codeword) is long enough to experience essentially all the states of the channel [59]. This situation occurs when the packet duration T is very large compared to the channel coherence time T_c. In that case, the fading statistical properties (e.g., mean and variance) can be efficiently inferred from the temporal samples.

An appropriate metric for this class of channels is the ergodic capacity, which is the average maximum transmission rate [3] supported by the channel while ensuring a vanishing error

[2] The notion of QoS here mainly refers to a target throughput with a certain block error rate (BLER).
[3] The maximum is reached in the case of a Gaussian input alphabet.

probability. This capacity is a function of the instantaneous channel SNR γ, i.e.,

$$\overline{C} \triangleq \mathrm{E}\left[\log_2\left(1+\gamma\right)\right]. \tag{2.18}$$

In practical link adaptation algorithms, such as transmit rate control, the ergodicity principle enables the receiver to estimate the average capacity by replacing the mathematical expectation in (2.18) by the long-term time average, i.e.,

$$\overline{C} \approx \frac{1}{T}\sum_{t=0}^{T-1}\log_2\left(1+\gamma_t\right). \tag{2.19}$$

2.6 Conclusions

In this chapter, we have revisited the main aspects of MIMO-ARQ relay systems that will be invoked throughout this thesis; we have shown that the three techniques are complementary in terms of multiplexing and diversity. Hence, a high multiplexing order MIMO transmission decreases the diversity it can afford, and therefore requires the activation of hybrid-ARQ to enhance it. The performance of the latter is, however, degraded in slow fading environments, which prompts the adoption of relaying nodes to deliver diversity in a cooperative fashion. These underlined capabilities can altogether be quantified using metrics such as average throughput, outage probability and ergodic capacity.

In the next chapters, we will take you in a journey where this complementarity between MIMO, H-ARQ and relaying becomes more fruitful through their joint design...

Chapter 3

Project-and-Forward Relaying over Dual-Hop MIMO Channels: Incentives and Theoretical Performance

3.1 Introduction

Multi-hop transmission has been widely used in low power sensor networks such as IEEE 802.15.4x, before being abandoned by the industry due to coverage limitations in mass deployments [60]. However, in mobile networks usually featuring high transmit powers, relays are rather deployed according to a simple dual-hop architecture where a source is connected to a destination through one relay node [61].

In amplify-and-forward dual-hop systems, the relay scales not only the signal—with either a fixed or CSI-dependent gain—but also the additive Gaussian noise; from the source to the destination, the noise propagates and is amplified to the extent that the end-to-end SNR and consequently the performance are quickly degraded. It is a detrimental effect that becomes even worse when the number of relay antennas increases, as the corresponding noises accumulate at each of the destination receive antennas. To sidestep this limitation, a variant of AF relaying, termed project-and-forward (PF), has been introduced in [15]; it consists on optimizing the number of relay active antennas by forwarding the degrees-of-freedom (DoF) of the received signal—yield by an orthogonal projection—instead of the signal itself; a few relay antennas as the rank of the source-relay MIMO channel are used, which dramatically reduces the noise accumulation at the destination and improves the end-to-end SNR [44]. Nonetheless, does practical radio conditions make PF a viable scheme?

Besides the independent Gaussian MIMO channel, where the channel rank is equal to the minimum of transmit and receive antennas; an inherent phenomenon in MIMO systems is the pinhole condition [62–64] that may arise when either the scattering radii, i.e., the radius of the cluster of scatterers, is small or the transmit-receive range is large. In that case, the fading energy travels through a very thin air pipe, called pinhole (or keyhole), causing the MIMO channel matrix to be rank-deficient [52], and the capacity to reduce to that of a single-input single-output (SISO) link [51]. As dictated by radio engineering rules, the relay is practically located at the cell-edge areas where coverage holes and low spectral-efficiencies are often reported [4]. In such a scenario, the range of the source-relay hop in the downlink direction is large to the extent that the corresponding MIMO channel rank drops notably, leading thereby to the so-called "pinhole" condition [52]. Conversely, the relay-destination channel is generally supposed to be full-rank, mainly due to the short distance between both nodes, as well as the rich scattering brought by obstructing structures (e.g., buildings) in both outdoor and outdoor-to-indoor environments [65]. Altogether then, PF relaying presents an interesting alternative to AF mode in rank deficient multi-antenna links, as well as when the relay is endowed with more antennas than the source; situations where the projection can optimize the relay antennas usage, and thereby alleviate the noise propagation.

While the authors have studied in [15] the diversity multiplexing trade-off (DMT) of AF and PF schemes over Rayleigh product links, we present in this chapter a novel end-to-end performance analysis of dual-hop PF systems over a realistic mixed MIMO-pinhole/Rayleigh relay channel. We derive analytical expressions for the probability density functions (PDFs) of both the first hop and the end-to-end SNRs, which are then used to infer the outage probability as well as the ergodic capacity whose formula is provided in terms of the bivariate Meijer G-function [66]. The asymptotic behavior is then derived using the residue theory, which yields important recommendations regarding the design of efficient PF-based relaying architectures. While the Meijer G-function [67, Eq. (9.301)] is a built-in routine in prevalent computing softwares such as MATHEMATICA, MATLAB and MAPLE, the bivariate Meijer G-function, to the best of our knowledge, is only available on MATHEMATICA with no general contour definition [68]. We therefore develop a fast MATLAB code with automated integration contour for this generalized function as a secondary contribution.

The remainder of the chapter is organized as follows. In Section 3.2, we introduce the pinhole/full-rank MIMO channel model. We also present the architecture of the project-and-forward relaying function. In Section 3.3, we first derive the PDFs of the SNRs, then we analyze the performance of the system in terms of the outage probability and the ergodic capacity. Section 3.4 addresses the asymptotic behavior to show the effect of the considered system parameters on the performance. Numerical results are provided in Section 3.5. The chapter is concluded in Section 3.6.

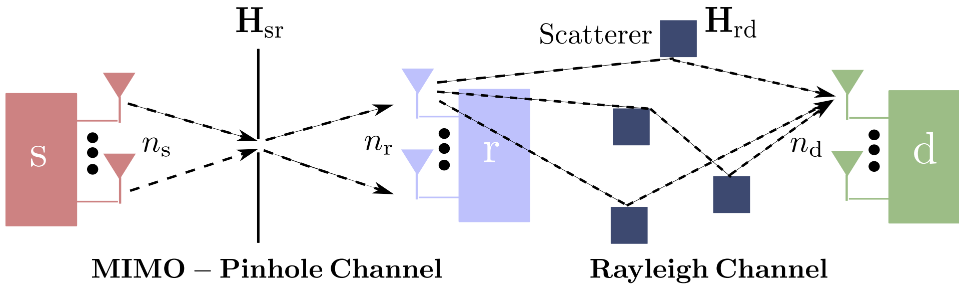

Figure 3.1: Mixed MIMO-pinhole and Rayleigh relay channel.

3.2 System Model

3.2.1 Mixed MIMO-Pinhole and Rayleigh Channel

We consider a dual-hop multi-antenna cooperative inband [1] transmission [3] where a n_{s}-antennas source is connected to a n_{d}-antennas destination through a n_{r}-antennas relay ($n_{\mathrm{s}}, n_{\mathrm{r}} > 1$). The cooperation is assumed *half-duplex*, spanning two consecutive slots where the source and the relay transmissions are orthogonal in time. The communication between each couple of nodes, $\epsilon \in \{\mathrm{s}, \mathrm{r}\}$ and $\epsilon' \in \{\mathrm{r}, \mathrm{d}\}$, takes place over an independent wireless link $\epsilon - \epsilon'$ experiencing an average propagation loss $\alpha_{\epsilon\epsilon'}$ and a small scale fading effect represented by a channel matrix $\mathbf{H}_{\epsilon\epsilon'} \in \mathbb{C}^{n_{\epsilon'} \times n_{\epsilon}}$, where

- $\mathbf{H}_{\mathrm{sr}}$ is supposed to be a pinhole channel. It is modeled as an outer product of two independent and uncorrelated Rayleigh fading vectors $\mathbf{g}_{\mathrm{s}} \in \mathbb{C}^{n_{\mathrm{s}} \times 1}$ and $\mathbf{g}_{\mathrm{r}} \in \mathbb{C}^{n_{\mathrm{r}} \times 1}$ [52], i.e.,

$$\mathbf{H}_{\mathrm{sr}} = \mathbf{g}_{\mathrm{r}} \mathbf{g}_{\mathrm{s}}^{\mathrm{H}}. \tag{3.1}$$

- $\mathbf{H}_{\mathrm{rd}}$ is a full-rank independent standard complex Gaussian matrix. Its entries are consequently Rayleigh distributed.

Both relay and destination received signals are corrupted by additive white Gaussian noise (AWGN) vectors $\mathbf{w}_{\mathrm{r}} \sim \mathcal{N}\left(\mathbf{0}_{n_{\mathrm{r}} \times 1}, \sigma^2 \mathbf{I}_{n_{\mathrm{r}}}\right)$ and $\mathbf{w}_{\mathrm{d}} \sim \mathcal{N}\left(\mathbf{0}_{n_{\mathrm{d}} \times 1}, \sigma^2 \mathbf{I}_{n_{\mathrm{d}}}\right)$, respectively. The corresponding average SNRs per hop are $\overline{\gamma}_{\mathrm{sr}} = \alpha_{\mathrm{sr}}^2 / \sigma^2$ and $\overline{\gamma}_{\mathrm{rd}} = \alpha_{\mathrm{rd}}^2 / \sigma^2$.

3.2.2 Project-and-Forward Relaying

Let $\mathbf{s} \in \mathbb{C}^{n_{\mathrm{s}} \times 1}$ denote a unitary precoded symbol vector transmitted by the source node. The $\mathrm{s} - \mathrm{r}$ communication model can be accordingly expressed as,

$$\mathbf{y}_{\mathrm{r}} = \alpha_{\mathrm{sr}} \mathbf{H}_{\mathrm{sr}} \mathbf{s} + \mathbf{w}_{\mathrm{r}} \in \mathbb{C}^{n_{\mathrm{r}} \times 1}. \tag{3.2}$$

[1]Contray to the outband mode, in inband mode both the source and the relay operate over the same frequency channel.

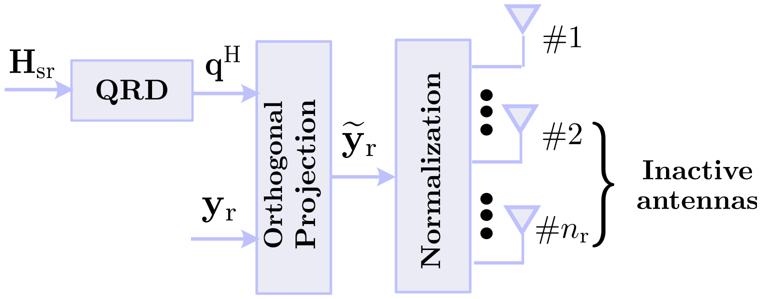

Figure 3.2: Project-and-Forward relaying building blocks.

The key idea of PF relaying is to extract and forward the DoFs of the received signal vector $\mathbf{y}_{\mathrm{r}}$ via a QR-based orthogonal projection [53]. Given that $\mathbf{H}_{\mathrm{sr}}$ is a pinhole channel, a single degree of freedom will be conveyed by the relay to be used in the estimation of the transmit vector $\mathbf{s}$ at the destination.

Let $\mathbf{H}_{\mathrm{sr}} = \mathbf{QR}$ denote the QR decomposition of $\mathbf{H}_{\mathrm{sr}}$, where $\mathbf{Q} \in \mathbb{C}^{n_{\mathrm{r}} \times n_{\mathrm{r}}}$ is a unitary matrix with $\mathbf{q} \in \mathbb{C}^{n_{\mathrm{r}} \times 1}$ standing for its first column vector, and $\mathbf{R} \in \mathbb{C}^{n_{\mathrm{r}} \times n_{\mathrm{s}}}$ is an upper triangular matrix whose $(n_{\mathrm{r}} - 1)$ bottom rows consist entirely of zeros, i.e.,

$$\mathbf{R} = \begin{bmatrix} \mathbf{h}_{\mathrm{r}} \\ \mathbf{0}_{(n_{\mathrm{r}}-1)\times n_{\mathrm{s}}} \end{bmatrix}. \tag{3.3}$$

The DoF $\hat{y}_{\mathrm{r}}$ is first obtained as

$$\widetilde{y}_{\mathrm{r}} = \mathbf{q}^{\mathrm{H}}\mathbf{y}_{\mathrm{r}} = \alpha_{\mathrm{sr}}\mathbf{h}_{\mathrm{r}}\mathbf{s} + \underbrace{\mathbf{q}^{\mathrm{H}}\mathbf{w}_{\mathrm{r}}}_{\widetilde{w}_{\mathrm{r}}} \in \mathbb{C}, \tag{3.4}$$

and is then normalized with a scaling factor $\alpha_{\mathrm{r}} = \left(\alpha_{\mathrm{sr}}^2 \left\|\mathbf{h}_{\mathrm{r}}\right\|_{\mathrm{F}}^2 + \sigma^2\right)^{-1/2}$ before being forwarded to the destination using only one relay antenna. Note that the statistical properties of noise term $\widetilde{w}_{\mathrm{r}}$ are maintained since $\mathbf{q}$ is a unitary vector.

To show the pure gain of PF scheme, relay antenna selection as well as receive diversity at the destination are not targeted by our analysis. The $\mathrm{r}-\mathrm{d}$ link is therefore a SISO Rayleigh channel whose fading coefficient h_{rd} is rid of antenna index, resulting in a simpler communication model as

$$y_{\mathrm{d}} = \alpha_{\mathrm{rd}}\alpha_{\mathrm{r}}h_{\mathrm{rd}}\widetilde{y}_{\mathrm{r}} + w_{\mathrm{d}} \in \mathbb{C}. \tag{3.5}$$

3.3 Analytical Performance Analysis

To assess the performance of PF system, we start this section by unveiling the probability density functions of the conditional SNRs. We then derive analytical expressions of the outage probability, the end-to-end SNR PDF and the ergodic capacity.[2]

3.3.1 Instantaneous SNRs Characterization

By invoking communication models (3.4) and (3.5), end-to-end SNR of the PF system can be expressed similarly to a dual-hop AF transmission [32], i.e.,

$$\gamma_{\mathrm{srd}} = \frac{\gamma_{\mathrm{sr}}\gamma_{\mathrm{rd}}}{\gamma_{\mathrm{sr}} + \gamma_{\mathrm{rd}} + 1}, \tag{3.6}$$

where the conditional terms $\gamma_{\mathrm{sr}} = \overline{\gamma}_{\mathrm{sr}} \left\|\mathbf{h}_{\mathrm{r}}\right\|_{\mathrm{F}}^2$ and $\gamma_{\mathrm{rd}} = \overline{\gamma}_{\mathrm{rd}} \left|h_{\mathrm{rd}}\right|^2$ represent the relay post-processing SNR and the destination receive SNR, respectively. Given that $\mathrm{r}-\mathrm{d}$ link is experiencing Rayleigh flat fading, γ_{rd} is exponentially distributed with the probability density function written as

$$f_{\gamma_{\mathrm{rd}}}(\gamma) = \frac{1}{\overline{\gamma}_{\mathrm{rd}}} \exp\left(-\frac{\gamma}{\overline{\gamma}_{\mathrm{rd}}}\right). \tag{3.7}$$

The PDF of SNR γ_{sr} is indirect, and is therefore given by the following lemma,

Lemma 3.3.1. *The* $\mathrm{s}-\mathrm{r}$ *instantaneous SNR* γ_{sr} *follows a distribution* $f_{\gamma_{\mathrm{sr}}}$ *expressed as*

$$f_{\gamma_{\mathrm{sr}}}(\gamma) = \frac{2}{\Gamma(n_{\mathrm{s}})\Gamma(n_{\mathrm{r}})\overline{\gamma}_{\mathrm{sr}}} \left(\frac{\gamma}{\overline{\gamma}_{\mathrm{sr}}}\right)^{\frac{n_{\mathrm{s}}+n_{\mathrm{r}}}{2}-1} K_{n_{\mathrm{r}}-n_{\mathrm{s}}}\left(2\sqrt{\frac{\gamma}{\overline{\gamma}_{\mathrm{sr}}}}\right). \tag{3.8}$$

Proof. To evaluate the PDF of γ_{sr}, we consider the equality $\mathbf{q}\mathbf{h}_{\mathrm{r}} = \mathbf{H}_{\mathrm{sr}} = \mathbf{g}_{\mathrm{r}}\mathbf{g}_{\mathrm{s}}^{\mathrm{H}}$ that stems from the aforementioned QR decomposition. Given that $\mathbf{q}$ is unitary, we infer that $\left\|\mathbf{h}_{\mathrm{r}}\right\|_{\mathrm{F}} = \left\|\mathbf{g}_{\mathrm{r}}\right\|_{\mathrm{F}} \left\|\mathbf{g}_{\mathrm{s}}\right\|_{\mathrm{F}}$, and due to the statistical independence between $\mathbf{g}_{\mathrm{s}}$ and $\mathbf{g}_{\mathrm{r}}$, the PDF of $\left\|\mathbf{h}_{\mathrm{r}}\right\|_{\mathrm{F}}^2$ can be shown to be

$$f_{\left\|\mathbf{h}_{\mathrm{r}}\right\|_{\mathrm{F}}^2}(\gamma) = \int_0^{+\infty} \frac{1}{\gamma_{\mathrm{r}}} f_{\left\|\mathbf{g}_{\mathrm{s}}\right\|_{\mathrm{F}}^2}\left(\frac{\gamma}{\gamma_{\mathrm{r}}}\right) f_{\left\|\mathbf{g}_{\mathrm{r}}\right\|_{\mathrm{F}}^2}(\gamma_{\mathrm{r}}) \mathrm{d}\gamma_{\mathrm{r}}. \tag{3.9}$$

By recalling that both $\mathbf{g}_{\mathrm{s}}$ and $\mathbf{g}_{\mathrm{r}}$ are Rayleigh fading vectors, we have $2\left\|\mathbf{g}_{\epsilon}\right\|_{\mathrm{F}}^2 \sim \mathcal{X}_{2n_{\epsilon}}^2, \epsilon \in \{\mathrm{s}, \mathrm{r}\}$. After some algebraic manipulations and by making use of (3.9) and [67, Eq. (3.471.9)], we obtain the PDF of γ_{sr} as shown in (3.8). ∎

For the sake of simplicity, the following notation will be used in the remainder of this chapter,

$$\begin{cases} \mu = \frac{n_{\mathrm{s}}+n_{\mathrm{r}}}{2} - 1, \\ \nu = n_{\mathrm{r}} - n_{\mathrm{s}}. \end{cases} \tag{3.10}$$

[2] In non-ergodic, i.e., block fading quasi-static channels, the outage probability is a meaningful measure that provides a lower bound on the block error probability. It is defined as the probability that the mutual information, as a function of the channel realization and the average SNR, is below the transmission rate [69].

3.3.2 Outage Probability

The outage probability in our relaying setup is expressed according to the definition (2.17) as

$$P_{\text{out}} = \Pr\left[\gamma_{\text{srd}} < \gamma_{\text{th}}\right] = \Pr\left[\frac{\gamma_{\text{sr}}\gamma_{\text{rd}}}{\gamma_{\text{sr}} + \gamma_{\text{rd}} + 1} < \gamma_{\text{th}}\right]. \tag{3.11}$$

To derive the corresponding analytical expression , let us prove the following lemma.

Lemma 3.3.2. *The outage probability can be expressed in terms of the PDF of γ_{sr} and the complementary CDF (CCDF) of γ_{rd} as follows,*

$$P_{\text{out}}\left(\gamma_{\text{th}}\right) = 1 - \int_0^{+\infty} \widetilde{F}_{\gamma_{\text{rd}}}\left[\gamma_{\text{th}} + \frac{\gamma_{\text{th}}^2 + \gamma_{\text{th}}}{\gamma}\right] f_{\gamma_{\text{sr}}}\left(\gamma + \gamma_{th}\right) \mathrm{d}\gamma. \tag{3.12}$$

Proof. Marginalization of (3.11) over γ_{sr} yields

$$\begin{aligned}
P_{\text{out}}\left(\gamma_{\text{th}}\right) &= \int_0^{+\infty} \Pr\left[\gamma_{\text{rd}}(\gamma - \gamma_{\text{th}}) < \gamma_{\text{th}}(\gamma + 1)\right] f_{\gamma_{\text{sr}}}\left(\gamma\right) \mathrm{d}\gamma \\
&= \int_0^{\gamma_{\text{th}}} \Pr\left[\gamma_{\text{rd}} > \frac{\gamma_{\text{th}}(\gamma + 1)}{\gamma - \gamma_{\text{th}}}\right] f_{\gamma_{\text{sr}}}\left(\gamma\right) \mathrm{d}\gamma + \int_{\gamma_{\text{th}}}^{+\infty} \Pr\left[\gamma_{\text{rd}} < \frac{\gamma_{\text{th}}(\gamma + 1)}{\gamma - \gamma_{\text{th}}}\right] f_{\gamma_{\text{sr}}}\left(\gamma\right) \mathrm{d}\gamma \\
&\overset{(1)}{=} \int_0^{\gamma_{\text{th}}} f_{\gamma_{\text{sr}}}\left(\gamma\right) \mathrm{d}\gamma + \int_{\gamma_{\text{th}}}^{+\infty} \Pr\left[\gamma_{\text{rd}} < \frac{\gamma_{\text{th}}(\gamma + 1)}{\gamma - \gamma_{\text{th}}}\right] f_{\gamma_{\text{sr}}}\left(\gamma\right) \mathrm{d}\gamma \\
&= \int_0^{+\infty} f_{\gamma_{\text{sr}}}\left(\gamma\right) \mathrm{d}\gamma - \int_{\gamma_{\text{th}}}^{+\infty} \left[1 - F_{\gamma_{\text{rd}}}\left(\frac{\gamma_{\text{th}}(\gamma + 1)}{\gamma - \gamma_{\text{th}}}\right)\right] f_{\gamma_{\text{sr}}}\left(\gamma\right) \mathrm{d}\gamma \\
&\overset{(2)}{=} 1 - \int_0^{+\infty} \widetilde{F}_{\gamma_{\text{rd}}}\left(\gamma_{\text{th}} + \frac{\gamma_{\text{th}}^2 + \gamma_{\text{th}}}{\gamma}\right) f_{\gamma_{\text{sr}}}\left(\gamma + \gamma_{\text{th}}\right) \mathrm{d}\gamma,
\end{aligned}$$

where (1) stems from the fact that $\Pr\left[\gamma_{\text{rd}} > \frac{\gamma_{\text{th}}(\gamma+1)}{\gamma - \gamma_{\text{th}}}\right] = 1$ holds since $\gamma - \gamma_{\text{th}} < 0$, and (2) follows from the equality $\int_0^{+\infty} f_{\gamma_{\text{sr}}}\left(\gamma\right) \mathrm{d}\gamma = 1$ given that $f_{\gamma_{\text{sr}}}$ is a PDF, and from the variable change $\gamma - \gamma_{\text{th}} \to \gamma$.

■

By recalling that the CCDF of γ_{rd} is $\exp\left(-\gamma/\bar{\gamma}_{\text{rd}}\right)$, and invoking lemmas 3.3.1 and 3.3.2, as well as making the change $x = \left(\frac{\gamma}{\gamma_{\text{th}}}\right) + 1$, we infer that

$$\begin{aligned}
P_{\text{out}}\left(\gamma_{\text{th}}\right) = 1 - 2\left(\frac{\gamma_{\text{th}}}{\bar{\gamma}_{\text{sr}}}\right)^{\mu+1} & \frac{e^{-\frac{\gamma_{\text{th}}}{\bar{\gamma}_{\text{rd}}}}}{\Gamma(n_{\text{s}})\Gamma(n_{\text{r}})} \\
& \times \underbrace{\int_1^{+\infty} x^{\mu} \exp\left(-\frac{\gamma_{\text{th}} + 1}{\bar{\gamma}_{\text{rd}}(x-1)}\right) K_{\nu}\left(2\sqrt{\frac{\gamma_{\text{th}}}{\bar{\gamma}_{\text{sr}}}x}\right) \mathrm{d}x}_{\mathcal{I}}.
\end{aligned} \tag{3.13}$$

A Taylor expansion of the exponential term $\exp\left(-\frac{\gamma_{\text{th}}+1}{\bar{\gamma}_{\text{rd}}(x-1)}\right)$ leads to an explicit formulation of $\mathcal{I}$ as

$$\mathcal{I} = \sum_{n=0}^{+\infty} \frac{(-1)^n}{n!} \left(\frac{\gamma_{\mathrm{th}}+1}{\overline{\gamma}_{\mathrm{rd}}}\right)^n \sum_{m=0}^{+\infty} \frac{\theta_{n,m}}{m!} \int_1^{+\infty} x^{\mu-n-m} K_\nu \left(2\sqrt{\frac{\gamma_{\mathrm{th}}}{\overline{\gamma}_{\mathrm{sr}}} x}\right) \mathrm{d}x, \tag{3.14}$$

where

$$\begin{cases} \theta_{n,m} = \frac{\Gamma(n+m)}{\Gamma(n)}, \\ \theta_{0,0} = 1. \end{cases} \tag{3.15}$$

Then, by combining (3.13) and (3.14) and using [67, Eq. (6.592.4)], an analytical expression of P_{out} is obtained after some simplifications as

$$P_{\mathrm{out}}(\gamma_{\mathrm{th}}) = 1 - \frac{e^{-\frac{\gamma_{th}}{\overline{\gamma}_{\mathrm{rd}}}}}{\Gamma(n_{\mathrm{s}})\Gamma(n_{\mathrm{r}})} \sum_{n=0}^{+\infty} \frac{(-1)^n}{n!} \left(\frac{\gamma_{\mathrm{th}}+1}{\overline{\gamma}_{\mathrm{rd}}}\right)^n \sum_{m=0}^{+\infty} \frac{\theta_{n,m}}{m!} \left(\frac{\gamma_{\mathrm{th}}}{\overline{\gamma}_{\mathrm{sr}}}\right)^{n+m+1} \times \mathrm{G}_{1,3}^{3,0}\left(\frac{\gamma_{\mathrm{th}}}{\overline{\gamma}_{\mathrm{sr}}} \middle| \begin{matrix} 0 \\ -1, \frac{\nu}{2}+\mu-n-m, -\frac{\nu}{2}+\mu-n-m \end{matrix}\right). \tag{3.16}$$

As detailed afterward, the infinite sums can be efficiently replaced by low order finite ones, while obtaining an exact match with Monte-Carlo simulations.

3.3.3 Probability Density Function

The PDF of the end-to-end SNR γ_{srd} is computed by first expanding the power $(\gamma_{\mathrm{th}}+1)^n$ in (3.16) into a finite sum using the Binomial theorem. The resulting expression is then differentiated with respect to γ_{th} via [70, Eq. 5], leading thereby to the analytical form

$$f_{\gamma_{\mathrm{srd}}}(\gamma) = \frac{e^{-\frac{\gamma}{\overline{\gamma}_{\mathrm{rd}}}}}{\Gamma(n_{\mathrm{s}})\Gamma(n_{\mathrm{r}})} \sum_{n=0}^{+\infty} \frac{(-1/\overline{\gamma}_{\mathrm{rd}})^n}{n!} \sum_{i=0}^{n} \binom{n}{i} \sum_{m=0}^{+\infty} \frac{\theta_{n,m}}{m!} \frac{\gamma^{n+m+i}}{\overline{\gamma}_{\mathrm{sr}}^{n+m+1}} \times \left[\frac{\gamma}{\overline{\gamma}_{\mathrm{rd}}} \cdot \mathrm{G}_{1,3}^{3,0}\left(\frac{\gamma}{\overline{\gamma}_{\mathrm{sr}}} \middle| \begin{matrix} 0 \\ -1, \frac{\nu}{2}+\mu-n-m, -\frac{\nu}{2}+\mu-n-m \end{matrix}\right) - \mathrm{G}_{2,4}^{3,1}\left(\frac{\gamma}{\overline{\gamma}_{\mathrm{sr}}} \middle| \begin{matrix} -(n+m+i+1), 0 \\ -1, \frac{\nu}{2}+\mu-n-m, -\frac{\nu}{2}+\mu-n-m, -(n+m+i) \end{matrix}\right)\right]. \tag{3.17}$$

3.3.4 Ergodic Capacity

In the case of the dual-hop PF system under consideration, the ergodic capacity can be expressed according to (2.18) as

$$\overline{C} = \frac{1}{2} \int_0^{+\infty} \log_2(1+\gamma) f_{\gamma_{\mathrm{srd}}}(\gamma) \mathrm{d}\gamma, \tag{3.18}$$

where the 1/2 distortion factor stems from the fact that one channel use (c.u.) of the end-to-end relay channel (3.5) corresponds to two temporal c.u. in a dual-hop transmission.

Combining (3.17) and Meijer G-function representations of the elementary functions [71, Eq. 11], $\gamma^p e^{-\frac{\gamma}{\overline{\gamma}_{\mathrm{rd}}}} = \overline{\gamma}_{\mathrm{rd}}^p \mathrm{G}_{0,1}^{1,0}\left(\frac{\gamma}{\overline{\gamma}_{\mathrm{rd}}}\middle| \begin{matrix} - \\ p \end{matrix}\right)$ and $\ln(1+\gamma) = \mathrm{G}_{2,2}^{1,2}\left(\gamma \middle| \begin{matrix} 1,1 \\ 1,0 \end{matrix}\right)$, the ergodic capacity can be rewritten in a further explicit form as

$$\overline{C} = \frac{1}{2\ln(2)\,\Gamma(n_{\mathrm{s}})\Gamma(n_{\mathrm{r}})} \sum_{k=0}^{+\infty} \frac{(-1/\overline{\gamma}_{\mathrm{rd}})^n}{n!} \sum_{i=0}^{n} \binom{n}{i} \sum_{m=0}^{+\infty} \frac{\theta_{n,m}}{m!\overline{\gamma}_{\mathrm{sr}}^{n+m+1}} \left(\mathcal{I}_{n,m,i} - \mathcal{J}_{n,m,i}\right), \tag{3.19}$$

where $\mathcal{I}_{n,m,i}$ and $\mathcal{J}_{n,m,i}$ are given by

$$\mathcal{I}_{n,m,i} = \overline{\gamma}_{\mathrm{rd}}^{n+m+i} \int_0^{+\infty} \mathrm{G}_{0,1}^{1,0}\left(\frac{\gamma}{\overline{\gamma}_{\mathrm{rd}}}\middle| \begin{matrix} - \\ n+m+i+1 \end{matrix}\right) \mathrm{G}_{2,2}^{1,2}\left(\gamma \middle| \begin{matrix} 1,1 \\ 1,0 \end{matrix}\right) \times \mathrm{G}_{1,3}^{3,0}\left(\frac{\gamma}{\overline{\gamma}_{\mathrm{sr}}}\middle| \begin{matrix} 0 \\ -1, \frac{\nu}{2}+\alpha-n-m, -\frac{\nu}{2}+\alpha-n-m \end{matrix}\right) \mathrm{d}\gamma, \tag{3.20}$$

and

$$\mathcal{J}_{n,m,i} = \overline{\gamma}_{\mathrm{rd}}^{n+m+i} \int_0^{+\infty} \mathrm{G}_{0,1}^{1,0}\left(\frac{\gamma}{\overline{\gamma}_{\mathrm{rd}}}\middle| \begin{matrix} - \\ n+m+i \end{matrix}\right) \mathrm{G}_{2,2}^{1,2}\left(\gamma \middle| \begin{matrix} 1,1 \\ 1,0 \end{matrix}\right) \times \mathrm{G}_{1,3}^{3,0}\left(\frac{\gamma}{\overline{\gamma}_{\mathrm{sr}}}\middle| \begin{matrix} (n+m+i+1), 0 \\ -1, \frac{\nu}{2}+\alpha-n-m, -\frac{\nu}{2}+\alpha-n-m, -(n+m+i) \end{matrix}\right) \mathrm{d}\gamma, \tag{3.21}$$

and can both be expressed in terms of the bivariate Meijer G-function using the integration identity [72, Eq. 12]. The ergodic capacity is consequently expressed as

$$\begin{aligned}\overline{C} = {} & \frac{1}{2\ln(2)\,\Gamma(n_{\mathrm{s}})\Gamma(n_{\mathrm{r}})} \sum_{n=0}^{+\infty} \frac{(-1)^n}{n!} \sum_{i=0}^{n} \binom{n}{i} \sum_{m=0}^{+\infty} \frac{\theta_{n,m}}{m!} \frac{\overline{\gamma}_{\mathrm{rd}}^{m+i+1}}{\overline{\gamma}_{\mathrm{sr}}^{n+m+1}} \\ & \times \Bigg[\mathrm{G}_{1,0:2,2:1,3}^{1,0:1,2:3,0}\left(\overline{\gamma}_{\mathrm{rd}}, \frac{\overline{\gamma}_{\mathrm{rd}}}{\overline{\gamma}_{\mathrm{sr}}} \middle| \begin{matrix} n+m+i+2 \\ - \end{matrix} \middle| \begin{matrix} 1,1 \\ 1,0 \end{matrix} \middle| \begin{matrix} 0 \\ -1, \frac{\nu}{2}+\mu-n-m, -\frac{\nu}{2}+\mu-n-m \end{matrix}\right) \\ & - \mathrm{G}_{1,0:2,2:2,4}^{1,0:1,2:3,1}\left(\overline{\gamma}_{\mathrm{rd}}, \frac{\overline{\gamma}_{\mathrm{rd}}}{\overline{\gamma}_{\mathrm{sr}}} \middle| \begin{matrix} n+m+i+1 \\ - \end{matrix} \middle| \begin{matrix} 1,1 \\ 1,0 \end{matrix} \middle| \begin{matrix} -(n+m+i+1), 0 \\ -1, \frac{\nu}{2}+\mu-n-m, -\frac{\nu}{2}+\mu-n-m, -(n+m+i) \end{matrix}\right) \Bigg]. \end{aligned} \tag{3.22}$$

3.4 Asymptotic Behavior

To highlight the effect of channel parameters on both the outage probability and the ergodic capacity, we study their asymptotic behaviors. Invoking [73, Theorem 1.7 and Theorem 1.11], expansions of the Mellin-Barnes integrals involved in the Meijer-G and bivariate Meijer-G functions can be derived by evaluating the residue of the corresponding integrands at the pole

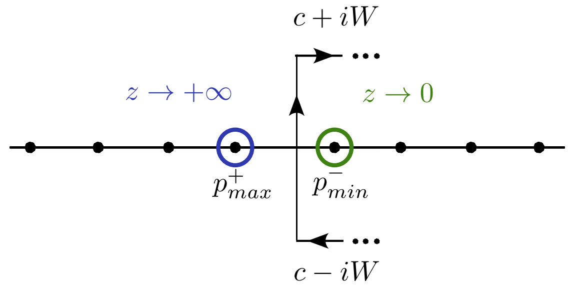

Figure 3.3: Complex contour of the Mellin-Barnes integral. W is set to a large value.

closest to the contour; the minimum pole on the right p^-_{min} for small Meijer-G arguments and the maximum pole on the left p^+_{max} for large ones, as depicted in Fig. 3.3. Moreover, the *Inside-Outside* theorem [74] states that the obtained result is further multiplied by -1 in case of clockwise-oriented contour (i.e., for small arguments).

3.4.1 Asymptotic Outage Probability

We study the asymptotic behavior of outage probability at low SNR threshold $\gamma_{\rm th}$. By keeping low order terms in (3.16), i.e., $n+m \leq 1$, and given that $\alpha + \nu/2 = n_{\rm r} - 1 \geq 1$ and $\alpha - \nu/2 = n_{\rm s} - 1 \geq 1$, we have $\pm\nu/2 + \alpha - n - m \geq 0 > -1$, and consequently, we evaluate the residue at -1. Since the contour is clockwise oriented in that case, the residue is multiplied by -1,

$$\begin{aligned}
&\mathrm{G}^{3,0}_{1,3}\left(\frac{\gamma_{\rm th}}{\overline{\gamma}_{\rm sr}}\middle| \begin{matrix} 0 \\ -1, \frac{\nu}{2}+\mu-n-m, -\frac{\nu}{2}+\mu-n-m \end{matrix}\right) \\
&= \frac{1}{2\pi j}\int_C \underbrace{\frac{\Gamma(-1-s)\,\Gamma\left(\frac{\nu}{2}+\mu-n-m-s\right)\Gamma\left(-\frac{\nu}{2}+\mu-n-m-s\right)}{\Gamma(-s)}\left(\frac{\gamma_{\rm th}}{\overline{\gamma}_{\rm sr}}\right)^s}_{g_0(s)}\mathrm{d}s \qquad (3.23) \\
&\approx -\mathrm{Res}\left[g_0(s), -1\right] = -\lim_{s\to -1}(s+1)\,g_0(s) \\
&= \Gamma\left(\frac{\nu}{2}+\mu-n-m+1\right)\Gamma\left(-\frac{\nu}{2}+\mu-n-m+1\right)\left(\frac{\gamma_{\rm th}}{\overline{\gamma}_{\rm sr}}\right)^{-1}. \qquad (3.24)
\end{aligned}$$

Applying (3.23) in (3.16) and replacing the exponential term by its first order approximation near zero, i.e., $\exp\left(-\frac{\gamma_{\rm th}}{\overline{\gamma}_{\rm rd}}\right) \approx 1 - \frac{\gamma_{\rm th}}{\overline{\gamma}_{\rm rd}}$, leads to

$$\begin{aligned}
P_{\rm out}(\gamma_{\rm th}) \overset{(small\,\gamma_{\rm th})}{\approx} & 1 - \frac{1}{\Gamma(n_{\rm s})\Gamma(n_{\rm r})}\sum_{n=0}^{+\infty}\frac{(-1)^n}{n!}\left(\frac{\gamma_{\rm th}+1}{\overline{\gamma}_{\rm rd}}\right)^n \sum_{m=0}^{+\infty}\frac{\theta_{n,m}}{m!} \\
& \times\Gamma\left(\frac{\nu}{2}+\mu-n-m+1\right)\Gamma\left(-\frac{\nu}{2}+\mu-n-m+1\right)\left(\frac{\gamma_{\rm th}}{\overline{\gamma}_{\rm sr}}\right)^{n+m}\left(1-\frac{\gamma_{\rm th}}{\overline{\gamma}_{\rm rd}}\right),
\end{aligned}$$

which yields the following asymptotic expression:

$$P_{\text{out}}\left(\gamma_{\text{th}}\right)=\left(1+\frac{1}{\left(n_{\text{s}}-1\right)\left(n_{\text{r}}-1\right)\overline{\gamma}_{\text{sr}}}\right)\frac{\gamma_{\text{th}}}{\beta\overline{\gamma}_{\text{sr}}}+o\left(\gamma_{\text{th}}\right), \tag{3.25}$$

where $\beta=\frac{\overline{\gamma}_{\text{rd}}}{\overline{\gamma}_{\text{sr}}}$ is the links balance parameter.

The contemplation of (3.25) provides interesting insights into the system design.

- **Leverage the r-d link:** The orthogonal projection enables to free some relay antennas resources as presented in 3.2.2. Given that the outage probability is governed by the $\mathrm{r}-\mathrm{d}$ link—as it decreases with high β—an interesting approach to improve the diversity and the throughput of the system under the pinhole condition is to leverage the $\mathrm{r}-\mathrm{d}$ link by performing either a signal-level space-time coding or spatial multiplexing of the relay DoFs, while activating adequate multi-antenna detection schemes at the destination. Such a strategy will be exhibited in chapter 4.

- **Benefit from the implicit combining gain:** The QR-based orthogonal projection of PF relaying is implicitly combining all space diversity branches of the $\mathrm{s}-\mathrm{r}$ channel. This results in e.g., a SNR gain proportional to $\left(n_{\text{s}}-1\right)\left(n_{\text{r}}-1\right)$ in low SNR regime $\left(\overline{\gamma}_{\text{sr}},\overline{\gamma}_{\text{rd}}\ll 1\right)$. This implicit combining becomes more interesting when the projection is performed jointly with hybrid-ARQ as will be shown in chapter 5.

3.4.2 Asymptotic Ergodic Capacity

Based on (**??**), the asymptotic behavior of the ergodic capacity is derived for different scenarios of the balance parameter β and the SNR $\overline{\gamma}_{\text{sr}}$. For that end, the bivariate Meijer-G terms in (**??**) are first expressed using Mellin-Barnes integrals as

$$\begin{aligned}
&\mathrm{G}^{1,0:1,2:3,0}_{1,0:2,2:1,3}\left(\overline{\gamma}_{\text{rd}},\frac{\overline{\gamma}_{\text{rd}}}{\overline{\gamma}_{\text{sr}}}\;\middle|\;\begin{matrix}n+m+i+2\\ -\end{matrix}\;\middle|\;\begin{matrix}1,1\\1,0\end{matrix}\;\middle|\;\begin{matrix}0\\ -1,\frac{\nu}{2}+\mu-n-m,-\frac{\nu}{2}+\mu-n-m\end{matrix}\right)\\
=\;&\frac{1}{\left(2\pi j\right)^{2}}\int_{C_1}\int_{C_2}\Gamma\left(n+m+i+2+s+t\right)\Gamma^{2}\left(s\right)\Gamma\left(1-s\right)\Gamma\left(-1-t\right)\\
&\times\Gamma\left(\frac{\nu}{2}+\mu-n-m-t\right)\Gamma\left(-\frac{\nu}{2}+\mu-n-m-t\right)\frac{\overline{\gamma}_{\text{rd}}^{s}\beta^{t}}{\Gamma\left(1+s\right)\Gamma\left(-t\right)}\mathrm{d}s\mathrm{d}t,
\end{aligned} \tag{3.26}$$

$$\begin{aligned}
&\mathrm{G}_{1,0:2,2:2,4}^{1,0:1,2:3,1}\left(\overline{\gamma}_{\mathrm{rd}}, \frac{\overline{\gamma}_{\mathrm{rd}}}{\overline{\gamma}_{\mathrm{sr}}} \,\middle|\, \begin{matrix} n+m+i+1 \\ - \end{matrix} \,\middle|\, \begin{matrix} 1,1 \\ 1,0 \end{matrix} \right. \\
&\qquad\qquad \left.\middle|\, \begin{matrix} -(n+m+i+1), 0 \\ -1, \frac{\nu}{2}+\mu-n-m, -\frac{\nu}{2}+\mu-n-m, -(n+m+i) \end{matrix}\right) \\
&= \frac{1}{(2\pi j)^2}\int_{C_1}\int_{C_2} \Gamma\left(n+m+i+1+s+t\right)\Gamma^2\left(s\right)\Gamma\left(1-s\right)\Gamma\left(n+m+i+2+t\right) \\
&\qquad \times\Gamma\left(-1-t\right)\Gamma\left(\frac{\nu}{2}+\mu-n-m-t\right)\Gamma\left(-\frac{\nu}{2}+\mu-n-m-t\right) \\
&\qquad \times\frac{\overline{\gamma}_{\mathrm{rd}}^{s}\beta^{t}}{\Gamma\left(1+s\right)\Gamma\left(-t\right)\Gamma\left(n+m+i+1+t\right)}\mathrm{d}s\mathrm{d}t. \qquad (3.27)
\end{aligned}$$

- **Case $\beta \to +\infty$:** we evaluate the residue of the first and second bivariate Meijer-G terms in (3.22) at the highest poles lying in the left-hand side of contour C_2, i.e., $t = -(n+m+i+2+s)$ and $t = -(n+m+i+1+s)$, respectively. After detailed residue calculations (see Appendix B.1) and by keeping only zeroth orders on $1/\beta$ we obtain the asymptotic expression

$$\overline{C} \underset{\beta\to+\infty}{\approx} \frac{1}{2\ln\left(2\right)\Gamma\left(n_{\mathrm{s}}\right)\Gamma\left(n_{\mathrm{r}}\right)}\mathrm{G}_{6,4}^{2,5}\left(\overline{\gamma}_{\mathrm{sr}}\,\middle|\, \begin{matrix} 1,1,1,1-n_{\mathrm{r}},1-n_{\mathrm{s}},0 \\ 1,1,0,0 \end{matrix}\right). \qquad (3.28)$$

- **Case $\beta, \overline{\gamma}_{\mathrm{sr}} \to +\infty$:** we approximate the Meijer-G term in (3.28) by computing the residue of the corresponding Mellin-Barnes integrand at $s = 0$ (See details in Appendix B.2), which leads to

$$\overline{C} \underset{\beta,\overline{\gamma}_{\mathrm{sr}}\to+\infty}{\approx} \frac{1}{2\ln\left(2\right)}\left[\ln\left(\overline{\gamma}_{\mathrm{sr}}\right) + \Psi^{(0)}\left(n_{\mathrm{s}}\right) + \Psi^{(0)}\left(n_{\mathrm{r}}\right)\right]. \qquad (3.29)$$

- **Case $\beta \to 0$:** which implies that $\overline{\gamma}_{\mathrm{rd}} = \beta\overline{\gamma}_{\mathrm{sr}} \to 0$. Evaluating the residue of the Mellin-Barnes integrands at $s = 1$ and $t = -1$, the asymptotic ergodic capacity is obtained as

$$\overline{C} \underset{\beta\to 0}{\approx} 0. \qquad (3.30)$$

These asymptotic capacity results draw attention to important system design directions.

- **PF is more interesting at cell-edge:** i.e., when the relay is closer to the destination ($\beta \to +\infty$), which is the likely scenario in practical deployments. In contrast, the capacity vanishes when the $\mathrm{s}-\mathrm{r}$ link SNR largely outperforms the $\mathrm{r}-\mathrm{d}$ one as demonstrated by (3.30).

- **Capacity is driven by the number of relay antennas:** when hybrid-ARQ is activated, the capacity can be further improved by virtually increasing the number of relay receive antennas by a joint projection over multi-transmission signals (see chapter 5).

Also, the multiplexing gain can be increased by performing a spatial multiplexing at the level of the relay (see chapter 4).

Scenario	Asymptotic $\overline{C}$	
$\beta \to +\infty$	$\frac{1}{2\ln(2)\Gamma(n_\mathrm{s})\Gamma(n_\mathrm{r})} \times \mathrm{G}_{6,4}^{2,5}\left(\overline{\gamma}_\mathrm{sr}\middle\vert \begin{matrix} 1,1,1,1-n_\mathrm{r},1-n_\mathrm{s},0 \\ 1,1,0,0 \end{matrix}\right)$	(3.31)
$\beta, \overline{\gamma}_\mathrm{sr} \to +\infty$	$\frac{1}{2\ln(2)}\left[\ln\left(\overline{\gamma}_\mathrm{sr}\right) + \psi^{(0)}\left(n_\mathrm{s}\right) + \psi^{(0)}\left(n_\mathrm{r}\right)\right]$	(3.32)
$\beta \to 0$	0	

Table 3.1: Ergodic capacity asymptotic expressions

3.5 Numerical Results

3.5.1 Settings

In this section, we present some numerical results to illustrate the theoretical analysis. Fig. 3.4, 3.5, and 3.6 show—for different antenna and average SNR setups—the exact and asymptotic results of both the end-to-end outage probability and the ergodic capacity, respectively. Throughout extensive numerical experiments, analytical curves are obtained by truncating the infinite sums to $K = 50$ and $L = 5$ terms. The exact match with Monte-Carlo simulation results confirms the accuracy of the theoretical analysis. To show the interest of PF relaying, AF simulations are provided for comparison. The bivariate Meijer G-function with automated contour—presented in the Appendix—was developed to enable the numerical evaluation of (16) in MATLAB environment.

3.5.2 Bivariate Meijer-G Implementation

The bivariate Meijer G-function, presented in Annex C, was developed to enable the numerical evaluation of (3.22) in MATLAB environment. In the generalized Meijer-G and H functions, the complex integration contour is closely (and critically) dependent on the parameters of the function. The implementations of the bivariate Meijer-G function in [68] and even that of the bivariate H-function [75], are settling for a static manual contour definition which is just not scalable for complicated and dynamic parameters (e.g., inside loops). In contrast, the proposed MATLAB code automates the integration contour definition, enabling a simple usage of the bivariate Meijer-G function in dynamic codes. A second contribution of our proposed code, is that it is based on the fast MATLAB routine *quad2d* rather than the slow *dblquad*. The difference is notable and appreciable from a running time point of view. Our proposed code is hence an improved (more general and automated) version of the existing implementation.

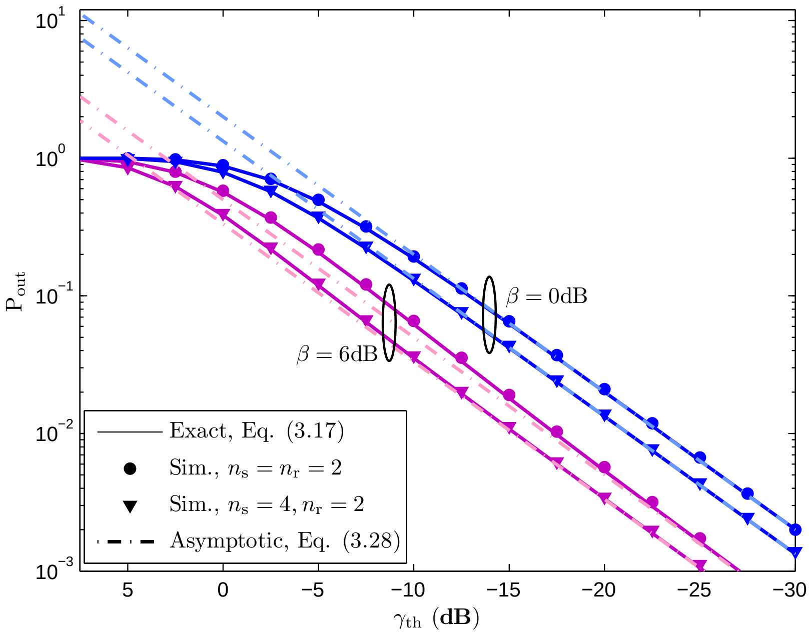

Figure 3.4: End-to-end outage probability versus γ_{th} for $\overline{\gamma}_{\mathrm{sr}} = 0$ dB..

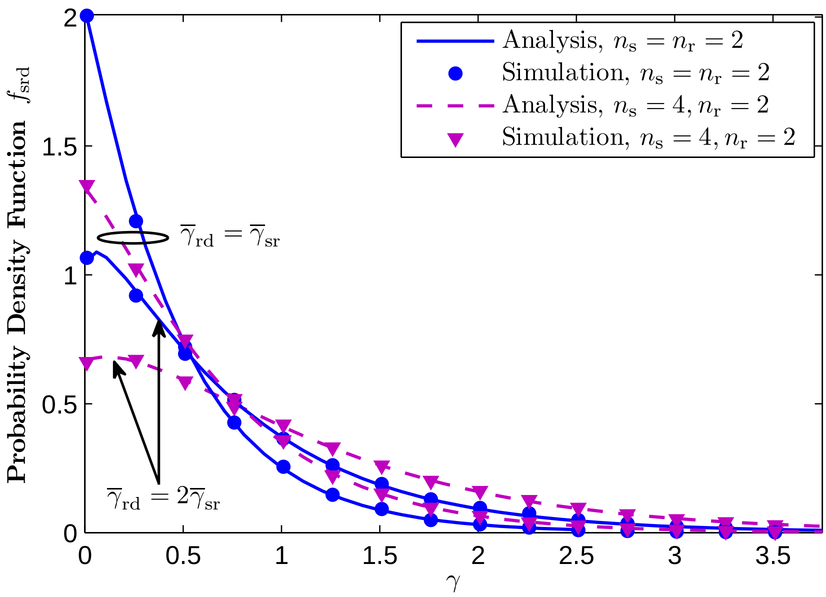

Figure 3.5: PDF of the end-to-end SNR for $\overline{\gamma}_{\mathrm{sr}} = 0$ dB.

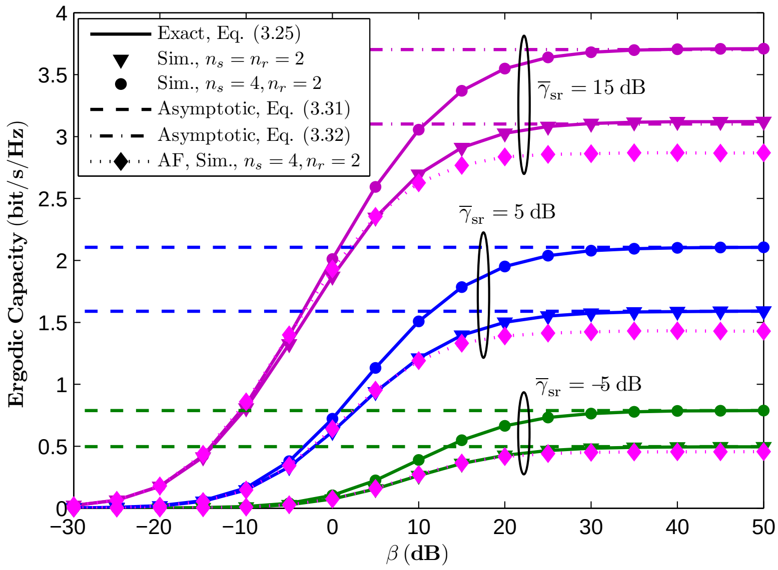

Figure 3.6: End-to-end ergodic capacity versus $\overline{\gamma}_{\mathrm{sr}}$ for different antenna configurations.

3.6 Conclusions

In this chapter, we have characterized the performance of PF system under the practical scenario of mixed MIMO-pinhole and Rayleigh dual-hop channel. Relying on a wide set of generalized mathematical functions, we have first derived analytical expressions of both the outage probability and the ergodic capacity. We have then invoked the residue theory to study the asymptotic behavior of these metrics and have shown that the performance is governed by the relay-destination link and the number of antennas. Accordingly, we have provided design recommendations to build efficient PF-based relaying schemes, exploiting the PF relay free antennas as well as the implicit combining brought by the projection operation. For numerical evaluation purposes, we have proposed a novel and fast MATLAB implementation of the bivariate Meijer-G function. Analytical curves have been confirmed with Monte-Carlo simulation results, and can be used by system designers to define SNR threshold for switching between PF and other relaying schemes in pinhole conditions.

So how one can build a PF-based relaying architecture to alleviate the half-duplex throughput loss in the MIMO relay channel? A question that the next chapter attempts to answer.

Chapter 4

PF-Based Cooperative Spatial Multiplexing over MIMO Broadband Systems

4.1 Introduction

Spatial multiplexing (SM) is a major ingredient to devise throughput-efficient transmission schemes over dual-hop MIMO broadband channels, usually suffering from spectral-efficiency deterioration induced by the half-duplex constraint. Indeed, from a radio design perspective, a relay may operate according to two distinct transmission modes. In *half-duplex* mode, the relay transmission and reception alternate in time. Hence, the transmission of one information symbol from the source to the destination occupies two channel uses, leading therefore to a throughput loss represented by the $1/2$ pre-log factor in the corresponding capacity expressions. Conversely, in *full-duplex* scheme, relay transmission and reception are concurrent which mitigates the aforementioned distortion factor [16]. Yet, the capacity can be significantly degraded from another angle: when a relay simultaneously transmits and receives over the same frequency channel, an interference link, dubbed loopback or echo interference link, is introduced from the relay transmitter to its receiver. Existing isolation and cancellation techniques [17, 18, 76] cannot perfectly prevent the relay transmit signal from leaking into its receiver. Consequently, a residual self-interference persists and adversely affects the effective signal-to-noise ratio (SNR) inside the capacity logarithm [19], especially in high transmit power regimes.

The skeptical performance of *full-duplex* radio transmission has urged the wireless community to sidestep the *half-duplex* throughput loss through different approaches. Hence, in [20] the authors propose a protocol where a base station (BS) consecutively serves K users and their corresponding relays in K orthogonal time slots. In time slot $K + 1$, all relays forward their received signals. The effective capacity of a single cooperative connection has to be multiplied by a factor $1/(1+1/K)$ instead of $1/2$ which enhances the throughput. In that case, the multiuser interference induced by the spatial reuse of the relay slot is handled via the adoption of distributed space-time codes (DSTC). In [23], the potential of fixed *half-duplex* relays is studied in a cellular context. To enable *full-duplex* operation, a policy is devised to let the relay reuse a second frequency channel, originally belonging to a neighboring cell, for its own transmissions. This results in a global outage and spectral-efficiency improvement. In [21], the throughput loss constraint is rather overcome by considering two *half-duplex* AF relays that alternately forward messages from a source to a destination. In order to decrease the inter-relay interference, one relay performs interference cancellation. This cooperation scheme turns the equivalent channel between the source and the destination into a frequency-selective channel. A maximum likelihood sequence estimator at the destination is then applied to extract the introduced diversity. Also, a two-way AF/DF relaying protocol is introduced in [25] where although the achievable rate in one direction suffers still from the pre-log factor $1/2$ but since two connections are realized in the same physical channel, the achieved sum-rate is higher than the single user rate over the *half-duplex* relay channel. In [26], the authors propose that a detect-and-forward (DetF) relay uses a modulation whose order is higher than the one at the source. The relaying phase duration is consequently reduced, yielding thereby interesting throughput gains.

In this chapter, we introduce a novel signal-level PF-based cooperative spatial multiplexing (CM) scheme for MIMO broadband transmissions. Unlike the previous strategies, it enables to shorten the relaying phase duration by multiplexing the signal DoFs over the relay antennas that have become vacant upon the orthogonal projection; a technique that does not require any extra resources (relay, frequency) or processing (symbol detection or re-mapping) at the relay, and turns out to be throughput-efficient over the whole SNR range compared to AF mode, and interestingly, becomes more powerful at cell edge. The derived frequency domain communication model masks the cooperation; as though the destination is receiving multiple transmissions from the source, which paves the way to run any joint detection and combining algorithms.

The remainder of the chapter is organized as follows. In Section 4.2, we introduce the MIMO relay channel model whereas we describe the broadcast phase processing in section 4.3. Section 4.4 details the building blocks of the relaying scheme including the signal-level spatial multiplexing procedure. The equivalent MIMO channel derivation and average throughput analysis are conducted in Section 4.5. Section 4.6 provides numerical results for different system settings. Finally, some conclusions are drawn in Section 4.7.

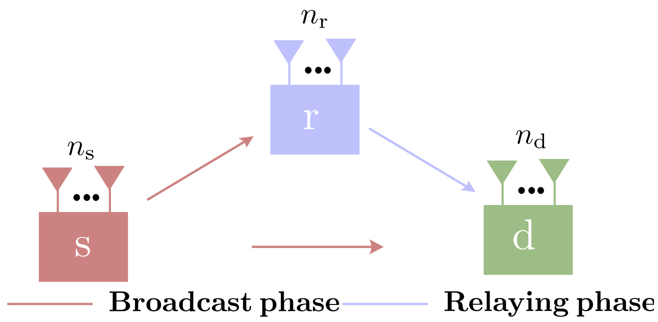

Figure 4.1: Orthogonal cooperation

4.2 MIMO Relay System Model

4.2.1 Channel Description

We consider a single carrier multi-antenna broadband cooperative uplink transmission involving a n_s antennas source, a n_r antennas relay, and a n_d antennas destination ($n_\mathrm{d} \geq n_\mathrm{r} \geq n_\mathrm{s}$). Communication between each couple of NEs, $\epsilon \in \{\mathrm{s}, \mathrm{r}\}$ and $\epsilon' \in \{\mathrm{r}, \mathrm{d}\}$, is established via a wireless link $\epsilon - \epsilon'$ corrupted by two fading effects:

- Large-scale fading: modeled by the average link loss $\alpha_{\epsilon\epsilon'} = d_{\epsilon\epsilon'}^{-\kappa/2}$ accounting for both free space attenuation and shadowing, with $d_{\epsilon\epsilon'}$ is the distance between nodes ϵ and ϵ' and κ is the path loss exponent.

- Small-scale fading: where each link $\epsilon - \epsilon'$ is supposed to be a block fading quasi-static frequency-selective MIMO channel of memory $L_{\epsilon\epsilon'} - 1$ (index $l = 0, \cdots, L_{\epsilon\epsilon'} - 1$). The lth path is represented by an independent standard complex Gaussian matrix $\mathbf{H}_{\epsilon\epsilon',l} \in \mathbb{C}^{n_{\epsilon'} \times n_\epsilon}$. Coefficients thereof have variance $1/L_{\epsilon\epsilon'}$ under a normalized equal power-delay profile. Therefore, the total average received power per each receive antenna (at both the relay and the destination) is equal to n_s when no large scale fading is considered.

4.2.2 Cooperation Protocol

As depicted in Fig. 4.1, the relay transmission is assumed *half-duplex*, spanning hence two consecutive phases. In this framework, we consider that the cooperation is orthogonal [26], i.e., the source broadcasts the whole data block during the first phase while it remains silent during the second phase when the relay forwards a processed version of the captured packet to the destination.

4.3 Broadcast Phase Processing

4.3.1 Signaling Scheme

We restrict the source to operate under the spatial multiplexing (SM) mode. During each broadcast phase, node s generates a $n_{\mathrm{s}} \times T$ symbol matrix $\mathbf{S}$,

$$\mathbf{S} \triangleq [\mathbf{s}_0, \ldots, \mathbf{s}_{T-1}], \tag{4.1}$$

where T (index $t = 0, \cdots, T-1$) is the total number of channel uses (c.u.), and $\mathbf{s}_t = [\mathrm{s}_{1,t}, \ldots, \mathrm{s}_{n_{\mathrm{s}},t}]^{\mathrm{T}} \in \mathcal{A}^{n_{\mathrm{s}}}$ is the symbol vector at c.u. t, with $\mathcal{A}$ is the alphabet of normalized constellation symbols. We assume that the source has no channel state information (CSI). Therefore, equal transmit power allocation is the optimal choice [51]. Symbols are considered to be zero-mean and independent in both space and time dimensions (deep interleaving assumption). Their cross-correlation is given by

$$\mathrm{E}\left[\mathbf{s}_t \mathbf{s}_{t'}^{\mathrm{H}}\right] = \delta_{tt'} \mathbf{I}_{n_{\mathrm{s}}}. \tag{4.2}$$

To prevent interblock interference, each packet is preceded by a cyclic prefix (CP) of length $L_{\mathrm{CP}} = \max\{L_{\mathrm{sd}}, L_{\mathrm{sr}}, L_{\mathrm{rd}}\}$.

4.3.2 Broadcast Phase Communication Model

At this level, the source proceeds by sending a prefixed version of packet $\mathbf{S}$ to both the destination and the relay. The corresponding CP-free baseband received signals can be respectively expressed as

$$\mathbf{y}_{\mathrm{d},t,1} = \alpha_{\mathrm{sd}} \sum_{l=0}^{L_{\mathrm{sd}}-1} \mathbf{H}_{\mathrm{sd},l} \mathbf{s}_{(t-l) \bmod T} + \mathbf{w}_{\mathrm{d},t,1} \in \mathbb{C}^{n_{\mathrm{d}} \times 1}, \tag{4.3}$$

$$\mathbf{y}_{\mathrm{r},t} = \alpha_{\mathrm{sr}} \sum_{l=0}^{L_{\mathrm{sr}}-1} \mathbf{H}_{\mathrm{sr},l} \mathbf{s}_{(t-l) \bmod T} + \mathbf{w}_{\mathrm{r},t} \in \mathbb{C}^{n_{\mathrm{r}} \times 1}, \tag{4.4}$$

where random vectors $\mathbf{w}_{\mathrm{d},t,1} \sim \mathcal{N}\left(\mathbf{0}_{n_{\mathrm{d}} \times 1}, \sigma^2 \mathbf{I}_{n_{\mathrm{d}}}\right)$ and $\mathbf{w}_{\mathrm{r},t} \sim \mathcal{N}\left(\mathbf{0}_{n_{\mathrm{r}} \times 1}, \sigma^2 \mathbf{I}_{n_{\mathrm{r}}}\right)$ denote the additive thermal noise.

4.4 Relaying Phase Processing

4.4.1 Frequency Domain Transformation

The relaying phase starts by transposing the stacked signal vector $\mathbf{y}_{\mathrm{r}} = \mathrm{vec}_T\{\mathbf{y}_{\mathrm{r},t}\}$ into the frequency domain. For that end, a block-wise communication model is constructed from (4.4) as

$$\mathbf{y}_{\mathrm{r}} = \alpha_{\mathrm{sr}} \mathbf{H}_{\mathrm{sr}} \mathbf{x} + \mathbf{w}_{\mathrm{r}}, \tag{4.5}$$

where $\mathbf{H}_{\mathrm{sr}}$ is a $n_{\mathrm{r}}T \times n_{\mathrm{s}}T$ block circulant matrix whose first column is

$$\left[\mathbf{H}_{\mathrm{sr},0}^{\mathrm{T}}, \cdots, \mathbf{H}_{\mathrm{sr},L_{\mathrm{sr}}-1}^{\mathrm{T}}, \mathbf{0}_{n_s \times n_r(T-L_{\mathrm{sr}})}\right]^{\mathrm{T}}. \tag{4.6}$$

$\mathbf{H}_{\mathrm{sr}}$ can therefore be block diagonalized in the Fourier basis, i.e., $\mathbf{H}_{\mathrm{sr}} = \mathbf{U}_{T,n_{\mathrm{r}}}^{\mathrm{H}} \mathbf{C}_{\mathrm{sr}} \mathbf{U}_{T,n_{\mathrm{s}}}$ where $\mathbf{C}_{\mathrm{sr}} \triangleq \operatorname{diag}\{\mathbf{C}_{\mathrm{sr},0}, \cdots, \mathbf{C}_{\mathrm{sr},T-1}\}$, and

$$\mathbf{C}_{\mathrm{sr},t} = \sum_{l=0}^{L_{\mathrm{sr}}-1} \mathbf{H}_{\mathrm{sr},l} \exp\left\{-j\frac{2\pi tl}{T}\right\} \in \mathbb{C}^{n_{\mathrm{r}} \times n_{\mathrm{s}}} \tag{4.7}$$

stands for the channel frequency response (CFR) at the t^{th} subcarrier. Hence, the frequency domain image of (4.5) is given by

$$\mathbf{y}_{\mathrm{r}}' = \alpha_{\mathrm{sr}} \mathbf{C}_{\mathrm{sr}} \mathbf{s}' + \mathbf{w}_{\mathrm{r}}' \in \mathbb{C}^{n_{\mathrm{r}}T}, \tag{4.8}$$

which can be expressed component-wise as

$$\mathbf{y}_{\mathrm{r},t}' = \alpha_{\mathrm{sr}} \mathbf{C}_{\mathrm{sr},t} \mathbf{s}_t' + \mathbf{w}_{\mathrm{r},t}' \in \mathbb{C}^{n_{\mathrm{r}} \times 1}. \tag{4.9}$$

According to (4.7), each matrix $\mathbf{C}_{\mathrm{sr},t}$ is a linear combination of independent standard Gaussian matrices. It follows that it is full rank, i.e., $\operatorname{rank}(\mathbf{C}_{\mathrm{sr},t}) = \min(n_{\mathrm{s}}, n_{\mathrm{r}}) = n_{\mathrm{s}}$.

4.4.2 Signal Reduction

By the QR decomposition technique [53], the CFR $\mathbf{C}_{\mathrm{sr},t}$ can be written as

$$\mathbf{C}_{\mathrm{sr},t} = \mathbf{Q}_t \mathbf{R}_t, \tag{4.10}$$

where the $n_{\mathrm{r}} \times n_{\mathrm{s}}$ matrix $\mathbf{Q}_t$ has orthogonal columns with unit norm and the $n_{\mathrm{s}} \times n_{\mathrm{s}}$ matrix $\mathbf{R}_t$ is upper triangular. Multiplying the received signal $\mathbf{y}_{\mathrm{r},t}'$ by $\mathbf{Q}_t^{\mathrm{H}}$ yields the sufficient statistic

$$\widetilde{\mathbf{y}'}_{\mathrm{r},t} = \mathbf{Q}_t^{\mathrm{H}} \mathbf{y}_{\mathrm{r},t}' = \alpha_{\mathrm{sr}} \mathbf{R}_t \mathbf{s}_t' + \widetilde{\mathbf{w}'}_{\mathrm{r},t} \in \mathbb{C}^{n_{\mathrm{s}} \times 1} \tag{4.11}$$

for the estimation of transmit vector $\mathbf{s}_t'$ at the destination side. Since $\mathbf{Q}_t$ is an unitary matrix, the statistical properties of the noise term $\widetilde{\mathbf{w}'}_{\mathrm{r},t} = \mathbf{Q}_t^{\mathrm{H}} \mathbf{w}_{\mathrm{r},t}'$ are maintained.

4.4.3 Signal-Level Spatial Multiplexing

In the extent that only n_s relay antennas are required to forward statistic $\widetilde{\mathbf{y}'}_{r,t}$ to node d, a spatial multiplexing can be performed on the $(n_{\mathrm{r}} - n_{\mathrm{s}})$ free antennas. It entails simultaneously transmitting k signal vectors of size $n_{\mathrm{s}} \times 1$ to the destination, where

$$k \triangleq \left\lceil \frac{n_{\mathrm{r}}}{n_{\mathrm{s}}} \right\rceil. \tag{4.12}$$

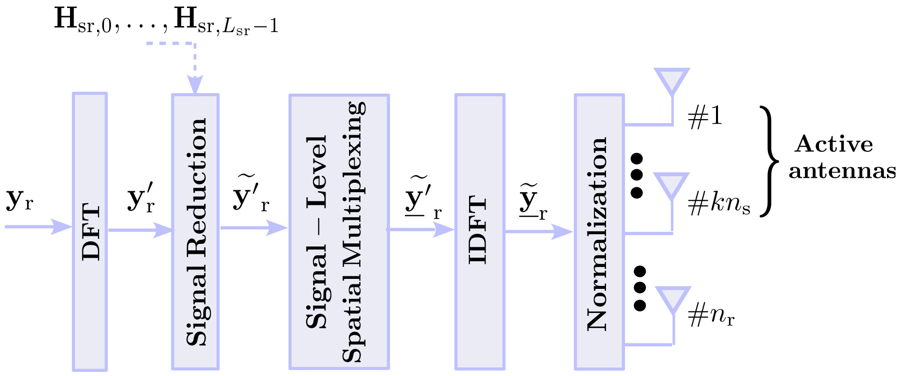

Figure 4.2: Relaying phase processing

The transmission unit of node r hence becomes a short packet of $kn_{\mathrm{s}} \times T_k$ signal samples, where actually, the new packet length $T_k = \frac{T}{k}$ is an integer since T is supposed to be a multiple of n_{r}. The t^{th} subcarrier signal $\widetilde{\underline{\mathbf{y}'}}_{\mathrm{r},t}$ is correspondingly constructed as

$$\widetilde{\underline{\mathbf{y}'}}_{\mathrm{r},t} \triangleq \left[\widetilde{\mathbf{y}'}^{\mathrm{T}}_{\mathrm{r},kt},\cdots,\widetilde{\mathbf{y}'}^{\mathrm{T}}_{\mathrm{r},k(t+1)-1}\right]^{\mathrm{T}} \in \mathbb{C}^{kn_{\mathrm{s}}\times 1}. \tag{4.13}$$

By invoking (4.11), we can write

$$\widetilde{\underline{\mathbf{y}'}}_{\mathrm{r},t} = \alpha_{\mathrm{sr}}\underline{\mathbf{R}}_t\underline{\mathbf{s}}'_t + \widetilde{\underline{\mathbf{w}'}}_{r,t},\ t = 0,\ldots,T_k-1 \tag{4.14}$$

with

$$\begin{cases} \underline{\mathbf{s}}'_t & \triangleq \left[\mathbf{s}'^{\mathrm{T}}_{kt},\cdots,\mathbf{s}'^{\mathrm{T}}_{k(t+1)-1}\right]^{\mathrm{T}} \in \mathbb{C}^{kn_{\mathrm{s}}}, \\ \underline{\mathbf{R}}_t & \triangleq \mathrm{diag}\left\{\mathbf{R}_{kt},\ldots,\mathbf{R}_{k(t+1)-1}\right\} \in \mathbb{C}^{kn_{\mathrm{s}}\times kn_{\mathrm{s}}}, \\ \widetilde{\underline{\mathbf{w}'}}_{\mathrm{r},t} & \triangleq \left[\widetilde{\mathbf{w}'}^{\mathrm{T}}_{\mathrm{r},kt},\cdots,\widetilde{\mathbf{w}'}^{\mathrm{T}}_{\mathrm{r},k(t+1)-1}\right]^{\mathrm{T}} \in \mathbb{C}^{kn_{\mathrm{s}}}. \end{cases} \tag{4.15}$$

The relay performs time domain conversion of the stacked signal $\widetilde{\underline{\mathbf{y}'}}_{\mathrm{r}} = \mathrm{vec}_{T_k}\left\{\widetilde{\underline{\mathbf{y}'}}_{\mathrm{r},t}\right\}$ via the application of a T_k-point inverse DFT as

$$\widetilde{\underline{\mathbf{y}}}_{\mathrm{r}} = \mathbf{U}^{\mathrm{H}}_{T_k,kn_{\mathrm{s}}}\widetilde{\underline{\mathbf{y}'}}_{\mathrm{r}}. \tag{4.16}$$

The resulting $kn_{\mathrm{s}} \times 1$ single carrier signal at channel use t is given by

$$\widetilde{\underline{\mathbf{y}}}_{\mathrm{r},t} = \alpha_{\mathrm{sr}}\sum_{l=0}^{T_k-1}\widetilde{\mathbf{H}}_{\mathrm{sr},l}\widetilde{\mathbf{s}}_{(t-l)\,\mathrm{mod}\,T_k} + \widetilde{\underline{\mathbf{w}}}_{\mathrm{r},t} \in \mathbb{C}^{kn_{\mathrm{s}}}, \tag{4.17}$$

where $\widetilde{\mathbf{s}} = \mathbf{U}^{\mathrm{H}}_{T_k,kn_s}\mathbf{s}'$ is affected by AWGN noise $\widetilde{\underline{\mathbf{w}}}_{\mathrm{r}} = \mathrm{vec}_{T_k}\left\{\widetilde{\underline{\mathbf{w}}}_{\mathrm{r},t}\right\}$. Due to the above QR decomposition, the energy of the equivalent source-relay multipath channel $\widetilde{\mathbf{H}}_{\mathrm{sr}}$ is dispersed

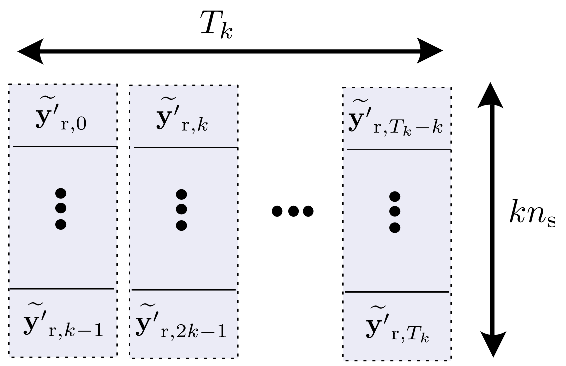

Figure 4.3: $kn_{\mathrm{s}} \times T_k$ signal packet resulting from spatial multiplexing

over T_k virtual paths. The lth path can be expressed as

$$\underset{0 \leq l \leq T_k - 1}{\widetilde{\mathbf{H}}_{\mathrm{sr},l}} = \sum_{t=0}^{T_k-1} \underline{\mathbf{R}}_t \exp\left\{ j \frac{2\pi t l}{T_k} \right\} \in \mathbb{C}^{kn_{\mathrm{s}} \times kn_{\mathrm{s}}}. \tag{4.18}$$

The time domain signal $\widetilde{\underline{\mathbf{y}}}_{\mathrm{r},t}$ is then normalized using its conditional covariance matrix,

$$\mathbf{\Xi}_{|\widetilde{\mathbf{H}}_{\mathrm{sr}}} = \mathrm{E}\left[\widetilde{\underline{\mathbf{y}}}_{\mathrm{r},t} \widetilde{\underline{\mathbf{y}}}_{\mathrm{r},t}^{\mathrm{H}} \mid \left\{ \widetilde{\mathbf{H}}_{\mathrm{sr},l} \right\} \right]. \tag{4.19}$$

Given the aforementioned assumption of deep space time interleaving, and the independence between symbols and noise vectors, (4.17) yields a developed expression of (4.19)

$$\mathbf{\Xi}_{|\widetilde{\mathbf{H}}_{\mathrm{sr}}} = \alpha_{\mathrm{sr}}^2 \sum_{l=0}^{T_k-1} \widetilde{\mathbf{H}}_{\mathrm{sr},l} \widetilde{\mathbf{H}}_{\mathrm{sr},l}^{\mathrm{H}} + \sigma^2 \mathbf{I}_{kn_{\mathrm{s}}}. \tag{4.20}$$

By considering the Cholesky factorization $\mathbf{\Xi}_{|\widetilde{\mathbf{H}}_{\mathrm{sr}}} = \mathbf{\Phi}\mathbf{\Phi}^{\mathrm{H}}$, the normalization consists on left multiplying $\widetilde{\underline{\mathbf{y}}}_{\mathrm{r},t}$ by $\mathbf{\Phi}^{-1}$.

4.4.4 Relaying Phase Communication Model

During the second phase, termed also "relaying phase", the normalized signal vector is mapped to kn_{s} relay antennas and transmitted towards node d. In the simplest case, these active antennas are selected according to a fixed mapping matrix,

$$\mathbf{P} = \begin{bmatrix} \mathbf{I}_{kn_{\mathrm{s}}} \\ \mathbf{0}_{(n_{\mathrm{r}} - kn_{\mathrm{s}}) \times kn_{\mathrm{s}}} \end{bmatrix}, \tag{4.21}$$

which is the strategy here, since the problem of antennas selection is out of the scope of this chapter. At the receiver side, the obtained signal after the elimination of CP is consequently expressed as

$$\mathbf{y}_{\mathrm{d},t,2} = \alpha_{\mathrm{rd}} \sum_{l=0}^{L_{\mathrm{rd}}-1} \mathbf{H}_{\mathrm{rd},l}\mathbf{P}\mathbf{\Phi}^{-1}\underline{\widetilde{\mathbf{y}}}_{\mathrm{r},(t-l)\mathrm{mod}T_k} + \widetilde{\mathbf{w}}_{\mathrm{d},t,2} \in \mathbb{C}^{n_{\mathrm{d}}\times 1}, \tag{4.22}$$

where $\widetilde{\mathbf{w}}_{\mathrm{d},t,2} \sim \mathcal{N}\left(\mathbf{0}_{n_{\mathrm{d}}\times 1}, \sigma^2\mathbf{I}_{n_{\mathrm{d}}}\right)$ denotes the additive Gaussian noise. By invoking (4.17) and (4.22), the sampled $n_{\mathrm{d}} \times 1$ signal vector $\mathbf{y}_{\mathrm{d},t,2}$ can be further developed as

$$\mathbf{y}_{\mathrm{d},t,2} = \alpha_{\mathrm{sr}}\alpha_{\mathrm{rd}} \sum_{l=0}^{L_{\mathrm{srd}}-1} \mathbf{H}_{\mathrm{srd},l}\widetilde{\mathbf{s}}_{(t-l)\mathrm{mod}T_k} + \mathbf{w}_{\mathrm{d},t,2}, \tag{4.23}$$

with $L_{\mathrm{srd}} = T_k + L_{\mathrm{rd}} - 1$, and

$$\underset{0\leq l\leq L_{\mathrm{srd}}-1}{\mathbf{H}_l^{\mathrm{srd}}} = \sum_{n=\max(0,l-L_{rd}+1)}^{\min(l,T_k-1)} \mathbf{H}_{\mathrm{rd},l-n}\mathbf{P}\mathbf{\Phi}^{-1}\widetilde{\mathbf{H}}_{\mathrm{sr},n} \in \mathbb{C}^{n_{\mathrm{d}}\times kn_{\mathrm{s}}}. \tag{4.24}$$

The corresponding noise $\mathbf{w}_{\mathrm{d},t,2}$ is given by

$$\mathbf{w}_{\mathrm{d},t,2} = \alpha_{\mathrm{rd}} \sum_{l=0}^{L_{\mathrm{rd}}-1} \mathbf{H}_{\mathrm{rd},l}\mathbf{P}\mathbf{\Phi}^{-1}\underline{\widetilde{\mathbf{w}}}_{\mathrm{r},(t-l)\mathrm{mod}T_k} + \widetilde{\mathbf{w}}_{\mathrm{d},t,2}, \tag{4.25}$$

and has conditional covariance matrix $\mathbf{\Lambda}_{|\mathbf{H}_{\mathrm{rd}}}$ (conditioned upon $\mathbf{H}_{\mathrm{rd}}$)

$$\begin{cases} \mathbf{\Lambda}_{|\mathbf{H}_{\mathrm{rd}}} = \sigma^2\left(\alpha_{\mathrm{rd}}^2 \sum_{l=0}^{\mathrm{L}_{rd}-1} \mathbf{\Lambda}_l\mathbf{\Lambda}_l^{\mathrm{H}} + \mathbf{I}_{n_{\mathrm{d}}}\right), \\ \mathbf{\Lambda}_l = \mathbf{H}_{\mathrm{rd},l}\mathbf{P}\mathbf{\Phi}^{-1}. \end{cases} \tag{4.26}$$

4.5 Average Throughput Analysis

In this section, we show that the presented cooperation scheme can be viewed as a transmission over a virtual MIMO channel whose expression is derived in the sequel. The system performance, in terms of average throughput, is then analyzed.

4.5.1 Equivalent MIMO Channel

By transposing the received signal packets $\mathbf{y}_{\mathrm{d},1} = \mathrm{vec}_T\left\{\mathbf{y}_{\mathrm{d},t;1}\right\}$ and $\mathbf{y}_{\mathrm{d},2} = \mathrm{vec}_{T_k}\left\{\mathbf{y}_{\mathrm{d},t,2}\right\}$ to the frequency domain

$$\begin{cases} \mathbf{y'}_{\mathrm{d},1} &= \mathbf{U}_{T,n_{\mathrm{s}}}\mathbf{y}_{\mathrm{d},1} \\ \mathbf{y'}_{\mathrm{d},,2} &= \mathbf{U}_{T_k,kn_{\mathrm{s}}}\mathbf{y}_{\mathrm{d},2} \end{cases}, \tag{4.27}$$

we get the following subcarriers communication models

$$\begin{cases} \mathbf{y'}_{\mathrm{d},t,1} &= \alpha_{\mathrm{sd}}\mathbf{C}_{\mathrm{sd},t}\mathbf{s}'_t + \mathbf{w'}_{\mathrm{d},t,1},\ t = 0,\ldots,T-1 \\ \mathbf{y'}_{\mathrm{d},t,2} &= \alpha_{\mathrm{sr}}\alpha_{\mathrm{rd}}\mathbf{C}_{\mathrm{srd},t}\underline{\mathbf{s}}'_t + \mathbf{w'}_{\mathrm{d},t,2},\ t = 0,\ldots,T_k-1 \end{cases}, \tag{4.28}$$

where $\{\mathbf{C}_{\mathrm{sd},t}\}$ and $\{\mathbf{C}_{\mathrm{srd},t}\}$ correspond to the CFRs of $\{\mathbf{H}_{\mathrm{sd},l}\}$ and $\{\mathbf{H}_{\mathrm{srd},l}\}$, respectively. To unify the channel inputs in (4.28), each k consecutive observations of $\mathbf{y'}_{\mathrm{d},1}$ are limped into one stacked vector

$$\underline{\mathbf{y}}'_{\mathrm{d},t,1} = \alpha_{\mathrm{sd}} \underline{\mathbf{C}}_{\mathrm{sd},t} \underline{\mathbf{s}}'_t + \underline{\mathbf{w}}'_{\mathrm{d},t,1},\ t = 0, \ldots, T_k - 1, \tag{4.29}$$

with

$$\begin{cases} \underline{\mathbf{y}}'_{\mathrm{d},t,1} & \triangleq \left[\mathbf{y'}^{\mathrm{T}}_{\mathrm{d},kt,1}, \cdots, \mathbf{y'}^{\mathrm{T}}_{\mathrm{d},k(t+1)-1,1}\right]^{\mathrm{T}} \in \mathbb{C}^{kn_{\mathrm{d}}}, \\ \underline{\mathbf{C}}_{\mathrm{sd},t} & \triangleq \mathrm{diag}\left\{\mathbf{C}_{\mathrm{sd},kt}, \ldots, \mathbf{C}_{\mathrm{sd},k(t+1)-1}\right\} \in \mathbb{C}^{kn_{\mathrm{d}} \times kn_{\mathrm{s}}}, \\ \underline{\mathbf{w}}'_{\mathrm{d},t,1} & \triangleq \left[\mathbf{w'}^{\mathrm{T}}_{\mathrm{d},kt}, \ldots, \mathbf{w'}^{\mathrm{T}}_{\mathrm{d},k(t+1)-1}\right]^{\mathrm{T}} \in \mathbb{C}^{kn_{\mathrm{d}}}. \end{cases} \tag{4.30}$$

Noise $\mathbf{w'}_{\mathrm{d},t,2}$ is colored, having the same covariance matrix $\mathbf{\Lambda}_{|\mathbf{H}_{\mathrm{rd}}}$ as $\mathbf{w}_{\mathrm{d},t,2}$. Consequently, we rather consider the Cholesky decomposition based whitened signal $\mathbf{\Omega}^{-1}\mathbf{y'}_{\mathrm{d},t,2}$ in the equivalent channel derivation, where $\mathbf{\Lambda}_{|\mathbf{H}_{\mathrm{rd}}} = \sigma^2 \mathbf{\Omega}\mathbf{\Omega}^{\mathrm{H}}$.

Based on (4.28) and (4.29), the considered relaying system can be represented by a virtual $(k+1)n_d \times kn_s$ MIMO channel whose expression at the t^{th} subcarrier ($t = 0, \ldots, T_k - 1$) is given by

$$\begin{bmatrix} \underline{\mathbf{y}}'_{\mathrm{d},t,1} \\ \mathbf{\Omega}^{-1}\mathbf{y'}_{\mathrm{d},t,2} \end{bmatrix} = \underbrace{\begin{bmatrix} \alpha_{\mathrm{sd}} \underline{\mathbf{C}}_{\mathrm{sd},t} \\ \alpha_{\mathrm{sr}}\alpha_{\mathrm{rd}} \mathbf{\Omega}^{-1} \mathbf{C}_{\mathrm{srd},t} \end{bmatrix}}_{\mathbf{C}_t} \underline{\mathbf{x}}'_t + \begin{bmatrix} \underline{\mathbf{w}}'_{\mathrm{d},t,1} \\ \mathbf{\Omega}^{-1}\mathbf{w'}_{\mathrm{d},t,2} \end{bmatrix}. \tag{4.31}$$

4.5.2 Average Throughput

To characterize the performance of the proposed cooperative spatial multiplexing scheme, average throughput is adopted as a metric. It is commonly a function of the factor k, the target spectral efficiency $\mathcal{S}$, and the average received SNR $\overline{\gamma}$,

$$\mathcal{T}(k, \mathcal{S}, \overline{\gamma}) = \mathrm{E}\left[u\right], \tag{4.32}$$

where u is a random variable (RV) taking values $\mathcal{S}$ and 0 with probabilities $1 - P_{\mathrm{out}}\left(k, \mathcal{S}, \overline{\gamma}\right)$ (in case of successful packet decoding) and $P_{\mathrm{out}}\left(k, \mathcal{S}, \overline{\gamma}\right)$ (when the decoding outcome is erroneous), respectively. Thus,

$$\mathrm{E}\left[u\right] = \mathcal{S}\left(1 - P_{\mathrm{out}}\left(k, \mathcal{S}, \overline{\gamma}\right)\right), \tag{4.33}$$

where $P_{\mathrm{out}}\left(k, \mathcal{S}, \overline{\gamma}\right)$ is the transmission's outage probability. It is defined in terms of the mutual information of the above equivalent MIMO channel (4.31) as

$$P_{\mathrm{out}}\left(k, \mathcal{S}, \overline{\gamma}\right) = \Pr\left\{\frac{1}{k+1} I\left(\mathbf{C}, \overline{\gamma}\right) < \mathcal{S}\right\}. \tag{4.34}$$

The $\frac{1}{k+1}$ distortion factor in (4.34) results from the fact that one channel use of the equivalent MIMO channel corresponds to $k+1$ effective c.u. of the system. The mutual information $I\left(\mathbf{C}, \overline{\gamma}\right)$ can be approximated by assuming a Gaussian input alphabet,

$$I\left(\mathbf{C},\overline{\gamma}\right)\approx\frac{1}{T_k}\sum_{t=0}^{T_k-1}\log_2\left(\det\left(\mathbf{I}_{(k+1)n_\mathrm{d}}+\frac{\overline{\gamma}}{n_\mathrm{s}}\mathbf{C}_t\mathbf{C}_t^\mathrm{H}\right)\right). \tag{4.35}$$

4.6 Simulation Results

4.6.1 Simulation Settings

In this section, average throughput performance of the presented signal-level cooperative spatial multiplexing scheme is evaluated via Monte-Carlo simulations. As a benchmark, we consider the *half-duplex* orthogonal AF relaying function, that actually, presents the same constraints as our system while being also signal-level oriented. To ensure a fair comparison, nodes of both systems must perceive the same SNRs. Let $\overline{\gamma}_{\epsilon\epsilon'}$ denote the average SNR per receive antenna over link $\epsilon-\epsilon'$. CM and AF SNR measurements are similar for links $\mathrm{s}-\mathrm{d}$ and $\mathrm{s}-\mathrm{r}$, i.e., $\overline{\gamma}_{\mathrm{s}\epsilon'}^{\mathrm{CM}}=\overline{\gamma}_{s\epsilon'}^{\mathrm{AF}}=\frac{\alpha_{s\epsilon'}^2 n_\mathrm{s}}{\sigma^2}$, $\epsilon'\in\{r,d\}$, while in link $\mathrm{r}-\mathrm{d}$ we have $\overline{\gamma}_{\mathrm{rd}}^{\mathrm{CM}}=\frac{\alpha_{\mathrm{rd}}^2 k n_\mathrm{s}}{\sigma^2}\leq\frac{\alpha_{\mathrm{rd}}^2 n_\mathrm{r}}{\sigma^2}=\overline{\gamma}_{\mathrm{rd}}^{\mathrm{AF}}$. To balance the relay-destination links, we increase the average transmit power of CM by a factor $\frac{n_\mathrm{r}}{k n_\mathrm{s}}$. The outage probability for AF relaying is computed using a 1/2 pre-log factor, i.e.,

$$P_{\mathrm{out}}^{\mathrm{AF}}\left(\mathcal{S},\overline{\gamma}\right)=\Pr\left\{\frac{1}{2}I_{\mathrm{AF}}<\mathcal{S}\right\}. \tag{4.36}$$

In all simulation scenarios, the source node is equipped with a single antenna ($n_\mathrm{s}=1$) since it is the typical uplink transmission scheme in MIMO broadband systems (e.g., LTE). Links $\mathrm{s}-\mathrm{d}$, $\mathrm{s}-\mathrm{r}$, and $r-d$ have the same length $L_{\mathrm{sd}}=L_{\mathrm{sr}}=L_{\mathrm{rd}}=3$. The path loss exponent is set to $\kappa=3$, and $T=128$ c.u. The average throughput we are computing corresponds to a target spectral efficiency $\mathcal{S}$ of n_s (bit/s/Hz) that could stem, for example, from a BPSK modulation (uncoded) or a higher order modulation with coding (e.g., QPSK with a $\frac{1}{2}$-rate encoder). The performance of CM over AF is however valid in both cases, since the two relaying schemes operate at the signal-level. Additional gains after decoding will scale-up respectively.

4.6.2 Performance Analysis

4.6.2.1 Average throughput versus SNR

It is noteworthy that the relay is located at the midpoint between nodes s and d so that the performance behavior can be relatively decorrelated with node r position. In the case of antennas configuration $(n_\mathrm{s},n_\mathrm{r},n_\mathrm{d})=(1,2,2)$, the CM scheme shrinks the relaying phase duration to the half ($k=2$) thus leading to a gain of 3 to 4 dB compared to AF over the entire SNR range. Such a difference becomes more accentuated when $(n_\mathrm{s},n_\mathrm{r},n_\mathrm{d})=(1,3,3)$. In Fig. 4.4 and 4.5, a 4 to 5 dB gap is observed between CM and AF since the first relay performs a spatial multiplexing on its 3 antennas ($k=3$). The CM throughput saturates at -9 dB ($\mathcal{T}=1$), whereas with AF one it only reaches 0.1 bit/s/Hz.

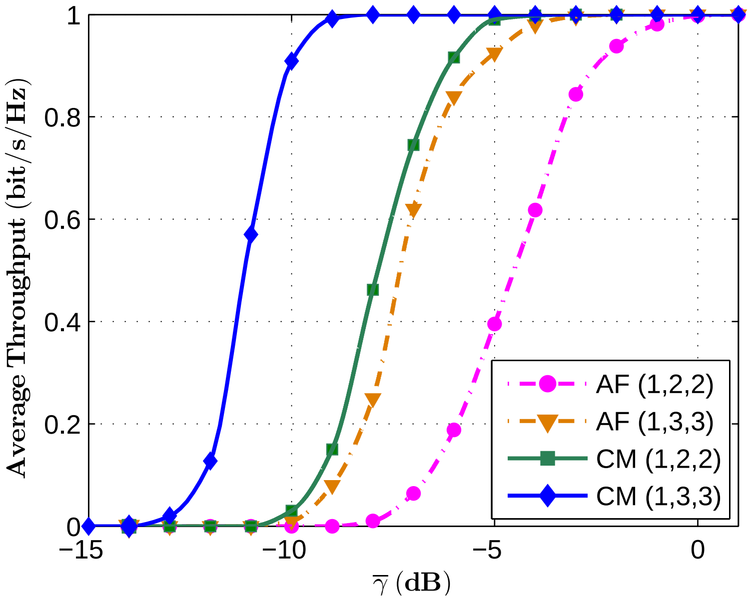

Figure 4.4: Average throughput for $n_s = 1$. The relay is at the medium of the source-destination link (i.e., $d_{sr} = 0.5$), $L_{sr} = L_{rd} = L_{sd} = 3$, and $\kappa = 3$.

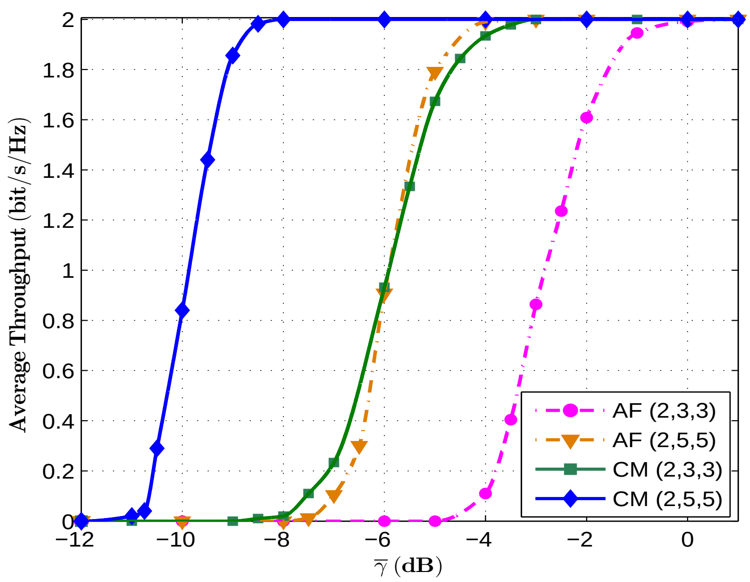

Figure 4.5: Average throughput for $n_s = 2$. The relay is at the medium of the soure-destination link (i.e., $d_{sr} = 0.5$), $L_{sr} = L_{rd} = L_{sd} = 3$, and $\kappa = 3$.

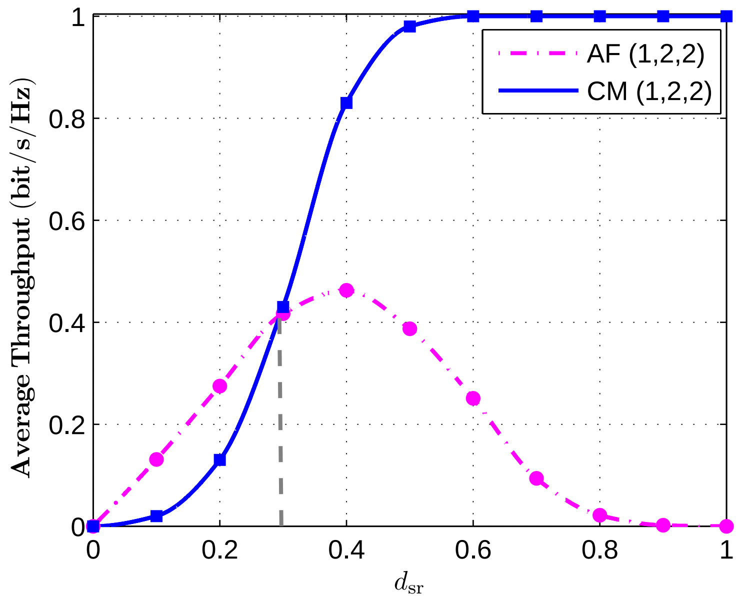

Figure 4.6: Average throughput versus d_{sr} at medium SNR, with $\overline{\gamma} = -5$ dB, $(n_{\mathrm{s}}, n_{\mathrm{r}}, n_{\mathrm{d}}) = (1, 2, 2)$, $L_{\mathrm{sr}} = L_{\mathrm{rd}} = L_{\mathrm{sd}} = 3$, and $\kappa = 3$.

4.6.2.2 Average throughput versus distance

Let us now focus on the medium SNR region, where average throughput trends can be concisely evaluated for various relay locations. Fig. 4.6 and 4.7 show that CM is mostly throughput-efficient than AF, and increases as node r moves away from the source. The rationale behind it is that in the surroundings of the source node ($d_{\mathrm{sr}} < 0.3$), the relay-destination range is large, leading to the so-called keyhole effect [52]. Consequently, the $\mathrm{r} - \mathrm{d}$ channel rank dramatically drops and the cooperative spatial multiplexing becomes impractical compared to AF strategy. Therefore, CM turns out to be an efficient relaying function for uplink throughput enhancement at cell edge.

4.7 Conclusions

In this chapter, a new signal-level cooperative spatial multiplexing scheme for broadband MIMO links has been presented. We have first extended the orthogonal projection concept to the MIMO-ISI channel via a frequency domain approach, which has served to extract the

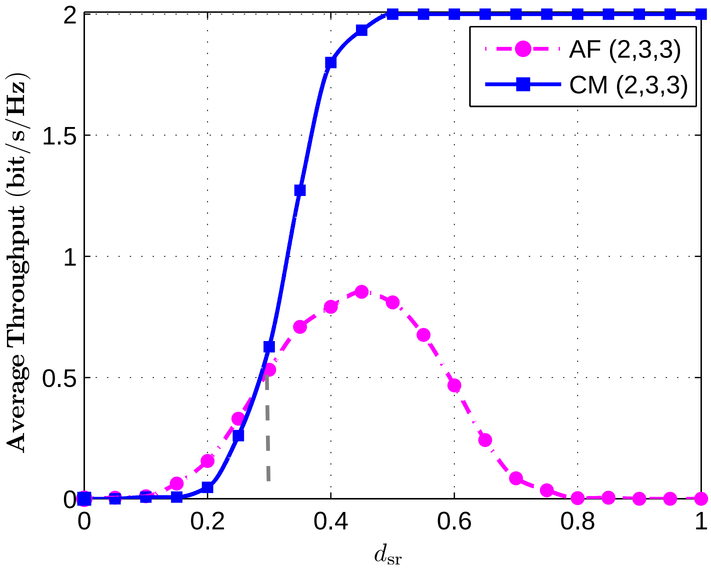

Figure 4.7: Average throughput versus $d_{\rm sr}$ at medium SNR, with $\overline{\gamma} = -3$ dB, $(n_{\rm s}, n_{\rm r}, n_{\rm d}) = (2, 3, 3)$, $L_{\rm sr} = L_{\rm rd} = L_{\rm sd} = 3$, and $\kappa = 3$.

degrees of freedom (DoFs) of the received signal and multiplex them over the relay free antennas, without resorting to any detection or re-mapping. Using the end-to-end mutual information to evaluate both the outage probability and average spectral-efficiency, it has been demonstrated that this multiplexing strategy allows for a noticeable reduction of the *half-duplex* latency, leading thereby to a great throughput enhancement. Besides, the derived communication model translates the relaying system into a point to point source-destination augmented size MIMO link, thus paving the way to adopt any joint detection and combining algorithms at the destination.

Chapter 5

Joint HARQ and PF Relaying for Single Carrier Broadband MIMO Systems

5.1 Introduction

In wireless systems, packet retransmission mechanisms play a crucial role in boosting the diversity gain. While conventional Automatic Repeat reQuest (ARQ) brings temporal diversity over block fading channels, cooperative communication, where one or multiple relays act as packet retransmitters, provides spatial diversity in the case of the so-called long-term (LT) quasi-static ARQ channels wherein all hybrid ARQ (HARQ) rounds of a single packet experience the same channel realization [5].

To convey a signal from the source to the destination, several relaying functions have been proposed. The well known ones are amplify-and-forward (AF), and decode-and-forward (DF). In the AF mode, the signal packet received from the transmitter is merely amplified and retransmitted towards the destination. The DF mode however consists on decoding then re-encoding the received data frame before forwarding it to the destination. While the first strategy suffers from noise amplification, the second one is corrupted by error propagation when the relay forwards an erroneously decoded data packet [10]. Alternatively, selective DF protocol, where the relay only transmits when it can reliably decode the data packet, has been introduced as an efficient method to reduce error propagation [12]. In their draft paper [15], the authors introduced project-and-forward (PF) as a new relaying scheme functioning over MIMO flat fading multihop relay channels. Hence, in a pure signal-level processing, a PF multi-antenna relay extracts and forwards only the degrees of freedom (DoF) contained in received signals, reducing hence the number of relay active antennas during the relaying phase and therefore the noise propagation effect at the destination. This approach leads to a power gain compared to the AF mode as well as a similar diversity gain at high signal-to-noise ratio (SNR), while presenting a lower complexity than DF that operates at the bit level.

A common limitation to all relaying schemes is that the diversity gain is increased at the cost of throughput loss due to the *half-duplex* constraint. To tackle this issue, different methods have been proposed. In addition to the schemes reported in Section 4.1, successive relaying using repetition coding has been introduced in [22] for a two-relay wireless network with flat fading. In [77], relay selection schemes have been designed for cooperative communication with DF relaying.

Under the *half-duplex* constraint, activating ARQ on the top of relaying function for rare erroneously decoded data packets enables the reduction of throughput loss. Several architectures focusing on the joint design of ARQ and relaying have raised recently. In [27], cooperative incremental redundancy HARQ scheme is devised jointly with Alamouti-based distributed space-time coding (DSTC). In [28], the authors consider a three-node relay system with HARQ on top of a hybrid relaying scheme, where the relay, based on its decoding status, switches between decode-and-forward (DF) and compress-and-forward (CF) [1] adaptively. This combined technique exhibits superior performance over direct transmission and conventional DF. In [29], a signal-level turbo packet combining strategy for multi-antenna multi-rate DF relay-assisted systems operating over broadband channel is introduced. Using *virtual antenna* concept, the authors design a MMSE-based frequency domain turbo packet combiner where each relaying slot is viewed as an additional set of virtual receive antennas. Block error rate (BLER) performance are provided to demonstrate the gains offered by the proposed combining scheme over the conventional soft information-based combining. In [30], the authors presents an alternative protocol where the source partitions the data packet into two subpackets, and broadcasts the first one to both the AF relay and the destination during the first slot. Slot 2 sees the reception of the second subpacket from the source simultaneously with a scaled version of subpacket 1 from the relay. This process is repeated at each ARQ round with the possibility to reverse the subpacket order to increase the diversity. The analysis of the joint source-relay-destination channel after two slots shows that both the average throughput and the outage probability are dramatically enhanced compared to classical AF strategy.

In this chapter, we design a new class of PF-based relays operating over single carrier frequency selective fading MIMO ARQ channels. The key idea is to consider ARQ transmissions as additional spatial diversity sources and perform a frequency domain orthogonal projection jointly over them. We show that near the high SNR region and at ARQ round k, our n_{r} antennas relay presents the same diversity gain as an AF relay with kn_{r} real antennas while realizing an important power gain over it.

The rest of the chapter is organized as follows: In Section 5.2, we present the general

[1] Compress-and-forward (CF) relaying schemes refer to cases where the relay forwards quantized, estimated or compressed (in the sense of distributed source coding) versions of its observation to the destination. The amount of extracted information depends on the capacity of the $\mathrm{r}-\mathrm{d}$ link. Indeed, it has been shown that CF outperforms DF when the relay is farther from the source (i.e., decoding is less reliable) and closer to the destination (i.e., more information can be conveyed to the destination through the $\mathrm{r}-\mathrm{d}$ channel) [78].

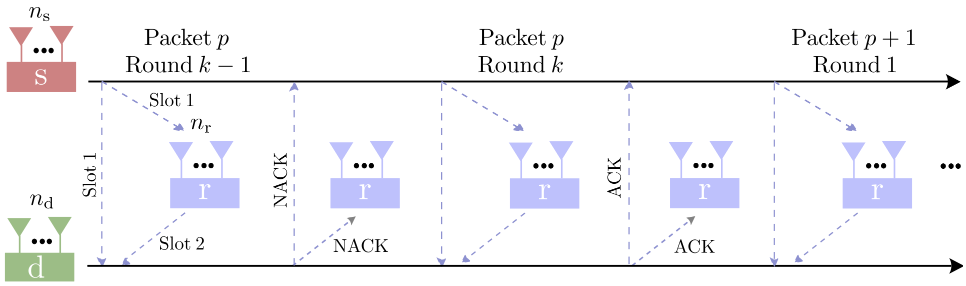

Figure 5.1: Relay ARQ protocol

framework of the considered system then introduce the adopted relay-aided ARQ transmission and its corresponding communication model. Section 5.3 details the different stages of the proposed joint-over-transmissions PF relaying scheme. The equivalent MIMO-ARQ channel and its performance analysis tools are presented in Section 5.4. Section 5.5 is devoted to numerical results. Finally, the chapter is concluded in Section 5.6.

5.2 Relay ARQ Communication Model

5.2.1 General Framework

We consider a single carrier broadband MIMO cooperative system that consists of a n_s-antennas source, a n_r-antennas relay, and a n_d-antennas destination ($n_\mathrm{r} \geq n_\mathrm{s}$). The relay node is equipped with a buffer where received signals are stored. The relaying mode is *half-duplex* oriented, requiring hence two consecutive time slots (TS) per data frame. The upper layer of the system supports an ARQ mechanism based on the *stop and wait* (SW) protocol and the well known Chase-type packet retransmission scheme, where the transmitter resends the same packet at each ARQ round. At the destination side, ARQ transmissions are combined prior to the decoding. If a packet is successfully decoded, a positive acknowledgment (ACK) message is returned to both the source and the relay through an error-free feedback channel with zero delay, letting the transmitter send the next frame. Otherwise, a negative acknowledgment (NACK) message is sent back indicating a decoding failure, and a retransmission is consequently performed by the source. If the decoding outcome is still erroneous after a preset maximum number of transmissions K (index $k = 1, \cdots, K$) is reached, an error is declared and the packet is deleted from both the source and the relay buffers. Each link $\epsilon - \epsilon'$, $\epsilon \in \{\mathrm{s}, \mathrm{r}\}$ and $\epsilon' \in \{\mathrm{r}, \mathrm{d}\}$, experiences two fading effects:

- Large-scale fading: where the average link loss $\alpha_{\epsilon\epsilon'}$, related to free space propagation and shadowing effect, is modeled as $\alpha_{\epsilon\epsilon'} = d_{\epsilon\epsilon'}^{-\kappa/2}$, with $d_{\epsilon\epsilon'}$ and κ being the range of link $\epsilon - \epsilon'$ and the path loss exponent, respectively.

- Small-scale fading: due to the broadband nature of the transmitted signals, each link $\epsilon - \epsilon'$ is assumed to be a block fading quasi-static MIMO-ISI channel of memory $L_{\epsilon\epsilon'} - 1$

(index $l = 0, \cdots, L_{\epsilon\epsilon'} - 1$). At ARQ round k, the lth path is represented by channel matrix $\mathbf{H}^{(k)}_{\epsilon\epsilon',l}$ whose coefficients are independent and identically distributed (i.i.d.) zero-mean circularly symmetric Gaussian random variables, having a variance $1/L_{\epsilon\epsilon'}$ under a normalized equal power-delay profile assumption. Therefore, the total average received power per each receive antenna (at both the relay and the receiver) is equal to n_s when no large scale fading is considered.

5.2.2 Relay-aided ARQ Transmission

At ARQ round k, the transmitter generates a data packet according to the so-called space-time bit interleaved coded modulation (ST-BICM) scheme. It is expressed as a $n_\mathrm{s} \times T$ symbol matrix $\mathbf{S}$,

$$\mathbf{S} \triangleq \left[\mathbf{s}_0, \ldots, \mathbf{s}_{T-1}\right], \tag{5.1}$$

where T (index $t = 0, \cdots, T-1$) is the total number of channel uses (c.u.), and $\mathbf{s}_t = \left[\mathrm{s}_{1,t}, \ldots, \mathrm{s}_{n_\mathrm{s},t}\right]^\mathrm{T} \in \mathcal{A}^{n_\mathrm{s}}$ is the symbol vector at c.u t, with $\mathcal{A}$ being the normalized constellation alphabet. We assume that the source has no channel state information (CSI). Therefore, equal transmit power allocation is the optimal choice [51]. Also, we suppose a sufficiently deep interleaving in such a way information bits entering the modulator are i.i.d. and equally likely. Consequently, symbols are zero mean and independent in both space and time dimensions. Their cross-correlation is given by

$$\mathrm{E}\left[\mathbf{s}_t \mathbf{s}_{t'}^\mathrm{H}\right] = \delta_{t,t'} \mathbf{I}_{n_\mathrm{s}}. \tag{5.2}$$

To prevent interblock interference (IBI), a cyclic prefix (CP) of length $L_\mathrm{CP} = \max\{L_\mathrm{sr}, L_\mathrm{rd}, L_\mathrm{sd}\}$ is appended to each transmitted packet in the system (i.e., at both the source and the relay nodes).

Now, let us focus on the progress of this relay ARQ transmission and the corresponding signal model. During the first slot, the transmitter broadcasts symbol frame $\mathbf{S}$ to both the destination and the relay. The CP-free baseband equivalent received signals at these two nodes can be respectively expressed as

$$\mathbf{y}^{(k)}_{\mathrm{d},t,1} = \alpha_\mathrm{sd} \sum_{l=0}^{L_\mathrm{sd}-1} \mathbf{H}^{(k)}_{\mathrm{sd},l} \mathbf{s}_{(t-l)\mathrm{mod}T} + \mathbf{w}^{(k)}_{\mathrm{d},t,1} \in \mathbb{C}^{n_\mathrm{d} \times 1}, \tag{5.3}$$

$$\mathbf{y}^{(k)}_{\mathrm{r},t} = \alpha_\mathrm{sr} \sum_{l=0}^{L_\mathrm{sr}-1} \mathbf{H}^{(k)}_{\mathrm{sr},l} \mathbf{s}_{(t-l)\mathrm{mod}T} + \mathbf{w}^{(k)}_{\mathrm{r},t} \in \mathbb{C}^{n_\mathrm{r} \times 1}. \tag{5.4}$$

In the second slot, the transmitter remains silent, while the relay projects and forwards signals $\left\{\mathbf{y}^{(k)}_{\mathrm{r},t}\right\}$ to the receiver according to the scheme presented in the next section.

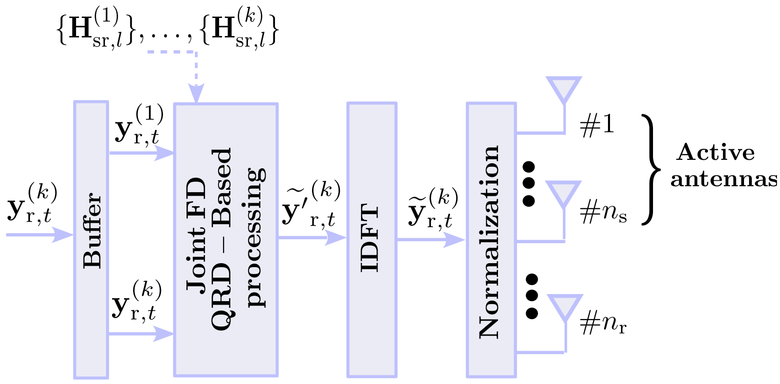

Figure 5.2: Relaying function at the kth ARQ transmission

5.3 Joint Over Transmissions Project and Forward Relaying

In this section, we design an efficient *project-and-forward* based relaying function for single carrier broadband hybrid ARQ-aided systems. As depicted in Fig. 5.2, frequency domain processing is employed to perform the orthogonal projection jointly over multiple ARQ transmissions. The resulting signal is converted to time domain, normalized, then transmitted to the destination.

5.3.1 Multi-Transmission Frequency Domain Signal Model

At the kth transmission, the relay makes use of the buffered signals $\mathbf{y}_{\mathrm{r},0}^{(1)}, \cdots, \mathbf{y}_{\mathrm{r},T-1}^{(k)}$ to construct, for each channel use t, a $kn_{\mathrm{r}} \times 1$ stacked signal vector $\underline{\mathbf{y}}_{\mathrm{r},t}^{(k)}$ as

$$\underline{\mathbf{y}}_{\mathrm{r},t}^{(k)} \triangleq \left[\mathbf{y}_{\mathrm{r},t}^{(1)^{\mathrm{T}}}, \cdots, \mathbf{y}_{\mathrm{r},t}^{(k)^{\mathrm{T}}}\right]^{\mathrm{T}}, \tag{5.5}$$

which is explicitly given by

$$\underline{\mathbf{y}}_{\mathrm{r},t}^{(k)} = \alpha_{\mathrm{sr}} \sum_{l=0}^{L_{\mathrm{sr}}-1} \underline{\mathbf{H}}_{\mathrm{sr},l}^{(k)} \mathbf{s}_{(t-l) \bmod T} + \underline{\mathbf{w}}_{\mathrm{r},t}^{(k)}, \tag{5.6}$$

where matrix $\underline{\mathbf{H}}_{\mathrm{sr},l}^{(k)} \in \mathbb{C}^{kn_{\mathrm{r}} \times n_{\mathrm{s}}}$ gathers the lth path channel matrices for the k transmissions,

$$\underline{\mathbf{H}}_{\mathrm{sr},l}^{(k)} \triangleq \begin{bmatrix} \mathbf{H}_{\mathrm{sr},l}^{(1)} \\ \vdots \\ \mathbf{H}_{\mathrm{sr},l}^{(k)} \end{bmatrix}, \tag{5.7}$$

and $\underline{\mathbf{w}}_{\mathrm{r},t}^{(k)} = \left[\mathbf{w}_{\mathrm{r},t}^{(1)^{\mathrm{T}}}, \cdots, \mathbf{w}_{\mathrm{r},t}^{(k)^{\mathrm{T}}}\right]^{\mathrm{T}} \in \mathbb{C}^{kn_{\mathrm{r}}}$ is a vector of zero-mean Gaussian noise with covariance $\sigma^2\mathbf{I}_{kn_{\mathrm{r}}}$. To jointly capture the k transmissions diversities, we arrange signals $\underline{\mathbf{y}}_{\mathrm{r},0}^{(k)}, \ldots, \underline{\mathbf{y}}_{\mathrm{r},T-1}^{(k)}$ into a $kn_{\mathrm{r}}T \times 1$ vector $\underline{\mathbf{y}}_{\mathrm{r}}^{(k)}$,

$$\underline{\mathbf{y}}_{\mathrm{r}}^{(k)} \triangleq \left[\underline{\mathbf{y}}_{\mathrm{r},0}^{(k)^{\mathrm{T}}}, \ldots, \underline{\mathbf{y}}_{\mathrm{r},T-1}^{(k)^{\mathrm{T}}}\right]^{\mathrm{T}}. \tag{5.8}$$

This yields the block-wise communication model expressed as

$$\underline{\mathbf{y}}_{\mathrm{r}}^{(k)} = \underline{\mathbf{H}}_{\mathrm{sr}}^{(k)}\mathbf{s} + \underline{\mathbf{w}}_{\mathrm{r}}^{(k)}, \tag{5.9}$$

where

$$\mathbf{s} \triangleq \left[\mathbf{s}_0^{\mathrm{T}}, \ldots, \mathbf{s}_{T-1}^{\mathrm{T}}\right]^{\mathrm{T}} \in \mathcal{A}^{n_{\mathrm{s}}T}, \tag{5.10}$$

$$\underline{\mathbf{w}}_{\mathrm{r}}^{(k)} \triangleq \left[\underline{\mathbf{w}}_{\mathrm{r},0}^{(k)^{\mathrm{T}}}, \ldots, \underline{\mathbf{w}}_{\mathrm{r},T-1}^{(k)^{\mathrm{T}}}\right]^{\mathrm{T}} \in \mathbb{C}^{kn_{\mathrm{r}}T\times 1}, \tag{5.11}$$

and $\underline{\mathbf{H}}_{\mathrm{sr}}^{(k)}$ is a $kn_{\mathrm{r}}T \times n_{\mathrm{s}}T$ block circulant matrix whose first column is

$$\left[\underline{\mathbf{H}}_{\mathrm{sr},0}^{(k)^{\mathrm{T}}}, \cdots, \underline{\mathbf{H}}_{\mathrm{sr},L_{\mathrm{sr}}-1}^{(k)^{\mathrm{T}}}, \mathbf{0}_{n_{\mathrm{s}}\times kn_{\mathrm{r}}(T-L_{\mathrm{sr}})}\right]^{\mathrm{T}}. \tag{5.12}$$

$\underline{\mathbf{H}}_{\mathrm{sr}}^{(k)}$ can therefore be block diagonalized in a Fourier basis as

$$\underline{\mathbf{H}}_{\mathrm{sr}}^{(k)} = \mathbf{U}_{T,kn_{\mathrm{r}}}^{\mathrm{H}}\mathbf{C}_{\mathrm{sr}}^{(k)}\mathbf{U}_{T,Nn_{\mathrm{s}}} \tag{5.13}$$

where

$$\mathbf{C}_{\mathrm{sr}}^{(k)} \triangleq \mathrm{diag}\left\{\mathbf{C}_{\mathrm{sr},0}^{(k)}, \cdots, \mathbf{C}_{\mathrm{sr},T-1}^{(k)}\right\} \in \mathbb{C}^{kNn_{\mathrm{r}}T\times Tn_{\mathrm{s}}}, \tag{5.14}$$

and $\mathbf{C}_{\mathrm{sr},t}^{(k)}$ is the channel frequency response (CFR) at the tth bin. It is expressed as

$$\mathbf{C}_{\mathrm{sr},t}^{(k)} = \sum_{l=0}^{L_{\mathrm{sr}}-1} \underline{\mathbf{H}}_{\mathrm{sr},l}^{(k)} \exp\left\{-j\frac{2\pi tl}{T}\right\} \in \mathbb{C}^{kn_{\mathrm{r}}\times n_{\mathrm{s}}}. \tag{5.15}$$

By applying the DFT to signal $\underline{\mathbf{y}}_{\mathrm{r}}^{(k)}$, we finally get the frequency domain signal model as

$$\underline{\mathbf{y}}'^{(k)}_{\mathrm{r}} = \alpha_{\mathrm{sr}}\mathbf{C}_{\mathrm{sr}}^{(k)}\mathbf{s}' + \underline{\mathbf{w}}'^{(k)}_{\mathrm{r}}, \tag{5.16}$$

where

$$\begin{cases} \underline{\mathbf{y}}'^{(k)}_{\mathrm{r}} \triangleq \left[\underline{\mathbf{y}}'^{(k)^{\mathrm{T}}}_{\mathrm{r},0}, \ldots, \underline{\mathbf{y}}'^{(k)^{\mathrm{T}}}_{\mathrm{r},T-1}\right]^{\mathrm{T}} \in \mathbb{C}^{kn_{\mathrm{r}}T}, \\ \mathbf{s}' \triangleq \left[\mathbf{s}'^{\mathrm{T}}_0, \ldots, \mathbf{s}'^{\mathrm{T}}_{T-1}\right]^{\mathrm{T}} \in \mathcal{A}^{n_{\mathrm{s}}T}, \\ \underline{\mathbf{w}}'^{(k)}_{\mathrm{r}} \triangleq \left[\underline{\mathbf{w}}'^{(k)}_{\mathrm{r},0}, \ldots, \underline{\mathbf{w}}'^{(k)}_{\mathrm{r},T-1}\right]^{\mathrm{T}} \in \mathbb{C}^{kn_{\mathrm{r}}T}. \end{cases} \tag{5.17}$$

5.3.2 Joint Over Transmissions QRD-based Projection

From (5.16), the $\mathrm{s}-\mathrm{r}$ channel can be viewed as a set of T flat fading $kn_\mathrm{r}\times n_\mathrm{s}$ MIMO channels. The component-wise communication model at the tth frequency bin can be described by

$$\underline{\mathbf{y}}'^{(k)}_{\mathrm{r},t} = \alpha_{\mathrm{sr}}\mathbf{C}^{(k)}_{\mathrm{sr},t}\mathbf{s}'_t + \underline{\mathbf{w}}'^{(k)}_{\mathrm{r},t}. \tag{5.18}$$

By invoking (5.15),$\mathbf{C}^{(k)}_{\mathrm{sr},t}$ is assumed full rank since it is a linear combination of independent Gaussian matrices. Therefore, the number of degrees of freedom (DoF) corresponding to the $kn_\mathrm{r}\times 1$ virtual signal vector $\underline{\mathbf{y}}'^{(k)}_{\mathrm{r},t}$ is equal to rank $\left(\mathbf{C}^{(k)}_{\mathrm{sr},t}\right) = \min\{kn_r, n_s\} = n_s$. As such, the relay can virtually convey the k transmissions using only n_s antennas. To extract these DoFs, let us take the QR decompositions [53] of matrices $\mathbf{C}^{(k)}_{\mathrm{sr},t}, t = 0,\cdots,T-1$,

$$\mathbf{C}^{(k)}_{\mathrm{sr},t} = \underline{\mathbf{Q}}^{(k)}_t\underline{\mathbf{R}}^{(k)}_t, \tag{5.19}$$

with

$$\begin{cases} \underline{\mathbf{Q}}^{(k)}_t = \begin{bmatrix} \mathbf{Q}^{(k)}_t & \mathbf{Q}'^{(k)}_t \end{bmatrix}, \\ \underline{\mathbf{R}}^{(k)}_t = \begin{bmatrix} \mathbf{R}^{(k)}_t \\ \mathbf{0}_{(kn_\mathrm{r}-n_\mathrm{s})\times n_\mathrm{s}} \end{bmatrix}, \end{cases} \tag{5.20}$$

where$\mathbf{Q}^{(k)}_t$ is a $(kn_\mathrm{r}\times n_\mathrm{s})$ matrix verifying $\mathbf{Q}^{(k)^\mathrm{H}}_t\mathbf{Q}^{(k)}_t = \mathbf{I}_{n_\mathrm{s}}$, and $\mathbf{R}^{(k)}_t$ is a $n_\mathrm{s}\times n_\mathrm{s}$ upper triangular matrix. The above QR decomposition can then be rewritten as

$$\mathbf{C}^{(k)}_{\mathrm{sr},t} = \mathbf{Q}^{(k)}_t\mathbf{R}^{(k)}_t \tag{5.21}$$

The relay perform the joint projection by applying $\mathbf{Q}^{(k)^\mathrm{H}}_t$ to $\underline{\mathbf{y}}'^{(k)}_{\mathrm{r},t}$ as

$$\widetilde{\mathbf{y}}'^{(k)}_{\mathrm{r},t} = \mathbf{Q}^{(k)^\mathrm{H}}_t\underline{\mathbf{y}}'^{(k)}_{\mathrm{r},t} = \alpha_{\mathrm{sr}}\mathbf{R}^{(k)}_t\mathbf{s}'_t + \underbrace{\mathbf{Q}^{(k)^\mathrm{H}}_t\underline{\mathbf{w}}'^{(k)}_{\mathrm{r},t}}_{\widetilde{\mathbf{w}}'^{(k)}_{\mathrm{r},t}}. \tag{5.22}$$

This processing can be expressed under a block-wise form by

$$\widetilde{\mathbf{y}}'^{(k)}_{\mathrm{r}} = \alpha_{\mathrm{sr}}\mathbf{R}^{(k)}\mathbf{s}' + \widetilde{\mathbf{w}}'^{(k)}_{\mathrm{r}}, \tag{5.23}$$

where

$$\begin{cases} \widetilde{\mathbf{y}}'^{(k)}_{\mathrm{r}} & \triangleq \left[\widetilde{\mathbf{y}}'^{(k)^\mathrm{T}}_{\mathrm{r},0},\ldots,\widetilde{\mathbf{y}}'^{(k)^\mathrm{T}}_{\mathrm{r},T-1}\right]^\mathrm{T} \in \mathbb{C}^{n_\mathrm{s}T}, \\ \mathbf{R}^{(k)} & \triangleq \mathrm{diag}\left\{\mathbf{R}^{(k)}_0,\ldots,\mathbf{R}^{(k)}_{T-1}\right\} \in \mathbb{C}^{n_\mathrm{s}T\times n_\mathrm{s}T}, \\ \widetilde{\mathbf{w}}'^{(k)}_{\mathrm{r}} & \triangleq \left[\widetilde{\mathbf{w}}'^{(k)^\mathrm{T}}_{\mathrm{r},0},\ldots,\widetilde{\mathbf{w}}'^{(k)^\mathrm{T}}_{\mathrm{r},T-1}\right]^\mathrm{T} \in \mathbb{C}^{n_\mathrm{s}T}. \end{cases} \tag{5.24}$$

The relay proceeds then by converting signal $\widetilde{\mathbf{y}'}_{\mathrm{r}}^{(k)}$ to the time domain as

$$\widetilde{\mathbf{y}}_{\mathrm{r}}^{(k)} = \mathbf{U}_{T,n_{\mathrm{s}}}^{\mathrm{H}} \widetilde{\mathbf{y}'}_{\mathrm{r}}^{(k)}. \tag{5.25}$$

The resulting $n_{\mathrm{s}} \times 1$ single carrier signal at channel use t is given by

$$\widetilde{\mathbf{y}}_{\mathrm{r},t}^{(k)} = \alpha_{\mathrm{sr}} \sum_{l=0}^{T-1} \widetilde{\mathbf{H}}_{\mathrm{sr},l}^{(k)} \mathbf{s}_{(t-l)\mathrm{mod}T} + \widetilde{\mathbf{w}}_{\mathrm{r},t}^{(k)}, \tag{5.26}$$

where $\widetilde{\mathbf{w}}_{\mathrm{r},t}^{(k)} \sim \mathcal{N}\left(\mathbf{0}_{n_{\mathrm{s}}\times 1}, \sigma^2 \mathbf{I}_{n_{\mathrm{s}}}\right)$ is the additive noise. Note that due to the multiplication of CFRs $\mathbf{C}_{\mathrm{sr},t}^{(k)}$ by $\mathbf{Q}_t^{(k)\mathrm{H}}$ in the frequency domain, the $\mathrm{s}-\mathrm{r}$ channel has been transformed into a virtual $n_{\mathrm{s}} \times n_{\mathrm{s}}$ multipath channel $\widetilde{\mathbf{H}}_{\mathrm{sr},l}^{(k)}$ with memory $T-1$, expressed as

$$\widetilde{\mathbf{H}}_{\mathrm{sr},l}^{(k)} = \sum_{t=0}^{T-1} \mathbf{R}_t^{(k)} \exp\left\{ j\frac{2\pi t l}{T} \right\} \in \mathbb{C}^{n_{\mathrm{s}}\times n_{\mathrm{s}}}. \tag{5.27}$$

5.3.3 Signal Normalization

Prior to its transmission over the forward channel, the signal $\widetilde{\mathbf{y}}_{\mathrm{r},t}^{(k)}$ is normalized. For that end, let us start by computing its conditional covariance matrix. We have

$$\mathbf{\Xi}_{|\underline{\mathbf{H}}_{\mathrm{sr}}^{(k)}}^{(k)} = \mathrm{E}\left[\widetilde{\mathbf{y}}_{\mathrm{r},t}^{(k)} \widetilde{\mathbf{y}}_{\mathrm{r},t}^{(k)\mathrm{H}} \mid \left\{ \underline{\mathbf{H}}_{\mathrm{sr},l}^{(k)} \right\} \right]. \tag{5.28}$$

Under the aforementioned assumption of deep space time interleaving, and the independence between symbols and noise vectors, we get from (4.17) the developed expression of the above covariance matrix as

$$\mathbf{\Xi}_{|\underline{\mathbf{H}}_{\mathrm{sr}}^{(k)}}^{(k)} = \alpha_{\mathrm{sr}} \sum_{l=0}^{T-1} \widetilde{\mathbf{H}}_{\mathrm{sr},l}^{(k)} \widetilde{\mathbf{H}}_{\mathrm{sr},l}^{(k)\mathrm{H}} + \sigma^2 \mathbf{I}_{n_{\mathrm{s}}}. \tag{5.29}$$

On the other hand, we make use of the following lemma,

Lemma 5.3.1. *Let $\{\mathbf{H}_l\}_{0\le l\le L-1}$ be a $M \times N$ sampled signal of length L, and $\{\mathbf{\Lambda}_l\}_{0\le l\le L-1}$ is its Fourier transform. We have*

$$\sum_{l=0}^{L-1} \mathbf{H}_l \mathbf{H}_l^{\mathrm{H}} = L \sum_{l=0}^{L-1} \mathbf{\Lambda}_l \mathbf{\Lambda}_l^{\mathrm{H}}. \tag{5.30}$$

Proof. Use the orthogonality of Fourier basis.

■

By recalling that matrices $\left\{\mathbf{R}_t^{(k)}\right\}_{0\le t\le T-1}$ are the T-point Fourier transforms of matrices $\left\{\widetilde{\mathbf{H}}_{\mathrm{sr},l}^{(k)}\right\}_{0\le l\le T-1}$, and using lemma 5.3.1, the conditional covariance matrix can be computed directly in the frequency domain as

$$\boldsymbol{\Xi}^{(k)}_{|\underline{\mathbf{H}}^{(k)}_{\mathrm{sr}}} = \alpha_{\mathrm{sr}} T \sum_{t=0}^{T-1} \mathbf{R}^{(k)}_t \mathbf{R}^{(k)^{\mathrm{H}}}_t + \sigma^2 \mathbf{I}_{n_\mathrm{s}}, \tag{5.31}$$

which reduces the calculation cost in terms of complex multiplications and additions. At this level, the relay node performs the Cholesky factorization of matrix $\boldsymbol{\Xi}^{(k)}_{|\underline{\mathbf{H}}^{(k)}_{\mathrm{sr}}}$,

$$\boldsymbol{\Xi}^{(k)}_{|\underline{\mathbf{H}}^{(k)}_{\mathrm{sr}}} = \boldsymbol{\Phi}^{(k)} \boldsymbol{\Phi}^{(k)^{\mathrm{H}}}. \tag{5.32}$$

Signal $\widetilde{\mathbf{y}}^{(k)}_{\mathrm{r},t}$ is thus normalized via left multiplication by $\boldsymbol{\Phi}^{(k)^{-1}}$, then forwarded to the destination using only n_s relay antennas. In that case, antenna selection is performed according to a fixed mapping matrix,

$$\mathbf{P} = \begin{bmatrix} \mathbf{I}_{n_\mathrm{s}} \\ \mathbf{0}_{(n_\mathrm{r}-n_\mathrm{s})\times n_\mathrm{s}} \end{bmatrix}. \tag{5.33}$$

A more accurate approach would be to select antennas based on a channel feedback from the receiver, but this is out of the scope of this scheme. We recall that the relay transmissions are also CP-based.

5.3.4 Second Slot Communication Model

After CP deletion, the obtained signal at the receiver side during TS 2 is written as

$$\mathbf{y}^{(k)}_{\mathrm{d},t,2} = \alpha_{\mathrm{rd}} \sum_{l=0}^{L_{\mathrm{rd}}-1} \mathbf{H}^{(k)}_{\mathrm{rd},l} \mathbf{P} \boldsymbol{\Phi}^{(k)^{-1}} \widetilde{\mathbf{y}}^{(k)}_{\mathrm{r},(t-l)\mathrm{mod}T} + \mathbf{w}^{(k)}_{\mathrm{d},t,2}. \tag{5.34}$$

with $\mathbf{w}^{(k)}_{\mathrm{d},t,2} \sim \mathcal{N}\left(\mathbf{0}_{n_\mathrm{d}\times 1}, \sigma^2 \mathbf{I}_{n_\mathrm{d}}\right)$ denoting the additive spatio-temporal noise component at the receiver.

5.4 Equivalent MIMO Channel and Theoretical Analysis Tools

From a signal processing point of view, the presented relay-aided ARQ transmission can be viewed as an equivalent MIMO channel whose expression is derived in the following. This enables to easily introduce the outage probability and the average spectral efficiency metrics adopted as system performance assessment tools.

5.4.1 Equivalent MIMO Channel

By invoking 5.3.3 and (5.34), the sampled received $n_\mathrm{s} \times 1$ signal vector at the receiver during TS 2 is developed as

$$\mathbf{y}_{\mathrm{d},t,2}^{(k)} = \alpha_{\mathrm{sr}}\alpha_{\mathrm{rd}} \sum_{l=0}^{L_{\mathrm{srd}}-1} \mathbf{H}_{\mathrm{srd},l}^{(k)} \mathbf{s}_{(t-l)\mathrm{mod}T} + \widetilde{\mathbf{w}}_{\mathrm{d},t,2}^{(k)}, \tag{5.35}$$

where $L_{\mathrm{srd}} = T + L_{\mathrm{rd}} - 1$, and

$$\underset{0\leq l\leq L_{\mathrm{srd}}-1}{\mathbf{H}_{\mathrm{srd},l}^{(k)}} = \sum_{n=\max(0,l-T+1)}^{\min(l,L_{\mathrm{rd}}-1)} \mathbf{H}_{\mathrm{rd},n}^{(k)} \mathbf{P} {\mathbf{\Phi}^{(k)}}^{-1} \widetilde{\mathbf{H}}_{\mathrm{sr},l-n}^{(k)}. \tag{5.36}$$

On the other hand, the corresponding accumulated noise $\widetilde{\mathbf{w}}_{\mathrm{d},t,2}^{(k)}$ is given by

$$\widetilde{\mathbf{w}}_{\mathrm{d},t,2}^{(k)} = \alpha_{\mathrm{rd}} \sum_{l=0}^{L_{\mathrm{rd}}-1} \mathbf{H}_{\mathrm{rd},l}^{(k)} \mathbf{P} {\mathbf{\Phi}^{(k)}}^{-1} \widetilde{\mathbf{w}}_{\mathrm{r},(t-l)\mathrm{mod}T}^{(k)} + \mathbf{w}_{\mathrm{d},t,2}^{(k)} \tag{5.37}$$

We compute its covariance matrix as

$$\mathbf{\Lambda}_{|\mathbf{H}_{\mathrm{sr}}^{(k)}}^{(k)} = \sigma^2 \left(\alpha_{\mathrm{rd}} \sum_{l=0}^{L_{\mathrm{rd}}-1} \mathbf{H}_{\mathrm{rd},l}^{(k)} \mathbf{P} {\mathbf{\Phi}^{(k)}}^{-1} {{\mathbf{\Phi}^{(k)}}^{-1}}^{\mathrm{H}} \mathbf{P}^{\mathrm{H}} {\mathbf{H}_{\mathrm{rd},l}^{(k)}}^{\mathrm{H}} + \mathbf{I}_{n_\mathrm{d}} \right).$$

Based on the Cholesky factorization of $\mathbf{\Lambda}_{|\mathbf{H}_{\mathrm{sr}}^{(k)}}^{(k)}$, expressed as

$$\mathbf{\Lambda}_{|\mathbf{H}_{\mathrm{sr}}^{(k)}}^{(k)} = \sigma^2 \mathbf{\Psi}^{(k)} {\mathbf{\Psi}^{(k)}}^{\mathrm{H}}, \tag{5.38}$$

the whitening of noise $\widetilde{\mathbf{w}}_{\mathrm{d},t,2}^{(k)}$ is performed by applying ${\mathbf{\Psi}^{(k)}}^{-1}$ to signal vector $\mathbf{y}_{\mathrm{d},t,2}^{(k)}$,

$$\widetilde{\mathbf{y}}_{\mathrm{d},t,2}^{(k)} = {\mathbf{\Psi}^{(k)}}^{-1} \mathbf{y}_{\mathrm{d},t,2}^{(k)}. \tag{5.39}$$

Now, let us express the equivalent $2n_\mathrm{d} \times n_\mathrm{s}$ MIMO channel at round k. From (5.3), (5.35) and (5.39), we get

$$\mathbf{y}_{\mathrm{d},t}^{(k)} = \sum_{l=0}^{L-1} \mathbf{H}_{l}^{(k)} \mathbf{s}_{(t-l)\mathrm{mod}T} + \mathbf{w}_{\mathrm{d},t}^{(k)}, \tag{5.40}$$

where $L = \max(L_{\mathrm{srd}}, L_{\mathrm{sd}}) = L_{\mathrm{srd}}$, and

$$\begin{cases} \mathbf{w}_{\mathrm{d},t}^{(k)} = \begin{bmatrix} \mathbf{w}_{\mathrm{d},t,1}^{(k)^{\mathrm{T}}} & \mathbf{\Psi}^{(k)^{-1}} \widetilde{\mathbf{w}}_{\mathrm{d},t,2}^{(k)^{\mathrm{T}}} \end{bmatrix}^{\mathrm{T}}, \\ \mathbf{y}_{\mathrm{d},t}^{(k)} = \begin{bmatrix} \mathbf{y}_{\mathrm{d},t,1}^{(k)^{\mathrm{T}}} & \widetilde{\mathbf{y}}_{\mathrm{d},t,2}^{(k)^{\mathrm{T}}} \end{bmatrix}^{\mathrm{T}}, \\ \mathbf{H}_l^{(k)} = \begin{bmatrix} \alpha_{\mathrm{sd}} \widetilde{\mathbf{H}}_{\mathrm{sd},l}^{(k)} \\ \alpha_{\mathrm{sr}} \alpha_{\mathrm{rd}} \mathbf{\Psi}^{(k)^{-1}} \mathbf{H}_{\mathrm{srd},l}^{(k)} \end{bmatrix}. \end{cases} \tag{5.41}$$

with

$$\widetilde{\mathbf{H}}_{\mathrm{sd},l}^{(k)} = \begin{cases} \mathbf{H}_{\mathrm{sd},l}^{(k)} & , 0 \le l \le L_{\mathrm{sd}} - 1 \\ \mathbf{0}_{n_{\mathrm{d}} \times n_{\mathrm{s}}} & , L_{\mathrm{sd}} \le l \le L \end{cases}. \tag{5.42}$$

Finally, the $2kn_{\mathrm{d}} \times n_{\mathrm{s}}$ multi-transmission MIMO channel can be described by

$$\underbrace{\begin{bmatrix} \mathbf{y}_{\mathrm{d},t}^{(1)} \\ \vdots \\ \mathbf{y}_{\mathrm{d},t}^{(k)} \end{bmatrix}}_{\underline{\mathbf{y}}_{\mathrm{d},t}^{(k)}} = \sum_{l=0}^{L-1} \underbrace{\begin{bmatrix} \mathbf{H}_l^{(1)} \\ \vdots \\ \mathbf{H}_l^{(k)} \end{bmatrix}}_{\underline{\mathbf{H}}_l^{(k)}} \mathbf{s}_{(t-l) \bmod T} + \underbrace{\begin{bmatrix} \mathbf{w}_{\mathrm{d},t}^{(1)} \\ \vdots \\ \mathbf{w}_{\mathrm{d},t}^{(k)} \end{bmatrix}}_{\underline{\mathbf{w}}_{\mathrm{d},t}^{(k)}}. \tag{5.43}$$

5.4.2 Outage Probability

By considering the above $2kn_{\mathrm{d}} \times n_{\mathrm{s}}$ virtual MIMO channel created at the kth ARQ round between the transmitting and receiving nodes, we can define a corresponding outage event that indicates that the channel is so poor such that the target data rate is not supported. In this case, the outage probability $P_{\mathrm{out}}(\overline{\gamma}, \mathcal{S})$ is the probability that the mutual information between $\mathbf{s}$ and $\underline{\mathbf{y}}_{\mathrm{d},t}^{(k)}$ at a given average signal-to-noise ratio (SNR) per receive antenna $\overline{\gamma}$, and channel realization $\left\{\underline{\mathbf{H}}_l^{(k)}\right\}$, is lower than the source information spectral efficiency $\mathcal{S}$. It can be expressed as

$$P_{\mathrm{out}}(\overline{\gamma}, \mathcal{S}) = \Pr\left\{ \frac{1}{2k} I\left(\mathbf{s}, \underline{\mathbf{y}}_{\mathrm{d},t}^{(k)} \mid \left\{\underline{\mathbf{H}}_l^{(k)}\right\}, \overline{\gamma}\right) < \mathcal{S} \right\}. \tag{5.44}$$

The mutual information $I\left(\mathbf{s}, \underline{\mathbf{y}}_{\mathrm{d},t}^{(k)} \mid \left\{\underline{\mathbf{H}}_l^{(k)}\right\}, \overline{\gamma}\right)$ represents the effective amount of information about $\mathbf{s}$ contained in $\underline{\mathbf{y}}_{\mathrm{d},t}^{(k)}$. It is approximated by assuming that the digital modulator delivers Gaussian i.i.d. symbols stream to the channel [57],

$$I\left(\mathbf{s}, \underline{\mathbf{y}}_{\mathrm{d},t}^{(k)} \mid \left\{\underline{\mathbf{H}}_l^{(k)}\right\}, \overline{\gamma}\right) \approx \frac{1}{T} \sum_{t=0}^{T-1} \log_2\left(\det\left(\mathbf{I}_{kn_{\mathrm{d}}} + \frac{\overline{\gamma}}{n_{\mathrm{s}}} \underline{\mathbf{C}}_t^{(k)} \underline{\mathbf{C}}_t^{(k)^{\mathrm{H}}}\right)\right),$$

where $\underline{\mathbf{C}}_t^{(k)}$ is the tth sample of the discrete Fourier transform (DFT) of $\left\{\underline{\mathbf{H}}_l^{(k)}\right\}$, i.e.,

$$\underline{\mathbf{C}}_t^{(k)} = \sum_{l=0}^{L-1} \underline{\mathbf{H}}_l^{(k)} \exp\left\{-j\frac{2\pi t}{T}(l)\mathrm{mod}T\right\}. \tag{5.45}$$

The $\frac{1}{2k}$ distortion factor in (5.44) is due to the fact that one c.u. of the virtual MIMO channel (5.43) corresponds to $2k$ temporal c.u. for the system.

5.4.3 Average Spectral Efficiency

To characterize the effectiveness by which the considered MIMO-ARQ system uses the transmission bandwidth, we make use of the average throughput metric defined for a maximum number of ARQ rounds K as [58]

$$\overline{\mathcal{T}} = \frac{\mathrm{E}\left[u\right]}{\mathrm{E}\left[n\right]}. \tag{5.46}$$

In (5.46), u is a random variable (RV) taking on values $\mathcal{S}$ and 0 with probabilities $1-\overline{P}_{\text{out}}\left(\overline{\gamma},\mathcal{S}\right)$ (in the case of successful packet decoding) and $\overline{P}_{\text{out}}\left(\overline{\gamma},\mathcal{S}\right)$ (when the decoding outcome is erroneous), respectively. Therefore,

$$\mathrm{E}\left[u\right] = \mathcal{S}\left(1-\overline{P}_{\text{out}}\left(\overline{\gamma},\mathcal{S}\right)\right), \tag{5.47}$$

with $\overline{P}_{\text{out}}\left(\overline{\gamma},\mathcal{S}\right)$ is the outage probability corresponding to (5.43), but without dividing the mutual information by k in (5.44). Indeed, this distortion effect can be modeled by the random variable n taking values in the set $\{1,\ldots,K\}$. This RV represents the number of ARQ rounds consumed to correctly decode a given data packet.

5.5 Simulation Results

5.5.1 Simulation Settings

In this section, we investigate via Monte-Carlo simulations on (5.44) and (5.46) the outage probability and the average throughput performances achieved by the JT-PF scheme, respectively. As a benchmark, we adopt a similar *half-duplex* cooperative MIMO-ARQ system where relaying is carried out according to a two-slotted amplify-and-forward (AF) function. Also, we consider that the AF relay has no buffering capability. To ensure a fair comparison, the two systems must have the same SNR levels in the three links, i.e. $\mathrm{s}-\mathrm{d}$, $\mathrm{s}-\mathrm{r}$, and $\mathrm{r}-\mathrm{d}$. By assuming identical large-scale fading conditions for both schemes, SNRs will depend only on small-scale fading parameters. As mentioned in subsection 5.2.1, the total average received power at each receive antenna is equal to the number of antennas of the corresponding transmitting node. Since the two systems have the same antennas configuration, they will present

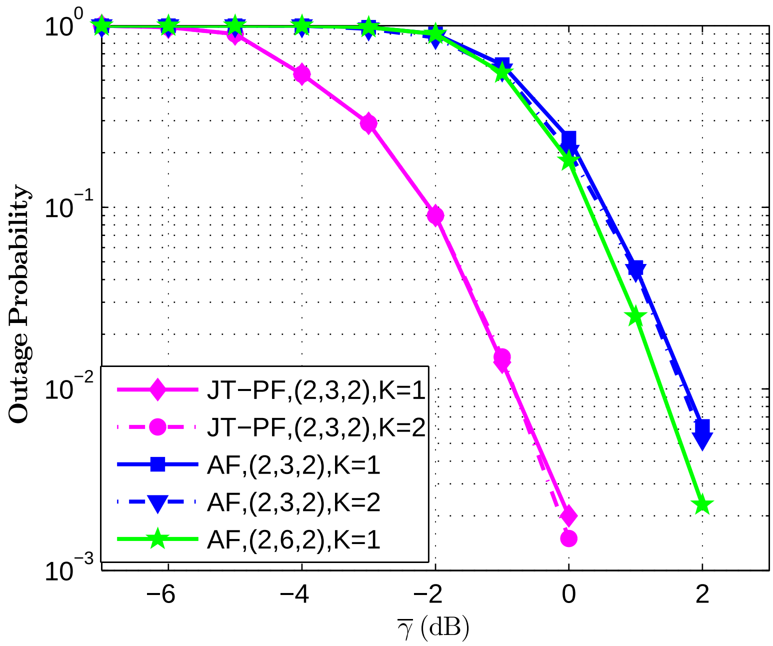

Figure 5.3: Outage probability versus $\overline{\gamma}$ for $(n_{\mathrm{s}}, n_{\mathrm{r}}, n_{\mathrm{d}}) = (2, 3, 2)$

similar SNR levels in links $\mathrm{s}-\mathrm{d}$ and $\mathrm{s}-\mathrm{r}$, where

$$\begin{cases} \overline{\gamma}^{\mathrm{PF}}_{\mathrm{sd}} = \overline{\gamma}^{\mathrm{AF}}_{\mathrm{sd}} = \frac{\alpha^2_{\mathrm{sd}} n_{\mathrm{s}}}{\sigma^2} = \overline{\gamma}, \\ \overline{\gamma}^{\mathrm{PF}}_{\mathrm{sr}} = \overline{\gamma}^{\mathrm{AF}}_{\mathrm{sr}} = \frac{\alpha^2_{\mathrm{sr}} n_{\mathrm{s}}}{\sigma^2}. \end{cases} \tag{5.48}$$

On the contrary, the mere SNR difference resides in link $\mathrm{r}-\mathrm{d}$. In fact, at ARQ round k, the JT-PF-based relay only requires n_{s} antennas out of n_{r} to forward the received signal. Therefore,

$$\begin{aligned} \overline{\gamma}^{\mathrm{PF}}_{\mathrm{rd}} &= \frac{\alpha^2_{\mathrm{rd}} n_{\mathrm{s}}}{\sigma^2} \\ &\leq \frac{\alpha^2_{\mathrm{rd}} n_{\mathrm{r}}}{\sigma^2} \quad = \overline{\gamma}^{\mathrm{AF}}_{\mathrm{rd}}. \end{aligned}$$

To balance the forward links of the two systems, we increase the average transmit power of the JT-PF relay by a factor $= \frac{n_{\mathrm{r}}}{n_{\mathrm{s}}}$.

For all simulation scenarios, all links have the same length $L_{\mathrm{sd}} = L_{\mathrm{sr}} = L_{\mathrm{rd}} = 3$, and without loss of generality, the relay is assumed to be at the medium of the direct link, i.e., $d_{\mathrm{sr}} + d_{\mathrm{rd}} = d_{\mathrm{sd}} = 1$ and $d_{\mathrm{sr}} = 0.5$ (in terms of normalized distances). The path loss exponent is set to $\kappa = 3$, and we choose $T = 128$ c.u. By considering a $\frac{1}{2}$-rate convolutional encoder and QPSK signaling at the transmitter, the target rate $\mathcal{S}$ is equal to n_{s} (bit/s/Hz).

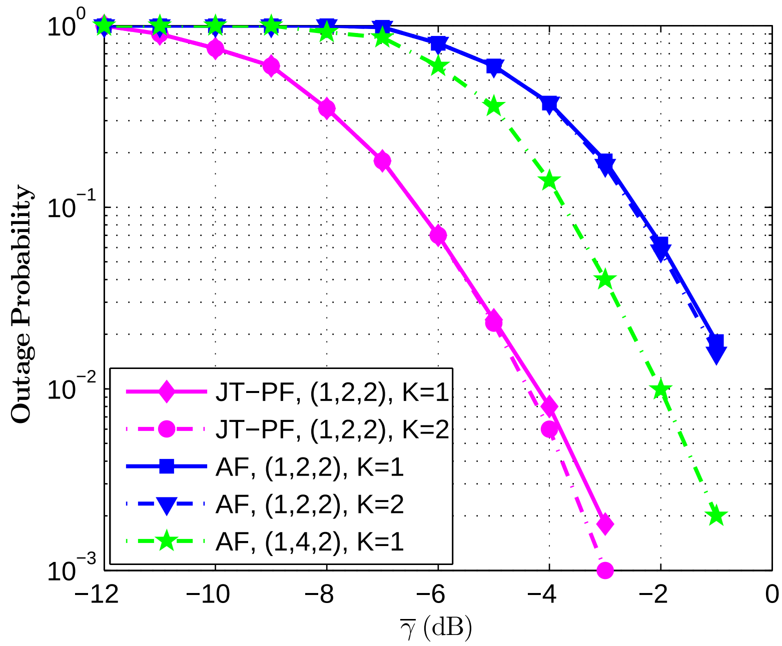

Figure 5.4: Outage probability versus $\overline{\gamma}$ for $(n_\mathrm{s}, n_\mathrm{r}, n_\mathrm{d}) = (1, 2, 2)$.

5.5.2 Performance Analysis

Both Fig. 5.3 and 5.4 show that JT-PF presents a concrete gain compared to AF. This is due to the reduction of the number of transmit antennas at the relay, minimizing thereby the noise hardening effect [15], and avoiding also overloaded antennas configuration (i.e., $n_\mathrm{r} > n_\mathrm{d}$). For instance, a gap of 2.3 dB is observed between the two schemes at 10^{-1} outage when $(n_\mathrm{s}, n_\mathrm{r}, n_\mathrm{d}) = (2, 3, 2)$ and $K = 1$ (i.e., no ARQ). At high SNR, JT-PF and AF achieve the same diversity gain since their outage probability curves' slopes are similar. When hybrid-ARQ is activated, JT-PF is operating on kn_r virtual receive antennas at ARQ round k. In high SNR region, it becomes diversity equivalent to the AF system with kn_r real relay antennas and no ARQ. For example, Fig. 5.4 demonstrates that when $\overline{\gamma} \geq -5$ dB, JT-PF with $(n_\mathrm{s}, n_\mathrm{r}, n_\mathrm{d}) = (1, 2, 2)$ and $K = 2$ has the same curve slope as AF with $(n_\mathrm{s}, n_\mathrm{r}, n_\mathrm{d}) = (1, 4, 2)$ and $K = 1$.

On the other hand, the proposed relaying scheme outperforms the AF in term of average throughput. While the first reaches the maximum throughput at 0 dB, the latter achieves it at $\overline{\gamma} \geq 2$ dB as depicted in Fig. 5.5. From Fig.5.6 we can see that the throughput performance gap between the two systems becomes clearer and approximately attains 4 dB for the entire SNR range.

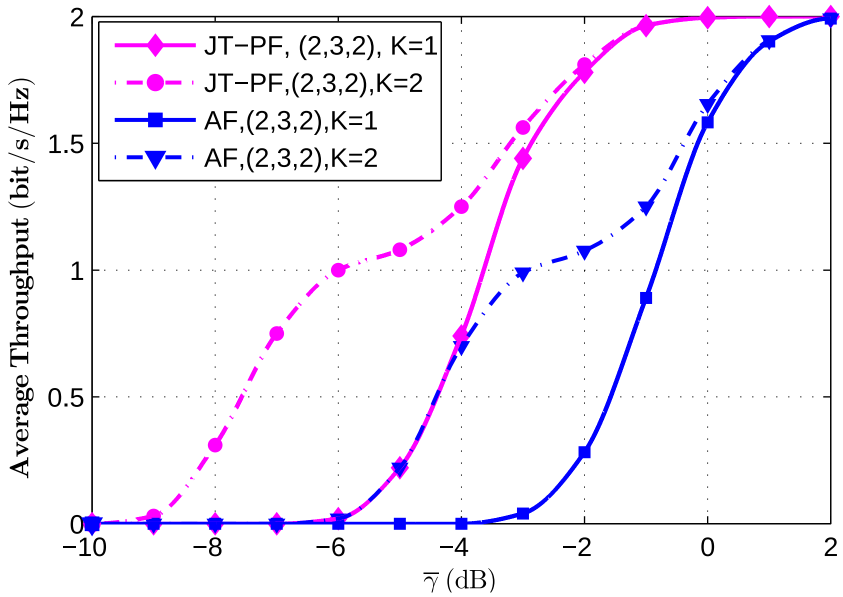

Figure 5.5: Average throughput versus $\overline{\gamma}$ for $(n_{\mathrm{s}}, n_{\mathrm{r}}, n_{\mathrm{d}}) = (2, 3, 2)$

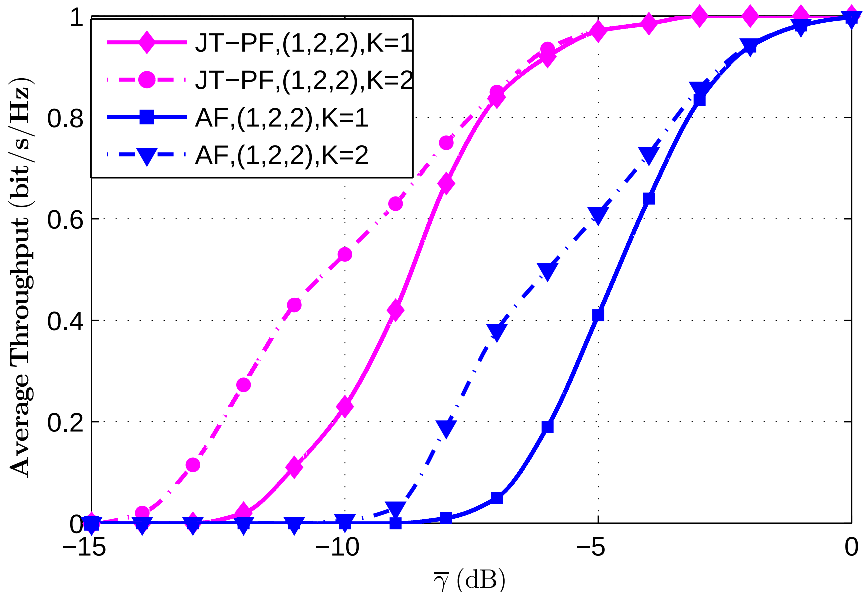

Figure 5.6: Average throughput versus $\overline{\gamma}$ for $(n_{\mathrm{s}}, n_{\mathrm{r}}, n_{\mathrm{d}}) = (1, 2, 2)$.

5.6 Conclusions

In this chapter, a new family of PF-based relays applicable to single carrier MIMO-ISI-ARQ channels has been presented. In a cross-layer approach, the proposed relay considers each ARQ transmission as an additional set of virtual antennas and carries out a joint projection over them. The devised frequency-domain communication model masks the cooperation in such a way the destination views the relay forwarded signals as direct retransmissions from the source, which enables to adopt any joint equalization and combining strategies at the destination side. Monte-Carlo simulations on the outage probability and the average throughput have shown the significant increase the system can provide in terms of diversity and SNR gains compared with AF relaying schemes. At high SNR regime and at ARQ round k, our n_r antennas relay presents the same diversity gain as an AF relay with kn_r real antennas.

Chapter 6

Conclusions

6.1 Summary of Contributions

In this dissertation, signal-level relaying strategies for single carrier broadband MIMO systems have been addressed in different frameworks. As a validation step, a novel end-to-end performance analysis of PF relaying under the practical scenario of mixed MIMO-pinhole and Rayleigh dual-hop channel has been initially conducted using a variety of generalized mathematical functions in Chapter 3. The asymptotic behavior of both the derived outage probability and ergodic capacity metrics have then been inferred using the residue theory; an artifact that yields expansions of the complex Mellin-Barnes integrals involved in the analysis. The obtained expressions have shown that the PF system performance is mainly governed by the relay-destination link and the number of antennas; whence it has been recommended—to build efficient PF-based relaying schemes—that we ought to exploit the PF relay free antennas as well as the implicit combining brought by the projection operation. For numerical evaluation purposes, we have developed a novel and fast MATLAB routine for the bivariate Meijer-G function, enabling an automated definition of the complex contour, since the existing MATHEMATICA version had settled only to a tricky manual implementation. Analytical curves have been confirmed with Monte-Carlo simulation results, and can be used by system designers to define SNR threshold for switching between PF and other relaying schemes in pinhole conditions.

In chapter 4, invoking the PF design guidelines stemming form the theoretical study, a new signal-level PF-based cooperative spatial multiplexing scheme has been devised to drastically improve the throughput in half-duplex relay-assisted broadband MIMO systems. For that end, the orthogonal projection has first been extended to the MIMO-ISI channel via a frequency domain approach. Accordingly, the degrees of freedom (DoFs) of the received signal have been extracted and multiplexed over the relay antennas that have been driven vacant by the so-called projection; a processing that does not require any detection or re-mapping. Besides, an adequate communication model has been derived in such a way to make the cooperation seamless for the destination; as though the relay signals are a direct retransmissions from the source, which paves the way to adopt any joint detection and combining algorithms at the destination. Based on the end-to-end mutual information, the average spectral-efficiency of the proposed spatial multiplexing strategy has been evaluated, and turns out to outperform AF's one in almost all relay locations, and—unlike the vanishing AF performance—it achieves the full modulation spectral-efficiency when the relay draws close to the destination.

Finally, PF-based relaying has been extended to the single carrier MIMO-ISI-ARQ channel in chapter 5, where through a cross-layer approach, the proposed relay considers each ARQ transmission as an additional set of virtual antennas and carries out a joint projection over them. The devised frequency-domain communication model masks the cooperation in such a way the destination views the relay forwarded signals as direct retransmissions from the source, which translates the relaying system into a point-to-point augmented size source-destination MIMO transmission. Using the outage probability and average throughput tools, it has been demonstrated that the introduced joint PF-ARQ architecture has higher performance in terms of diversity and SNR gains compared with AF relaying schemes; at high SNR regime and at ARQ round k, our n_r antennas relay presents the same diversity gain as an AF relay with kn_r real antennas.

6.2 Future Research Directions

Having outlined the thesis contributions, several research axes remain open to future investigations:

1. Extend the analysis conducted for the pinhole channel to the general case of arbitrary rank MIMO channels for both AF and PF schemes.

2. As PF relaying optimizes the number of relay active antennas, we might study its energy-efficiency with respect to a practical channel rank probability distribution.

3. While the presented performance analysis has focused on the pure gain brought by PF relaying, the inclusion of both space-time coding and diversity combining (e.g., MRC) effects would help to draw supplementary conclusions with respect to system design.

4. The wide set of mathematical tools, including the used generalized functions (Meijer-G functions of one and two variables), their more general versions (Fox-H and I functions), as well as the residue theory might be used to characterize the performance of 5G wireless communication systems in a variety of channel models.

5. The introduced PF-based spatial multiplexing and hybrid-ARQ architectures operate over the MIMO uncorrelated Rayleigh broadband channel, whose rank depends only on the number of antennas. This framework might be extended to the case of arbitrary rank-deficient MIMO channels with antennas correlation to reflect the impact.

Appendix A

Some Generalized Functions Definitions

A.1 Meijer-G Function

The Meijer-G function is defined in terms of a Mellin-Barnes integral as [67, Eq. (9.301)]

$$\mathrm{G}_{p,q}^{m,n}\left(z\,\middle|\,\begin{matrix}a_1,\ldots,a_p\\ b_1,\ldots,b_q\end{matrix}\right)=\frac{1}{2\pi j}\int_C\frac{\prod_{l=1}^{m}\Gamma\left(b_l-s\right)\prod_{l=1}^{n}\Gamma\left(1-a_l+s\right)}{\prod_{l=m+1}^{q}\Gamma\left(1-b_l+s\right)\prod_{l=n+1}^{p}\Gamma\left(a_l-s\right)}z^s\mathrm{d}s,\qquad\text{(A.1)}$$

where

- $0 \le m \le q$ and $0 \le n \le p$,
- The poles of $\Gamma\left(b_k - s\right)$ must not coincide with the poles of $\Gamma\left(1 - a_l + s\right)$ for any k and l (where $k = 1, \ldots, m$; $l = 1, \ldots, n$),
- The contour C is any path running from $c - j\infty$ to $c + j\infty$, where the constant c is chosen in such a way that the poles of the functions $\Gamma\left(1 - a_l + s\right)$ lie to the left, and the poles of the function $\Gamma\left(b_k - s\right)$ lie to the right of C (for $k = 1, 2, \ldots, m$ and $l = 1, 2, \ldots, n$). In this case, the conditions under which the integral (A.1) converges are of the form $p + q < 2(m + n)$, $|\arg z| < \left(m + n - \frac{p+q}{2}\right)\pi$,
- The values $z = 0$ is excluded.

A.2 Bivariate Meijer-G Function

The bivariate Meijer-G function is defined as [66, 79]

$$\begin{aligned}
&\mathrm{G}_{p_1,q_1:p_2,q_2:p_3,q_3}^{n_1,0:m_2,n_2:m_3,n_3}\left(z_1, z_2 \left| \begin{matrix} a_1,\ldots,a_{p_1} \\ b_1,\ldots,b_{q_1} \end{matrix} \right| \begin{matrix} c_1,\ldots,c_{p_2} \\ d_1,\ldots,d_{q_2} \end{matrix} \left| \begin{matrix} e_1,\ldots,e_{p_3} \\ f_1,\ldots,f_{q_3} \end{matrix} \right.\right) \\
=\ & \frac{1}{(2\pi j)^2}\int_{C_1}\int_{C_2} \frac{\prod_{l=1}^{n_1}\Gamma(a_l+s+t)\prod_{l=1}^{n_2}\Gamma(1-c_l+s)}{\prod_{l=n_1+1}^{p_1}\Gamma(1-a_l-s-t)\prod_{l=1}^{q_1}\Gamma(b_l+s+t)\prod_{l=n_2+1}^{p_2}\Gamma(c_l-s)} \\
&\times \frac{\prod_{l=1}^{m_2}\Gamma(d_l-s)\prod_{l=1}^{n_3}\Gamma(1-e_l+t)\prod_{l=1}^{m_3}\Gamma(f_l-t)}{\prod_{l=m_2+1}^{q_2}\Gamma(1-d_l+s)\prod_{l=n_3+1}^{p_3}\Gamma(e_l-t)\prod_{l=m_3+1}^{q_3}\Gamma(1-f_l+t)} z_1^s z_2^t \mathrm{d}s\,\mathrm{d}t,
\end{aligned} \tag{A.2}$$

where

- Contour C_k $(k = 1, 2)$ is any path running from $c_k - j\infty$ to $c_k + j\infty$, such that the poles of the functions of the form $\Gamma(\delta_l + z_k)$ lie to the left, and the poles of the functions $\Gamma(\delta_l - z_k)$ lie to the right,
- Positive integers $n_1, p_1, q_1, n_2, m_2, p_2, q_2, n_3, m_3, p_3, q_3$ satisfy the following inequalities: $q_2, q_3 \geq 1$, $p_1 \geq 0$, $0 \leq n_1 \leq p_1$, $0 \leq n_2 \leq p_2$, $0 \leq n_3 \leq p_3$, $0 \leq m_2 \leq q_2$, and $0 \leq m_3 \leq q_3$,
- The values $z_1 = 0$ and $z_2 = 0$ are excluded.

Appendix B

Derivation of the Capacity Asymptotic Expressions

B.1 Case $\beta \to +\infty$

The bivariate Meijer-G terms in (3.22) can be expressed in terms of the Mellin-Barnes integrals as

$$\begin{aligned} J_1 &= \mathrm{G}_{1,0:2,2:1,3}^{1,0:1,2:3,0}\left(\overline{\gamma}_{\mathrm{rd}}, \tfrac{\overline{\gamma}_{\mathrm{rd}}}{\overline{\gamma}_{\mathrm{sr}}} \;\middle|\; \begin{matrix} n+m+i+2 \\ - \end{matrix} \;\middle|\; \begin{matrix} 1,1 \\ 1,0 \end{matrix} \;\middle|\; \begin{matrix} 0 \\ -1, \frac{\nu}{2}+\mu-n-m, -\frac{\nu}{2}+\mu-n-m \end{matrix}\right) \\ &= \frac{1}{(2\pi j)^2}\int_{C_1}\int_{C_2}\Gamma\left(n+m+i+2+s+t\right)\Gamma^2\left(s\right)\Gamma\left(1-s\right)\Gamma\left(-1-t\right) \\ &\quad\times\Gamma\left(\frac{\nu}{2}+\mu-n-m-t\right)\Gamma\left(-\frac{\nu}{2}+\mu-n-m-t\right)\frac{\overline{\gamma}_{\mathrm{rd}}^{s}\beta^{t}}{\Gamma\left(1+s\right)\Gamma\left(-t\right)}\mathrm{d}s\mathrm{d}t, \end{aligned} \tag{B.1}$$

$$\begin{aligned} J_2 &= \mathrm{G}_{1,0:2,2:2,4}^{1,0:1,2:3,1}\left(\overline{\gamma}_{\mathrm{rd}}, \tfrac{\overline{\gamma}_{\mathrm{rd}}}{\overline{\gamma}_{\mathrm{sr}}} \;\middle|\; \begin{matrix} n+m+i+1 \\ - \end{matrix} \;\middle|\; \begin{matrix} 1,1 \\ 1,0 \end{matrix} \right. \\ &\qquad\qquad \left.\middle|\; \begin{matrix} -(n+m+i+1), 0 \\ -1, \frac{\nu}{2}+\mu-n-m, -\frac{\nu}{2}+\mu-n-m, -(n+m+i) \end{matrix}\right) \\ &= \frac{1}{(2\pi j)^2}\int_{C_1}\int_{C_2}\Gamma\left(n+m+i+1+s+t\right)\Gamma^2\left(s\right)\Gamma\left(1-s\right)\Gamma\left(n+m+i+2+t\right) \\ &\qquad\times\Gamma\left(-1-t\right)\Gamma\left(\frac{\nu}{2}+\mu-n-m-t\right)\Gamma\left(-\frac{\nu}{2}+\mu-n-m-t\right) \\ &\qquad\times\frac{\overline{\gamma}_{\mathrm{rd}}^{s}\beta^{t}}{\Gamma\left(1+s\right)\Gamma\left(-t\right)\Gamma\left(n+m+i+1+t\right)}\mathrm{d}s\mathrm{d}t \end{aligned} \tag{B.2}$$

According to [73, Theorem 1.7], the integral over C_1 can be approximated for $\beta \to +\infty$ by evaluating the residue at the closest pole to the contour C_1 from the left-hand side, i.e., at

$t = -(n+m+i+2+s)$. In that case, the contour is anti-clockwise oriented and the result is not multiplied by -1,

$$
\begin{aligned}
&\underbrace{\begin{aligned}\frac{1}{2\pi j}\int_{C_1} &\Gamma\left(n+m+i+2+s+t\right)\Gamma\left(-1-t\right)\\ &\times\Gamma\left(\frac{\nu}{2}+\mu-n-m,-t\right)\Gamma\left(-\frac{\nu}{2}+\mu-n-m,-t\right)\times\frac{\beta^{t}}{\Gamma\left(-t\right)}\,\mathrm{d}t\end{aligned}}_{g_1(t)}\\
\approx\;& \operatorname{Res}\left[g_1(t),-\left(n+m+i+2+s\right)\right]\\
=\;& \lim_{t\to-(n+m+i+2+s)}\left(t+n+m+i+2+s\right)g_1\left(t\right)\\
=\;& \Gamma\left(n+m+i+1+s\right)\Gamma\left(\frac{\nu}{2}+\mu+i+2+s\right)\Gamma\left(-\frac{\nu}{2}+\mu+i+2+s\right)\\
&\times\frac{\beta^{-(n+m+i+2+s)}}{\Gamma\left(n+m+i+2+s\right)}.
\end{aligned}
\tag{B.3}
$$

Therefore we have

$$
\begin{aligned}
J_1 \approx\;& \beta^{-(n+m+i+2)}\times\frac{1}{2\pi j}\int_{C_2}\Gamma\left(\frac{\nu}{2}+\mu+i+2+s\right)\Gamma\left(-\frac{\nu}{2}+\mu+i+2+s\right)\\
&\times\frac{\Gamma\left(n+m+i+1+s\right)\Gamma^2\left(s\right)\Gamma\left(1-s\right)}{\Gamma\left(1+s\right)\Gamma\left(n+m+i+2+s\right)}\left(\frac{\overline{\gamma}_{\mathrm{rd}}}{\beta}\right)^{s}\mathrm{d}s\\
\approx\;& \beta^{-(n+m+i+2)}\mathrm{G}_{5,3}^{1,5}\left(\overline{\gamma}_{\mathrm{sr}}\left|\begin{matrix}1,1,-\left(n+m+i\right),-\left(n_{\mathrm{r}}+i\right),-\left(n_{\mathrm{s}}+i\right)\\ 1,0,-\left(n+m+i+1\right)\end{matrix}\right.\right).
\end{aligned}
\tag{B.4}
$$

Similarly, we evaluate the residue of integral J_2 at $t = -(n+m+i+1+s)$ which yields

$$
\begin{aligned}
J_2 \approx\;& \beta^{-(n+m+i+1)}\times\frac{1}{2\pi j}\int_{C_2}\Gamma\left(\frac{\nu}{2}+\mu+i+1+s\right)\Gamma\left(-\frac{\nu}{2}+\mu+i+1+s\right)\\
&\times\frac{\Gamma\left(n+m+i+s\right)\Gamma^2\left(s\right)\Gamma^2\left(1-s\right)}{\Gamma\left(1+s\right)\Gamma\left(n+m+i+1+s\right)}\left(\frac{\overline{\gamma}_{\mathrm{rd}}}{\beta}\right)^{s}\mathrm{d}s\\
\approx\;& \beta^{-(n+m+i+1)}\mathrm{G}_{6,4}^{2,5}\left(\overline{\gamma}_{\mathrm{sr}}\left|\begin{matrix}1,1,-\left(n+m+i-1\right),-\left(n_{\mathrm{r}}+i-1\right),-\left(n_{\mathrm{s}}+i-1\right),0\\ 1,1,0,-\left(n+m+i\right)\end{matrix}\right.\right).
\end{aligned}
\tag{B.5}
$$

Keeping only low order terms on $1/\beta$ leads to the expression (3.4.2) in Table 3.1.

■

B.2 Case $\beta, \overline{\gamma}_{\rm sr} \to +\infty$

The Meijer-G function in (3.28) can be written in terms of the Mellin-Barnes integral as

$$\begin{aligned} J_3 &= \mathrm{G}_{6,4}^{2,5}\left(\overline{\gamma}_{\rm sr}\middle| \begin{matrix} 1,1,1,1-n_{\rm r},1-n_{\rm s},0 \\ 1,1,0,0 \end{matrix}\right) \\ &= \frac{1}{2\pi j}\int_C \underbrace{\frac{\Gamma^2\left(1-s\right)\Gamma^3\left(s\right)\Gamma\left(n_{\rm r}+s\right)\Gamma\left(n_{\rm s}+s\right)}{\Gamma^2\left(1+s\right)\Gamma\left(-s\right)}\overline{\gamma}_{\rm sr}^{s}}_{g_2(s)}\,\mathrm{d}s. \end{aligned}$$

For $\overline{\gamma}_{\rm sr} \to +\infty$, we approximate J_3 by evaluating the residue of the integrand at the closest pole to C from the left-hand side, i.e., $s = 0$. For that end, we recall the residue formula for poles with arbitrary order k,

$$\mathrm{Res}\left[g(s), s_0\right] = \frac{1}{(k-1)!}\lim_{s\to s_0}\frac{\mathrm{d}^{k-1}}{\mathrm{d}s^{k-1}}\left[\left(s-s_0\right)^k g(s)\right]. \tag{B.6}$$

Given that pole 0 is of order 3, we have

$$J_3 \approx \mathrm{Res}\left[g_2(s), 0\right] \approx \frac{1}{2}\lim_{s\to 0}\frac{\mathrm{d}^2}{\mathrm{d}s^2}\left[s^3 g_2(s)\right]. \tag{B.7}$$

By recalling that

$$\begin{cases} \frac{\mathrm{d}}{\mathrm{d}s}\left[\Gamma\left(s\right)\right] &= \Gamma\left(s\right)\Psi^{(0)}\left(s\right), \\ \frac{\mathrm{d}}{\mathrm{d}s}\left[\overline{\gamma}_{\rm sr}^{s}\right] &= \ln\left(\overline{\gamma}_{\rm sr}\right)\overline{\gamma}_{\rm sr}^{s}, \\ \Psi^{(0)}\left(s\right) &= \ln\left[\Gamma\left(s\right)\right], \end{cases} \tag{B.8}$$

algebraic manipulations yield

$$J_3 \approx \Gamma(n_{\rm s})\Gamma(n_{\rm r})\left[\ln\left(\overline{\gamma}_{\rm sr}\right) + \Psi^{(0)}\left(n_{\rm s}\right) + \Psi^{(0)}\left(n_{\rm r}\right)\right]. \tag{B.9}$$

Plugging (B.9) into (3.28) leads to (3.29).

■

Appendix C

Bivariate Meijer-G Routine

```
function out = Bivariate_Meijer_G(am1, ap1, bn1, bq1, cm2, cp2, dn2, dq2, em3,...
ep3,fn3, fq3, x, y)

%***************************** Integrand definition ******************************
F = @(s,t)(GammaProd(am1,s+t).* GammaProd(1-cm2,s).* GammaProd(dn2,-s)...
.* GammaProd(1-em3,t).* GammaProd(fn3,-t).* (x.^s) .* (y.^t)) ...
./(GammaProd(1-ap1,-(s+t)).* GammaProd(bq1,s+t).* GammaProd(cp2,-s)...
.* Gam  maProd(1-dq2,s).* GammaProd(ep3,-t) .* GammaProd(1-fq3,t));
%****************************** Contour definition ******************************
% cs
Sups = min(dn2); Infs = -max(1-cm2);
cs = (Sups + Infs)/2;% s between Sups and Infs
% ct
Supt = min(fn3); Inft = max([-am1-cs em3-1]);% t>-am1-s,s=cs
ct = Supt - ((Supt - Inft)/10);% t between Supt and Inft
% W
W = 10;
% quad2d settings
Tol = 10^-5; MaxEval = 2000;% increase MaxEval for higher W
%****************************** Bivariate Meijer G ******************************
out = (-1/(2*pi)^2)*quad2d(F,cs-j*W,cs+j*W,ct-j*W,ct+j*W,'AbsTol',Tol,...
'RelTol',Tol,'MaxFunEvals',MaxEval,'Singular',true);
%***************************** GammaProd subfunction ****************************
    function output = GammaProd(p,z)
    [pp zz] = meshgrid(p,z);
        if (isempty(p)) output = ones(size(z));
        else output = reshape(prod(gamma(pp+zz),2),size(z));
        end
    end
% The gamma function here is the complex gamma, available in
% www.mathworks.com/matlabcentral/fileexchange/3572-gamma
end
```

Bibliography

[1] M. Dohler, R. Heath, A. Lozano, C. Papadias, and R. Valenzuela, “Is the PHY layer dead?,” *IEEE Communications Magazine,* vol. 49, no. 4, pp. 159–165, Apr. 2011.

[2] R. Q. Hu, Y. Qian, and C. Q. Li, “Spectrum and energy efficient heterogeneous wireless networks,” in Tutorial (T5), *IEEE Wireless Communications and Networking Conference (WCNC’13),* Shanghai, China, Apr. 2013.

[3] A. Damnjanovic, J. Montojo, Y. Wei, T. Ji, T. Luo, M. Vajapeyam, T. Yoo, O. Song, and D. Malladi, “A survey on 3GPP heterogeneous networks,” *IEEE Wireless Communications,* vol. 18, no. 3, pp. 10–21, Jun. 2011.

[4] Y. Sambo, M. Shakir, K. Qaraqe, E. Serpedin, and M. Imran, “Expanding cellular coverage via cell-edge deployment in heterogeneous networks: Spectral efficiency and backhaul power consumption perspectives,” *IEEE Communications Magazine,* vol. 52, no. 6, pp. 140–149, Jun. 2014.

[5] H. El Gamal, G. Caire, and M. Damen, “The MIMO ARQ channel: Diversity-multiplexing-delay tradeoff,” *IEEE Transactions on Information Theory,* vol. 52, no. 8, pp. 3601–3621, Aug. 2006.

[6] A. Sendonaris, E. Erkip, and B. Aazhang, “User cooperation diversity. part II. implementation aspects and performance analysis,” *IEEE Transactions on Communications,* vol. 51, no.11, pp. 1939–1948, Nov. 2003.

[7] A. Sendonaris, E. Erkip, and B. Aazhang, “User cooperation diversity. part I. system description,” *IEEE Transactions on Communications,* vol. 51, no. 11, pp. 1927–1938, Nov. 2003.

[8] J. Laneman, G. W. Wornell, and D. Tse, “An efficient protocol for realizing cooperative diversity in wireless networks,” *in IEEE International Symposium on Information Theory (ISIT’01),* Washington, DC, USA, pp. 294–, 2001.

[9] J. Laneman and G. W. Wornell, “Distributed space-time-coded protocols for exploiting cooperative diversity in wireless networks,” *IEEE Transactions on Information Theory,* vol. 49, no. 10, pp. 2415–2425, Oct. 2003.

[10] J. Laneman, D. Tse, and G. W. Wornell, "Cooperative diversity in wireless networks: Efficient protocols and outage behavior," *IEEE Transactions on Information Theory,* vol. 50, no. 12, pp. 3062–3080, Dec. 2004.

[11] R. Nabar, H. Bolcskei, and F. Kneubuhler, "Fading relay channels: Performance limits and space-time signal design," *IEEE Journal on Selected Areas in Communications,* vol. 22, no. 6, pp. 1099–1109, Aug. 2004.

[12] F. Onat, H. Yanikomeroglu, and S. Periyalwar, "Relay-assisted spatial multiplexing in wireless fixed relay networks," in *IEEE Global Telecommunications Conference (GLOBE-COM'06),* San Francisco, CA, USA, pp. 1–6, Nov. 2006.

[13] D. Chen and J. Laneman, "Modulation and demodulation for cooperative diversity in wireless systems," *IEEE Transactions on Wireless Communications,* vol. 5, no. 7, pp. 1785–1794, Jul. 2006.

[14] T. Wang, A. Cano, G. Giannakis, and J. Laneman, "High-performance cooperative demodulation with decode-and-forward relays," *IEEE Transactions on Communications,* vol. 55, no. 7, pp. 1427–1438, Jul. 2007.

[15] S. Yang and J.-C. Belfiore, "Diversity of MIMO multihop relay channels-part I: Amplify-and-forward.", [Online] available at http://arxiv.org/abs/0708.0386.

[16] H. Ju, E. Oh, and D. Hong, "Catching resource-devouring worms in next-generation wireless relay systems: Two-way relay and full-duplex relay," *IEEE Communications Magazine,* vol. 47, no. 9, pp. 58–65, September 2009.

[17] M. Duarte, C. Dick, and A. Sabharwal, "Experiment-driven characterization of full-duplex wireless systems," *IEEE Transactions on Wireless Communications,* vol. 11, no. 12, pp. 4296–4307, Dec. 2012.

[18] M. Duarte and A. Sabharwal, "Full-duplex wireless communications using off-the-shelf radios: Feasibility and first results," in *Forty Fourth Asilomar Conference on Signals, Systems and Computers (ASILOMAR'10),* Pacific Grove, CA, pp. 1558–1562, Nov. 2010.

[19] M. Khafagy, A. Ismail, M.-S. Alouini, and S. Aissa, "Efficient cooperative protocols for full-duplex relaying over Nakagami-m fading channels," *IEEE Transactions on Wireless Communications,* vol. 14, no. 6, pp. 3456–3470, Jun. 2015.

[20] O. Munoz, A. Agustin, and J. Vidal, "Cellular capacity gains of cooperative MIMO transmission in the downlink," in *International Zurich Seminar on Communications,* Zurich, Switzerland, pp. 22–26, 2004.

[21] T. Oechtering and A. Sezgin, "A new cooperative transmission scheme using the space-time delay code," in *ITG Workshop on Smart Antennas*, Munich, Germany, pp. 41–48, Mar. 2004.

[22] Y. Fan, C. Wang, J. Thompson, and H. Poor, "Recovering multiplexing loss through successive relaying using repetition coding," *IEEE Transactions on Wireless Communications,* vol. 6, no. 12, pp. 4484–4493, Dec. 2007.

[23] H. Hu, H. Yanikomeroglu, D. Falconer, and S. Periyalwar, "Range extension without capacity penalty in cellular networks with digital fixed relays," in *IEEE Global Telecommunications Conference (GLOBECOM'04)* , Dallas, Texas, USA, vol. 5, pp. 3053–3057, Nov. 2004.

[24] A. Ribeiro, X. Cai, and G. Giannakis, "Opportunistic multipath for bandwidth-efficient cooperative networking," in *IEEE International Conference on Acoustics, Speech, and Signal Processing (ICASSP'04),* Montreal, Quebec, Canada, vol. 4, pp. 549–552, May 2004.

[25] B. Rankov and A. Wittneben, "Spectral efficient protocols for half-duplex fading relay channels," *IEEE Journal on Selected Areas in Communications,* vol. 25, no. 2, pp. 379–389, Feb. 2007.

[26] M. Benjillali, L. Szczecinski, and M.-S. Alouini, "A spectrally efficient detect-and-forward scheme with two-tier adaptive cooperation," *IEEE Transactions on Communications,* vol. 59, no. 9, pp. 2367–2372, Sep. 2011.

[27] R. Narasimhan, "Throughput-delay performance of half-duplex hybrid-ARQ relay channels," in *IEEE International Conference on Communications (ICC'08)*, Beijing, China, pp. 986–990, May 2008.

[28] Y. Qi, R. Hoshyar, and R. Tafazolli, "On the performance of HARQ with hybrid relaying schemes," in *IEEE International Conference on Communications (ICC'09)*, Dresden, Germany, pp. 1–6, Jun. 2009.

[29] H. Chafnaji, T. Ait-Idir, H. Yanikomeroglu, and S. Saoudi, "Signal-level turbo packet combining for multi-rate relay-assisted systems over multi-antenna broadband channels," in *IEEE Global Telecommunications Conference (GLOBECOM'10),* Miami, Florida, USA, pp. 1–5, Dec. 2010.

[30] Z. El Moutaouakkil, T. Ait-Idir, H. Yanikomeroglu, and S. Saoudi, "Relay ARQ strategies for single carrier MIMO broadband amplify-and-forward cooperative transmission," in *IEEE 21st International Symposium on Personal Indoor and Mobile Radio Communications (PIMRC'10)*, Istanbul, Turkey, pp. 713–717, Sep. 2010.

[31] M. O. Hasna and M.-S. Alouini, "Outage probability of multihop transmission over Nakagami fading channels," *IEEE Communications Letters,* vol. 7, no. 5, pp. 216–218, May 2003.

[32] M. O. Hasna and M.-S. Alouini, "End-to-end performance of transmission systems with relays over Rayleigh fading channels," *IEEE Transactions on Wireless Communications,* vol. 2, no. 6, pp. 1126–1131, Nov. 2003.

[33] M. O. Hasna and M.-S. Alouini, "Optimal power allocation for relayed transmissions over Rayleigh fading channels," *IEEE Transactions on Wireless Communications,* vol. 3, no. 6, pp. 1999–2004, Nov. 2004.

[34] M. O. Hasna and M.-S. Alouini, "Harmonic mean and end-to-end performance of transmission systems with relays," *IEEE Transactions on Communications,* vol. 52, no. 1, pp. 130–135, Jan. 2004.

[35] G. Karagiannidis, "Performance bounds of multihop wireless communications with blind relays over generalized fading channels," *IEEE Transactions on Wireless Communications,* vol. 5, no. 3, pp. 498–503, Mar. 2006.

[36] G. Karagiannidis, "Moments-based approach to the performance analysis of equal gain diversity in Nakagami-m fading," *IEEE Transactions on Communications,* vol. 52, no. 5, pp. 685–690, May 2004.

[37] H. Suraweera, R. H. Louie, Y. Li, G. Karagiannidis, and B. Vucetic, "Two hop amplify-and-forward transmission in mixed Rayleigh and Rician fading channels," *IEEE Communications Letters,* vol. 13, no. 4, pp. 227–229, Apr. 2009.

[38] H. Suraweera, G. Karagiannidis, and P. Smith, "Performance analysis of the dual-hop asymmetric fading channel," *IEEE Transactions on Wireless Communications,* vol. 8, no. 6, pp. 2783–2788, Jun. 2009.

[39] O. Souihli and T. Ohtsuki, "Cooperative diversity can mitigate keyhole effects in wireless MIMO systems," in *IEEE Global Telecommunications Conference (GLOBECOM'09)*, Honolulu, Hawaii, USA, pp. 1–6, Nov. 2009.

[40] O. Souihli and T. Ohtsuki, "The MIMO relay channel in the presence of keyhole effects," in *IEEE International Conference on Communications (ICC'10)*, Cape Town, South Africa, pp. 1–5, May 2010.

[41] T. Duong, H. Suraweera, T. Tsiftsis, H. Zepernick, and A. Nallanathan, "OSTBC transmission in MIMO AF relay systems with keyhole and spatial correlation effects," in *IEEE International Conference on Communications (ICC'11)*, Kyoto, Japan, pp. 1–6, Jun. 2011.

[42] M. Benjillali and L. Szczecinski, "A simple detect-and-forward scheme in fading channels," *IEEE Communications Letters,* vol. 13, no. 5, pp. 309–311, May 2009.

[43] G. Caire, G. Taricco, and E. Biglieri, "Bit-interleaved coded modulation," *IEEE Transactions on Information Theory,* vol. 44, no. 3, pp. 927–946, May 1998.

[44] H. Chergui, T. Ait-Idir, M. Benjillali, and S. Saoudi, "Joint-over-transmissions project and forward relaying for single carrier broadband MIMO ARQ systems," in *IEEE 73rd Vehicular Technology Conference (VTC Spring'11)* , Budapest, Hungary, pp. 1–5, May 2011.

[45] K. J. Kim, T. Duong, and X.-N. Tran, "Performance analysis of cognitive spectrum-sharing single-carrier systems with relay selection," *IEEE Transactions on Signal Processing,* vol. 60, no. 12, pp. 6435–6449, Dec. 2012.

[46] L. Wang, K. J. Kim and H. Poor, "Security enhancement of cooperative single carrier systems," *IEEE Transactions on Information Forensics and Security,* vol. 10, no. 1, pp. 90–103, Jan. 2015.

[47] L. Wang, *Physical Layer Security in Wireless Networks: Design and Enhancement.* PhD thesis, Queen Mary University of London, 2015.

[48] E. W. Barnes, "A new development in the theory of the hypergeometric functions," in *London Math. Society,* vol. s2–6, no. 1, pp. 141–177, 1908.

[49] C. Berrou, A. Glavieux, and P. Thitimajshima, "Near Shannon limit error-correcting coding and decoding: Turbo-codes," in *IEEE International Conference on Communications (ICC'93)*, Geneva, Switzerland, vol. 2, pp. 1064–1070, May 1993.

[50] C. Douillard, M. Jezequel, C. Berrou, A. Picart, P. Didier, and A. Glavieux, "Iterative correction of intersymbol interference: Turbo-equalization," *European Transactions on Telecommunications,* vol. 6, no. 5, pp. 507–511, 1995.

[51] I. Emre Telatar, "Capacity of multi-antenna Gaussian channels," *European Transactions on Telecommunications,* vol. 10, no. 6, pp. 585–595, Nov.–Dec. 1999.

[52] D. Gesbert, H. Bolcskei, D. Gore, and A. Paulraj, "Outdoor MIMO wireless channels: Models and performance prediction," *IEEE Transactions on Communications,* vol. 50, no. 12, pp. 1926–1934, Dec. 2002.

[53] G. H. Golub and C. F. Van Loan, *Matrix Computations.* The John Hopkins University Press, 3rd ed., 1996.

[54] L. Zheng and D. Tse, "Diversity and multiplexing: a fundamental tradeoff in multiple-antenna channels," *IEEE Transactions on Information Theory,* vol. 49, no. 5, pp. 1073–1096, May 2003.

[55] H. El Gamal, G. Caire, and M. Damen, "The MIMO ARQ channel: Diversity multiplexing delay tradeoff," *IEEE Transactions on Information Theory,* vol. 52, no. 8, pp. 3601–3621, Aug. 2006.

[56] H. Samra and Z. Ding, "New MIMO ARQ protocols and joint detection via sphere decoding," *IEEE Transactions on Signal Processing,* vol. 54, no. 2, pp. 473–482, Feb. 2006.

[57] T. Ait-Idir and S. Saoudi, "Turbo packet combining strategies for the MIMO-ISI-ARQ channel," *IEEE Transactions on Communications,* vol. 57, no. 12, pp. 3782–3793, Dec. 2009.

[58] G. Caire and D. Tuninetti, "The throughput of hybrid-ARQ protocols for the Gaussian collision channel," *IEEE Transactions on Information Theory,* vol. 47, no. 5, pp. 1971–1988, Jul. 2001.

[59] E. Biglieri, *Coding for Wireless Channels.* Springer Science & Business Media, 2005.

[60] K. Zheng, S. Ou, J. Alonso-Zarate, M. Dohler, F. Liu, and H. Zhu, "Challenges of massive access in highly dense LTE-advanced networks with machine-to-machine communications," *IEEE Wireless Communications,* vol. 21, no. 3, pp. 12–18, Jun. 2014.

[61] S. Nagata, Y. Yan, X. Gao, A. Li, H. Kayama, T. Abe, and T. Nakamura, "Investigation on system performance of L1/L3 relays in LTE-advanced downlink," in *IEEE 73rd Vehicular Technology Conference (VTC Spring'11),* Budapest, Hungary, pp. 1–5, May 2011.

[62] D. Chizhik, G. Foschini, M. Gans, and R. Valenzuela, "Keyholes, correlations, and capacities of multielement transmit and receive antennas," *IEEE Transactions on Wireless Communications,* vol. 1, no. 2, pp. 361–368, Apr. 2002.

[63] S. Loyka and A. Kouki, "On MIMO channel capacity, correlations, and keyholes: analysis of degenerate channels," *IEEE Transactions on Communications,* vol. 50, no. 12, pp. 1886–1888, Dec. 2002.

[64] H. Shin and J. H. Lee, "Capacity of multiple-antenna fading channels: spatial fading correlation, double scattering, and keyhole," *IEEE Transactions on Information Theory,* vol. 49, no. 10, pp. 2636–2647, Oct. 2003.

[65] H. T. Nguyen, J. B. Andersen, and G. F. Pedersen, "Characterization of the indoor outdoor to indoor MIMO radio channel at 2.140 GHz," *Wireless Personal Communications,* vol. 35, no. 3, pp. 289–309, Nov. 2005.

[66] B. L. Sharma and R. F. A. Abiodun, "Generating function for generalized function of two variables," *American Mathematical Society,* vol. 46, no. 1, pp. 69–72, Oct. 1974.

[67] I. S. Gradshteyn and I. M. Ryzhik, *Table of Integrals, Series, and Products.* Academic Press, 7th ed., 2007.

[68] I. Ansari, S. Al-Ahmadi, F. Yilmaz, M. Alouini, and H. Yanikomeroglu, "A new formula for the BER of binary modulations with dual-branch selection over generalized-K composite fading channels," *IEEE Transactions on Communications,* vol. 59, no. 10, pp. 2654–2658, Oct. 2011.

[69] D. Tse and P. Viswanath, *Fundamentals of Wireless Communication.* New York, NY, USA, Cambridge University Press, 2005.

[70] [Online] http://functions.wolfram.com/HypergeometricFunctions/MeijerG/20/01/01/.

[71] V. S. Adamchik and O. S. Marichev, "The algorithm for calculating integrals of hypergeometric type functions and its realization in REDUCE system," in *International Symposium on Symbolic and Algebraic Computation,* Tokyo, Japan, pp. 212–224, Aug. 1990.

[72] S. C. Gupta, "Integrals involving products of G-functions," in *Proceedings of the National Academy of Sciences,* India, vol. 39(A), pp. 103–200, 1969.

[73] A. Kilbas, *H-Transforms: Theory and Applications.* Analytical Methods and Special Functions, CRC Press, 2004.

[74] T. Rowland and E. W. Weisstein, "Inside–Outside theorem, MathWorld -a Wolfram web resource." [Online] available at http://mathworld.wolfram.com/Inside-OutsideTheorem.html.

[75] K. Peppas, "A new formula for the average bit error probability of dual-hop amplify-and-forward relaying systems over generalized shadowed fading channels," *IEEE Wireless Communications Letters,* vol. 1, no. 2, pp. 85–88, Apr. 2012.

[76] M. Jain, J. I. Choi, T. Kim, D. Bharadia, S. Seth, K. Srinivasan, P. Levis, S. Katti, and P. Sinha, "Practical, real-time, full-duplex wireless," in *the 17th Annual International Conference on Mobile Computing and Networking (MobiCom'11)*, New York, NY, USA, pp. 301–312, Sep. 2011.

[77] R. Tannious and A. Nosratinia, "Spectrally-efficient relay selection with limited feedback," *IEEE Journal on Selected Areas in Communications,* vol. 26, no. 8, pp. 1419–1428, Oct. 2008.

[78] Y.-W. P. Hong, W.-J. Huang, and C.-C. J. Kuo, *Cooperative Communications and Networking: Technologies and System Design.* Springer US, 2010.

[79] B. L. Sharma, "On the generalised function of two variables," *Ann. Soc. Sci. Bruxelles,* vol. 79, no. 1, pp. 26–40, 1965.

Publications List

- H. Chergui, M. Benjillali, and S. Saoudi, "Performance Analysis of Project-and-Forward Relaying in Mixed MIMO-Pinhole and Rayleigh Dual-Hop Channel", *IEEE Communications Letters* (Accepted), Dec. 2015.

- H. Chergui, T. Ait-Idir, M. Benjillali, and S. Saoudi, "Signal Level Cooperative Spatial Multiplexing for Throughput Enhancement in MIMO Broadband Systems", in *IEEE Wireless Communications and Networking Conference (WCNC'13)*, Shanghai, China, pp. 3535–3539, Apr. 2013

- H. Chergui, T. Ait-Idir, M. Benjillali, and S. Saoudi, "Joint-over-transmissions project and forward relaying for single carrier broadband MIMO ARQ systems," in *IEEE 73rd Vehicular Technology Conference (VTC Spring'11)*, Budapest, Hungary, pp. 1–5, May 2011.

Signal-Level Relaying Strategies for Broadband MIMO ARQ Communications

(Résumé de Thèse de Doctorat)

Hatim Chergui

Institut TELECOM/TELECOM Bretagne, UMR CNRS 3192 Lab-STICC, Technopôle Brest-Iroise, France

Email: chergui@ieee.org

I. Introduction

Le relayage coopératif, multiple-input multiple-output (MIMO) et hybrid-ARQ sont des techniques primordiales pour améliorer le débit et la qualité des transmissions sans-fil sur les canaux large-bande ; l'analyse de performance permet d'en évaluer les gains conséquents, mais également dévoile les compromis qu'elles incluent : la diversité spatiale des relais est obtenue aux dépens de la capacité suite à la contrainte half-duplex ; la déficience de rang du canal multi-antenne aux bordures de la cellule, où les relais sont généralement déployés, entrave l'activation du multiplexage spatio-temporel ; la diversité temporelle du hybrid-ARQ se trouve rapidement dégradée par la nature quasi-statique et long-terme des environnement à évanouissement lent. Cette thèse essaie de surmonter ces enjeux inhérents en proposant une conception conjointe des trois techniques pour les communications sur les canaux MIMO-ARQ limités par les interférences entre symboles (IES). Dans une approche niveau-signal, nous exploitons la déficience de rang du canal source-relais—découlant de la distribution des réflecteurs et/ou du nombre d'antennes—en s'appuyant sur un relayage de type project-and-forward (PF). Le concept de projection est premièrement validé à travers l'analyse de sa performance sur un canal mixte MIMO-pinhole/Rayleigh à évanouissement plat, et ce en utilisant des fonctions mathématiques généralisées. En invoquant la théorie des résidus, nous étudions le comportement asymptotique du système, ce qui mène à des recommandations sur la conception des schémas de relayage basés sur PF. Nous appliquons ensuite le concept de projection orthogonale aux canaux MIMO à IES pour alléger la contrainte half-duplex. Ainsi, nous introduisons une architecture de multiplexage spatial coopératif à base de PF pour réduire la durée de la phase de relayage, sans recourir toutefois à la détection ou la remodulation au niveau du relais. Le modèle de communication mis en place permet d'assimiler le système de relayage à une transmission point à point MIMO, ce qui permet d'adopter les techniques de détection et de combinaison conjointes côté destination. Finalement, nous introduisons une conception inter-couches, où la projection est effectuée conjointement sur des transmissions MIMO-ARQ multiples, augmentant ainsi le gain de diversité et l'efficacité spectrale.

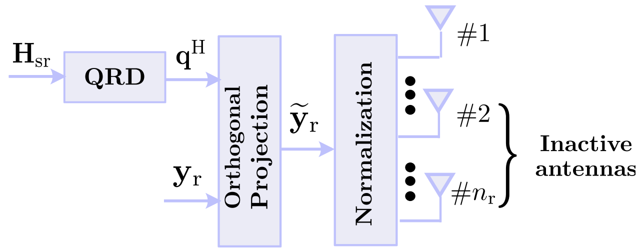

FIGURE 1. Les blocs du relayage Project-and-Forward sous un canal de rang 1.

II. RELAYAGE PROJECT-AND-FORWARD

Tandis que les schémas de relayage de type *amplify-and-forward* (AF) possèdent une architecture de faible complexité, leur performance se trouve facilement limitée par l'amplification du bruit ; un effet qui s'accentue dans le contexte MIMO où les bruits relayés par les antennes du relais finissent par s'accumuler sur chaque antenne de la destination. Pour alléger une tel inconvénient, une variante du AF dite *project-and-forward* (PF) a été introduite dans [1] : en transférant les degrés de liberté du signal reçu—dont le nombre est égal au rang ρ du canal MIMO source-relais—la puissance moyenne du bruit est réduite par un facteur $\rho/n_{\rm r}$, où $n_{\rm r}$ est le nombre d'antennes du relais ; **une stratégie qui s'avère avoir un haut potentiel sur des canaux source-relais MIMO avec déficience de rang ainsi que dans les cas où le relais possède plus d'antennes que la source.**

Le traitement requis par PF est purement niveau signal, avec certes une complexité supérieure à celle de AF, mais qui demeure toujours inférieure aux schémas detect-and-forward (DetF) et donc également à decode-and-forward (DF). La Table I dresse une comparaison rapide du nombre d'opérations à virgule flottante pour quelques classes de relayage dans le scénario d'un canal MIMO $n_{\rm r} \times n_{\rm s}$ à évanouissement par bloc, avec un paquet de longueur T symboles.

Schéma de Relayage	Type	Complexité
AF (aveugle)	Niveau Signal	$n_{\rm r}T$
AF (avec estimation du canal)	Niveau Signal	$(4n_{\rm s}+3)+n_{\rm r}T$
PF	Niveau Signal	$3n_{\rm s}^2(n_{\rm r}-n_{\rm s}/3)+(2n_{\rm r}^2-n_{\rm r})$ $+\rho(4n_{\rm s}-2\rho+3)+n_{\rm r}T$
DetF (basé sur MMSE)	Niveau Symbole	$12n_{\rm s}^3+n_{\rm s}^2(8n_{\rm r}+2)+3n_{\rm s}n_{\rm r}-n_{\rm r}+\|\mathcal{A}\|\,n_{\rm r}T$

TABLE I
COMPLEXITÉ DES SCHÉMAS DE RELAYAGE.

Existe-il alors des conditions pratiques où la stratégie PF est viable ? et quelle serait, dans ce cas, sa performance ?

III. RELAYAGE PROJECT-AND-FORWARD : OPPORTUNITÉS ET ANALYSE DE PERFORMANCE

A. *Opportunités*

Outre le canal MIMO Gaussien indépendant dont le rang est égal au minimum du nombre d'antennes émettrices et réceptrices ; un phénomène inhérent aux systèmes MIMO est la condition "pinhole" [2], [3], [4] qui surgit lorsque le rayon de la zone de réflecteurs est petit ou la distance séparant l'émetteur du récepteur est grande. Les trajets ayant une énergie non négligeable se trouvent tous confinés dans un tuyau aérien virtuel semblable à une fente de serrure (d'où le nom anglais *pinhole ou keyhole*), ce qui réduit le rang du canal MIMO à l'unité [5], et sa capacité à celle d'un lien *single-input single-output* (SISO) [6]. Tel que dicté par les règles de l'ingénierie, un relais est pratiquement déployé aux bordures de la cellule où les trous de couverture ainsi que les faibles efficacités spectrales sont souvent rapportés [7]. De ce fait, la longueur du bond source-relais dans le sens descendant

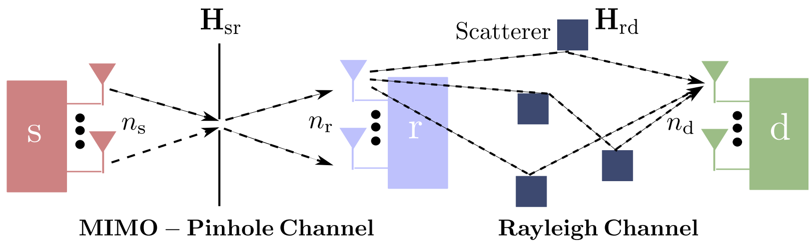

FIGURE 2. Canal double-bond mixte MIMO-pinhole/Rayleigh.

est aussi large que, suite à l'analyse ci-dessus, le rang du canal MIMO correspondant est réduit à l'unité, conduisant ainsi à la condition "pinhole" [5]. En revanche, la petite distance séparant le relais de la destination et la richesse de ce lien en terme de réflecteurs décorrélés—assurés par les structures bloquantes (ex. bâtiments) en milieux indoor et outdoor-to-indoor [8]—favorisent un canal relais-destination à rang plein.

B. Analyse de Performance

Pour caractériser un tel canal double-bond mixte de type MIMO-pinhole/Rayleigh, on a recours à la probabilité de coupure et la capacité ergodique. Ainsi, pour une source à n_{s} antennes connectée à une destination à n_{d} antennes à travers un relais possédant n_{r} antennes ($n_{\mathrm{s}}, n_{\mathrm{r}} > 1$), ces deux métriques ont été mises en évidence comme suit :

1) Probabilité de Coupure: Suite au calcul des densités de probabilité des RSBs instantanés des deux bonds, la probabilité de coupure P_{out} a été exprimée en termes des nombres des antennes, des rapports signal-sur-bruit (RSBs) moyens des deux bonds $\overline{\gamma}_{\mathrm{sr}}$ et $\overline{\gamma}_{\mathrm{rd}}$, et du seuil de coupure γ_{th} par la formule

$$P_{\mathrm{out}}\left(\gamma_{\mathrm{th}}\right) = 1 - \frac{e^{-\frac{\gamma_{\mathrm{th}}}{\overline{\gamma}_{\mathrm{rd}}}}}{\Gamma(n_{\mathrm{s}})\Gamma(n_{\mathrm{r}})} \sum_{n=0}^{+\infty} \frac{(-1)^n}{n!} \left(\frac{\gamma_{\mathrm{th}}+1}{\overline{\gamma}_{\mathrm{rd}}}\right)^n \sum_{m=0}^{+\infty} \frac{\theta_{n,m}}{m!} \left(\frac{\gamma_{\mathrm{th}}}{\overline{\gamma}_{\mathrm{sr}}}\right)^{n+m+1} \times \mathrm{G}_{1,3}^{3,0}\left(\frac{\gamma_{\mathrm{th}}}{\overline{\gamma}_{\mathrm{sr}}} \middle| \begin{array}{c} 0 \\ -1, \frac{\nu}{2}+\mu-n-m, -\frac{\nu}{2}+\mu-n-m \end{array}\right), \tag{1}$$

où le coefficient $\theta_{n,m}$ est explicité par

$$\begin{cases} \theta_{n,m} = \frac{\Gamma(n+m)}{\Gamma(n)}, \\ \theta_{0,0} = 1. \end{cases} \tag{2}$$

et $\mathrm{G}_{\cdot,\cdot}^{\cdot,\cdot}(\cdot \mid \cdot)$ représente la fonction G de Meijer.

2) Capacité Ergodique: La capacité ergodique du système considéré a été également montrée égale à

$$\overline{C} = \frac{1}{2\ln(2)\,\Gamma(n_\mathrm{s})\Gamma(n_\mathrm{r})} \sum_{n=0}^{+\infty} \frac{(-1)^n}{n!} \sum_{i=0}^{n} \binom{n}{i} \sum_{m=0}^{+\infty} \frac{\theta_{n,m}}{m!} \frac{\overline{\gamma}_\mathrm{rd}^{m+i+1}}{\overline{\gamma}_\mathrm{sr}^{n+m+1}}$$
$$\times \Bigg[\mathrm{G}^{1,0:1,2:3,0}_{1,0:2,2:1,3}\left(\overline{\gamma}_\mathrm{rd}, \tfrac{\overline{\gamma}_\mathrm{rd}}{\overline{\gamma}_\mathrm{sr}} \,\middle|\, \begin{matrix} n+m+i+2 \\ - \end{matrix} \,\middle|\, \begin{matrix} 1,1 \\ 1,0 \end{matrix} \,\middle|\, \begin{matrix} 0 \\ -1, \frac{\nu}{2}+\mu-n-m, -\frac{\nu}{2}+\mu-n-m \end{matrix} \right)$$
$$- \mathrm{G}^{1,0:1,2:3,1}_{1,0:2,2:2,4}\left(\overline{\gamma}_\mathrm{rd}, \tfrac{\overline{\gamma}_\mathrm{rd}}{\overline{\gamma}_\mathrm{sr}} \,\middle|\, \begin{matrix} n+m+i+1 \\ - \end{matrix} \,\middle|\, \begin{matrix} 1,1 \\ 1,0 \end{matrix} \,\middle|\, \begin{matrix} -(n+m+i+1), 0 \\ -1, \frac{\nu}{2}+\mu-n-m, -\frac{\nu}{2}+\mu-n-m, -(n+m+i) \end{matrix} \right) \Bigg]., \tag{3}$$

où $\mathrm{G}^{\cdot,\cdot:\cdot,\cdot:\cdot,\cdot}_{\cdot,\cdot:\cdot,\cdot:\cdot,\cdot}(\cdot,\cdot \mid \cdot \mid \cdot \mid \cdot)$ est la fonction G de Meijer à deux variables [9] qui, à notre connaissance, ne possède qu'une implémentation à contour fixe sur le logiciel MATHEMATICA [10]. De ce fait, une routine rapide et avec contour automatisé a été développée sous MATLAB pour cette fonction généralisée (cf. Annexe).

C. Comportement Asymptotique

Les comportements asymptotiques de la probabilité de coupure ainsi que de la capacité ergodique ont été obtenus en exprimant d'abord les fonctions G de Meijer en termes d'intégrales de Mellin-Barnes qui, en fonction du régime d'intérêt (haut ou faible RSB), sont approximés via la théorie des résidus. Les formules qui en ont résulté ont permis de tirer des recommandations sur la conception des systèmes de relayage basés sur PF.

1) Probabilité de Coupure Asymptotique: Dans le haut RSB, cette probabilité est approximée par

$$P_\mathrm{out}(\gamma_\mathrm{th}) = \left(1 + \frac{1}{(n_\mathrm{s}-1)(n_\mathrm{r}-1)\,\overline{\gamma}_\mathrm{sr}}\right) \frac{\gamma_\mathrm{th}}{\beta\overline{\gamma}_\mathrm{sr}} + o(\gamma_\mathrm{th}), \tag{4}$$

où $\beta = \frac{\overline{\gamma}_\mathrm{rd}}{\overline{\gamma}_\mathrm{sr}}$ est le facteur de balancement des deux bonds.

L'interprétation de (4) fournit des directives pour la conception du système ;

- **Capitaliser sur le lien r-d :** La projection orthogonale permet de libérer des ressources antennaires au niveau du relais comme montré dans II. Dans la mesure où la probabilité de coupure est gouvernée par le lien $\mathrm{r-d}$—puisqu'elle décroit avec l'augmentation deβ—une approche intéressante pour améliorer la diversité et le débit du système sous la condition "pinhole" est d'exploiter le lien $\mathrm{r-d}$ via un codage spatio-temporel ou un multiplexage spatial des degrés de libertés du signal, tout en activant des schéma de détection MIMO adéquats côté destination. Cette stratégie est présentée à la section IV.
- **Bénéficier du gain de combinaison implicite :** La projection orthogonale du relayage PF—basée sur la décomposition QR—permet de combiner implicitement toutes les branches de diversité spatiales du canal $\mathrm{s-r}$. Ceci conduit par exemple à un gain de RSB proportionnel à $(n_\mathrm{s}-1)(n_\mathrm{r}-1)$ dans le régime de faible RSB ($\overline{\gamma}_\mathrm{sr}, \overline{\gamma}_\mathrm{rd} \ll 1$). Ce gain devient plus intéressant quand la projection est menée conjointement avec hybrid-ARQ, comme exposé dans la section V.

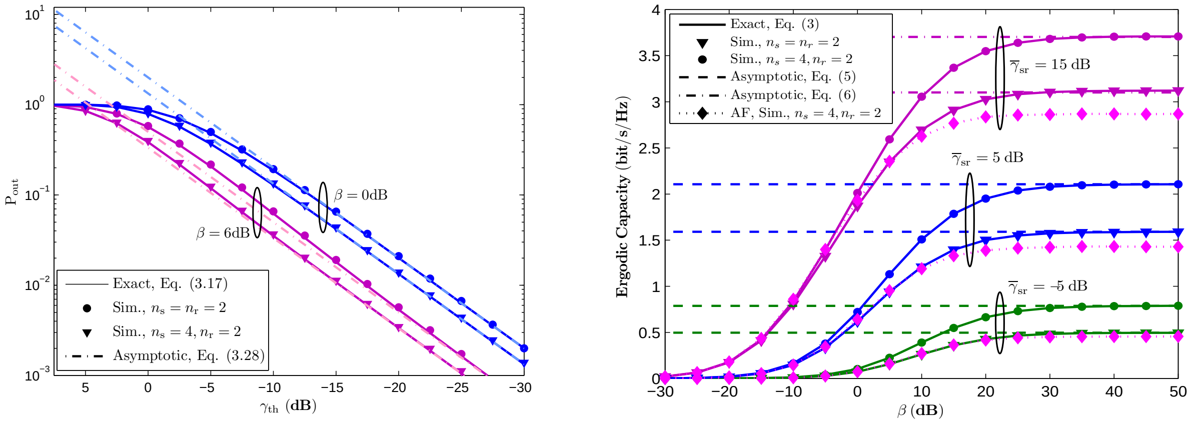

(a) (b)

FIGURE 3. (a) Probabilité de coupure de bout-en-bout versus γ_{th} pour $\overline{\gamma}_{\mathrm{sr}} = 0$ dB. (b) Capacité ergodique de bout-en-bout versus $\overline{\gamma}_{\mathrm{sr}}$ pour différentes configurations antennaires.

2) Capacité Ergodique Asymptotique: Des approximations de la capacité ergodique ont été obtenues pour différents scenarii du RSB $\overline{\gamma}_{\mathrm{sr}}$ et du facteur de balancement β comme suit :

Scénario	$\overline{C}$ Asymptotique	
$\beta \to +\infty$	$\frac{1}{2\ln(2)\Gamma(n_{\mathrm{s}})\Gamma(n_{\mathrm{r}})} \times \mathrm{G}_{6,4}^{2,5}\left(\overline{\gamma}_{\mathrm{sr}} \middle\vert \begin{matrix} 1,1,1,1-n_{\mathrm{r}},1-n_{\mathrm{s}},0 \\ 1,1,0,0 \end{matrix}\right)$	(5)
$\beta, \overline{\gamma}_{\mathrm{sr}} \to +\infty$	$\frac{1}{2\ln(2)}\left[\ln\left(\overline{\gamma}_{\mathrm{sr}}\right) + \psi^{(0)}\left(n_{\mathrm{s}}\right) + \psi^{(0)}\left(n_{\mathrm{r}}\right)\right]$	(6)
$\beta \to 0$	0	

TABLE II
EXPRESSIONS ASYMPTOTIQUE DE LA CAPACITÉ ERGODIQUE

Ces formules s'apprêtent à plusieurs interprétations pratiques :

– **PF est plus intéressant aux bordures de la cellule :** c.à.d, le relais est plus proche de la destination ($\beta \to +\infty$), ce qui est aussi le scénario le plus probable en pratique. En revanche, la capacité s'annule lorsque le RSB du lien $\mathrm{s}-\mathrm{r}$ dépasse largement celui du lien $\mathrm{r}-\mathrm{d}$ comme le montre la Table II.

– **La capacité est tributaire du nombre d'antennes au relais :** avec l'activation du hybrid-ARQ, la capacité peut être améliorée en augmentant virtuellement le nombre d'antennes au relais via une projection conjointe sur plusieurs transmissions ARQ (cf. V), ou encore augmenter le gain de multiplexage en menant un multiplexage spatial sur les antennes libres du relais (cf. IV).

IV. MULTIPLEXAGE SPATIAL COOPÉRATIF BASÉ SUR PF POUR LES SYSTÈMES MIMO LARGE BANDE

A. Concept

On considère une transmission multi-antenne mono-porteuse large-bande uplink, où une source à n_{s} antennes est connectée à une destination à n_{d} antennes via un relais équipé de n_{r} antennes ($n_{\mathrm{d}} \geq n_{\mathrm{r}} \geq n_{\mathrm{s}}$) selon le protocole de coopération représenté par la Figure 4. En guise de simplicité, et sans perte de généralité, les canaux MIMO liant chaque couple de nœuds sont supposés Gaussiens.

Afin de réduire la contrainte half-duplex et la perte de débit qui en résulte, on introduit, au niveau du relais, un module de multiplexage spatial niveau signal qui ne requiert ainsi aucune détection ou décodage. Après la réception d'un paquet de signaux

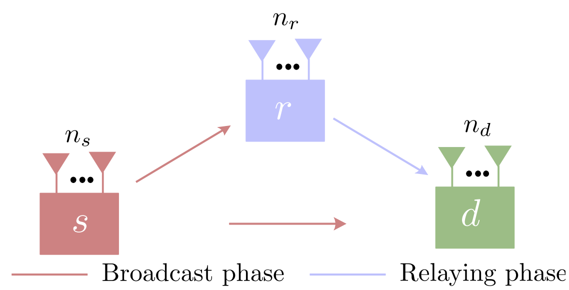

Figure 4. Coopération orthogonale

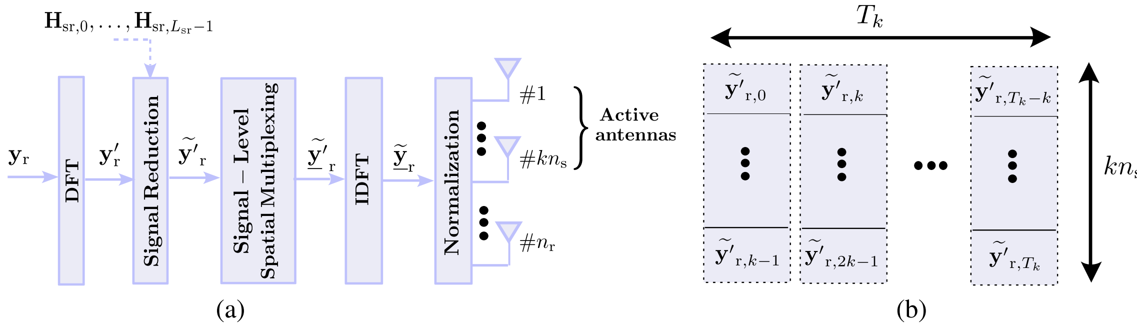

FIGURE 5. (a) Blocs du multiplexage coopératif (b) Nouveau paquet de taille $kn_{\mathrm{s}} \times T_k$ résultant du multiplexage spatial.

de dimension $n_{\mathrm{r}} \times T$, le relais applique, à chaque instant t $(t = 1, \ldots, T)$, **une projection orthogonale fréquentielle** pour extraire les degrés de libertés (DDLs) du signal reçu qui sont en nombre de $\min(n_{\mathrm{s}}, n_{\mathrm{r}}) = n_{\mathrm{s}}$. Dans la mesure où seulement n_{s} sont suffisantes pour transférer les DDLs, un multiplexage spatial peut être réalisé sur les $(n_{\mathrm{r}} - n_{\mathrm{s}})$ antennes libres. Ainsi, k vecteurs de DDL de taille $n_{\mathrm{s}} \times 1$ peuvent être simultanément transmis vers la destination, où

$$k \triangleq \left\lfloor \frac{n_{\mathrm{r}}}{n_{\mathrm{s}}} \right\rfloor, \tag{7}$$

ce qui résulte en un paquet de taille $kn_{\mathrm{s}} \times T_k$, avec $T_k = T/k$. La chaîne de traitement ainsi que le nouveau paquet sont illustrés sur la Figure 5.

Le modèle de communication adopté finit par assimiler le système coopératif à une transmission MIMO point-à-point ; son expression à la $t$ème sous-porteuse $(t = 0, \ldots, T_k - 1)$ du domaine fréquentiel est donné par

$$\begin{bmatrix} \underline{\mathbf{y}}'_{\mathrm{d},t,1} \\ \mathbf{\Omega}^{-1}\mathbf{y}'_{\mathrm{d},t,2} \end{bmatrix} = \underbrace{\begin{bmatrix} \alpha_{\mathrm{sd}}\underline{\mathbf{C}}_{\mathrm{sd},t} \\ \alpha_{\mathrm{sr}}\alpha_{\mathrm{rd}}\mathbf{\Omega}^{-1}\mathbf{C}_{\mathrm{srd},t} \end{bmatrix}}_{\mathbf{C}_t} \underline{\mathbf{x}}'_t + \begin{bmatrix} \underline{\mathbf{w}}'_{\mathrm{d},t,1} \\ \mathbf{\Omega}^{-1}\mathbf{w}'_{\mathrm{d},t,2} \end{bmatrix}, \tag{8}$$

où $\mathbf{C}_t$ est la réponse fréquentielle à la $t$ème sous-porteuse. **Ceci ouvre la piste aux concepteurs pour réutiliser tous les algorithmes de détection conjointe MIMO.**

B. Analyse du Débit

En calculant l'information mutuelle du canal équivalent (8) en fonction du RSB moyen par antennes réceptrice $\overline{\gamma}$,

$$I\left(\mathbf{C},\overline{\gamma}\right)\approx\frac{1}{T_k}\sum_{t=0}^{T_k-1}\log_2\left(\det\left(\mathbf{I}_{(k+1)n_{\mathrm{d}}}+\frac{\overline{\gamma}}{n_{\mathrm{s}}}\mathbf{C}_t\mathbf{C}_t^{\mathrm{H}}\right)\right),\tag{9}$$

le débit moyen peut être calculé selon la formule suivante

$$\mathcal{T}=\mathcal{S}\left(1-P_{\mathrm{out}}\left(k,\mathcal{S},\overline{\gamma}\right)\right),\tag{10}$$

où $\mathcal{S}$ est l'efficacité spectrale de l'émetteur (ex. pour $n_{\mathrm{s}}=2$ et QPSK-$1/2$, on a $\mathcal{S}=2$), et $P_{\mathrm{out}}\left(k,\mathcal{S},\overline{\gamma}\right)$ est la probabilité de coupure du canal équivalent donnée par

$$P_{\mathrm{out}}\left(k,\mathcal{S},\overline{\gamma}\right)=\Pr\left\{\frac{1}{k+1}I\left(\mathbf{C},\overline{\gamma}\right)<\mathcal{S}\right\}.\tag{11}$$

Le coefficient de distorsion $\frac{1}{k+1}$ dans (11) découle du fait qu'une utilisation du canal MIMO équivalent (8) correspond à $k+1$ utilisation temporelles du système coopératif.

Les résultats de simulation Monte-Carlo, représentés sur la Figure 6, montrent le gain de débit important du multiplexage spatial coopératif (CM) par rapport au schéma AF sur tout l'intervalle du RSB. **De plus, en contraste au AF dont la performance est quasi-nulle à côté de la destination, le CM garde une tendance croissante de débit avec le rapprochement du relais de la destination, ce qui prouve l'efficacité d'un tel mode de relayage aux bordures de la cellule.**

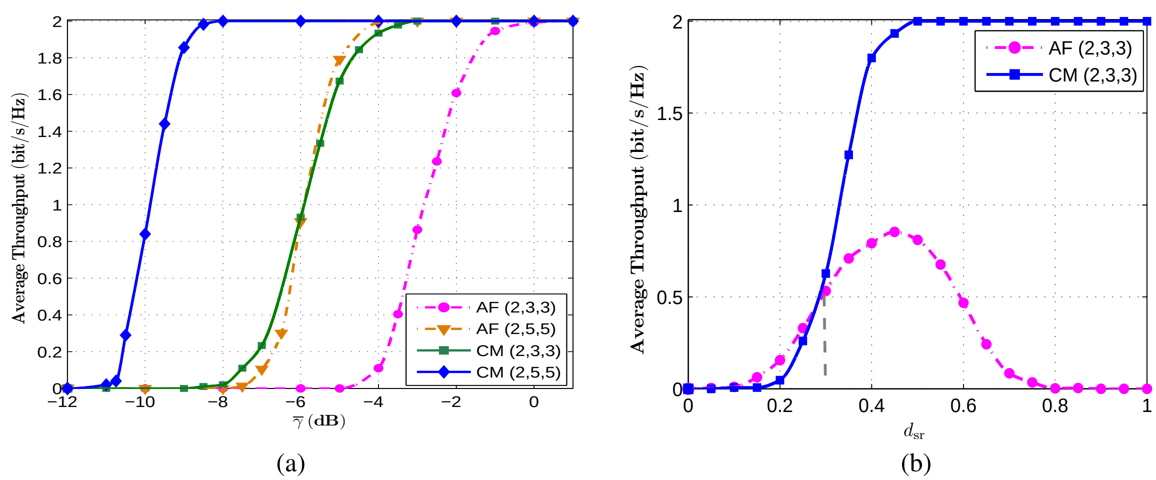

FIGURE 6. (a) Débit moyen pour $n_{\mathrm{s}}=2$. Le relais est située à mi-distance entre la source et la destination (c.à.d, $d_{\mathrm{sr}}=0.5$), $L_{\mathrm{sr}}=L_{\mathrm{rd}}=L_{\mathrm{sd}}=3$, et $\kappa=3$. (b) Débit moyen versus d_{sr} au RSB moyen, avec $\overline{\gamma}=-3$ dB, $(n_{\mathrm{s}},n_{\mathrm{r}},n_{\mathrm{d}})=(2,3,3)$, $L_{\mathrm{sr}}=L_{\mathrm{rd}}=L_{\mathrm{sd}}=3$, et $\kappa=3$.

V. CONCEPTION CONJOINTE DE HARQ ET PF POUR LES SYSTÈMES MIMO MONO-PORTEUSE LARGE BANDE

A. *Principe de Base*

Pour améliorer le gain de diversité des systèmes coopératifs tout en gardant une complexité niveau-signal, on propose une nouvelle classe de relayage basée PF pour les canaux MIMO-ARQ sélectifs en fréquence opérant selon la configuration illustrée à la Figure 7-(a). Le principe de base est que le relais voit chaque retransmission temporelle comme une source additionnelle de diversité spatiale ; au $k$ème round le processus ARQ entre la source et le relais peut être assimilé à une communication point-à-point

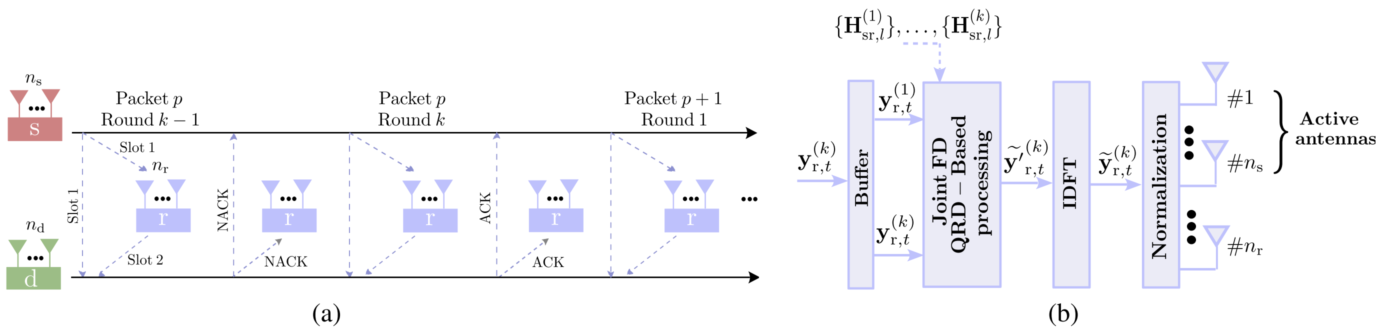

FIGURE 7. (a) Protocole Relais-ARQ (b) Chaîne de traitement du relais à la $k$ème transmission ARQ

sur un canal MIMO $kn_\mathrm{r} \times n_\mathrm{s}$ dont la définition du $l$ème trajet est donnée par

$$\underline{\mathbf{H}}_{\mathrm{sr},l}^{(k)} \triangleq \begin{bmatrix} \mathbf{H}_{\mathrm{sr},l}^{(1)} \\ \vdots \\ \mathbf{H}_{\mathrm{sr},l}^{(k)} \end{bmatrix}. \tag{12}$$

Le relais ensuite applique une projection orthogonale dans le domaine fréquentiel conjointement sur le vecteur composé des signaux reçus sur les k transmissions tel que représenté par la Figure 7-(b). Le modèle de communication de bout-en-bout masque la coopération de telle sorte que la communication est vue comme une simple transmission sur un canal MIMO $2kn_\mathrm{d} \times n_\mathrm{s}$ point-à-point ayant une réponse fréquentielle $\underline{\mathbf{C}}_t^{(k)}$ à la $t$ème sous-porteuse. Ceci facilite l'analyse de performance du système et permet aux concepteurs de réutiliser tous les algorithmes de détection MIMO conjointe côté destination.

B. Diversité et Débit

L'information mutuelle du canal équivalent peut être exprimée, sous l'hypothèse que le modulateur fournit des symboles Gaussiens indépendant, par la formule suivante

$$I\left(\mathbf{s}, \underline{\mathbf{y}}_{\mathrm{d},t}^{(k)} \mid \left\{\underline{\mathbf{H}}_l^{(k)}\right\}, \overline{\gamma}\right) \approx \frac{1}{T}\sum_{t=0}^{T-1} \log_2\left(\det\left(\mathbf{I}_{kn_\mathrm{d}} + \frac{\overline{\gamma}}{n_\mathrm{s}} \underline{\mathbf{C}}_t^{(k)} \underline{\mathbf{C}}_t^{(k)^\mathrm{H}}\right)\right), \tag{13}$$

de laquelle découle la probabilité de coupure du système

$$P_\mathrm{out}\left(\overline{\gamma}, \mathcal{S}\right) = \Pr\left\{\frac{1}{2k} I\left(\mathbf{s}, \underline{\mathbf{y}}_{\mathrm{d},t}^{(k)} \mid \left\{\underline{\mathbf{H}}_l^{(k)}\right\}, \overline{\gamma}\right) < \mathcal{S}\right\}. \tag{14}$$

Le débit moyen est évalué ensuite par

$$\mathcal{T} = \frac{\mathcal{S}\left(1 - \overline{P}_\mathrm{out}\left(\overline{\gamma}, \mathcal{S}\right)\right)}{\mathrm{E}\left[n\right]}, \tag{15}$$

où $n \in \{1, \ldots, K\}$ est une variable aléatoire modélisant le nombre de round consommés pour décoder correctement un paquet.

Les simulations Monte-Carlo de la probabilité de coupure ainsi que du débit moyen montrent l'amélioration remarquable en termes du gain de diversité et du RSB en comparaison au schémas AF. Dans le régime du haut RSB et au $k$ème round par exemple, **le relais JT-PF à n_r antennes réalise le même gain de diversité qu'un relais AF équipé de kn_r antennes,** comme prouvé par les pentes des courbes de la probabilité de coupure Figure 8-(a).

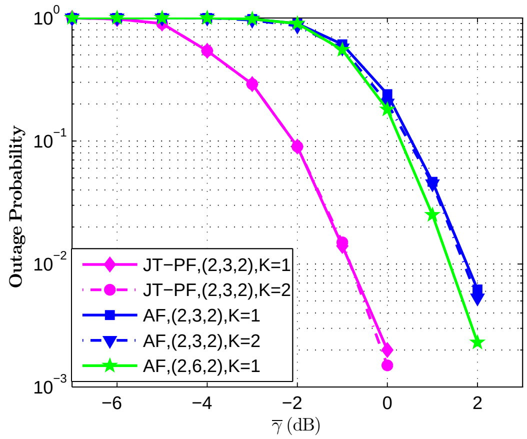

(a)

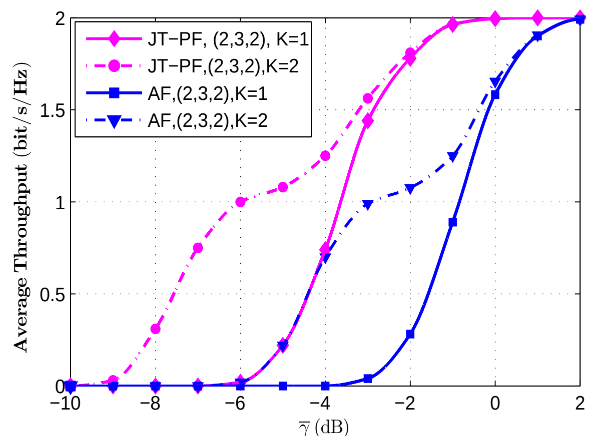

(b)

FIGURE 8. (a) Probabilité de coupure versus $\overline{\gamma}$ pour $(n_{\mathrm{s}}, n_{\mathrm{r}}, n_{\mathrm{d}}) = (2, 3, 2)$ (b) Débit moyen versus $\overline{\gamma}$ pour $(n_{\mathrm{s}}, n_{\mathrm{r}}, n_{\mathrm{d}}) = (2, 3, 2)$

VI. CONCLUSIONS

Outre la revue de littérature du relayage MIMO, cette thèse a été marquée par une multitude de nouvelles contributions.

– Au moment où le relayage PF n'avait connu aucuns travaux de recherche après l'article introductif [1], cette thèse a établi un complet d'analyse et conception de systèmes de relayage à base de PF pour les canaux MIMO large bande pratiques. Notre papier initial [11] est devenu ainsi une référence dans le domaine du relayage PF, avec des citations dans des articles de revue de grande renommée (cf. [12], [13]) et thèse (cf. [14]).

– La performance du relayage PF a été étudiée dans le scénario réaliste d'un canal mixte à double bond MIMO-pinhole /Rayleigh ; et des expressions analytiques inédites de la probabilité de coupure ainsi que de la capacité ergodique ont été démontrées.

– En appliquant la théorie des résidus sur les intégrales de Mellin-Barnes, il a été montré comment développer des expressions asymptotiques pour les fonctions généralisées les plus compliquées. Le comportement asymptotique du schéma PF a été en conséquence déduit, ce qui a permis de dégager des recommandations sur la conception des systèmes basés PF.

– La projection orthogonale, qui s'appuie sur la décomposition QR, a été étendue pour inclure les canaux MIMO-IES via une approche fréquentielle. Les modèles de communication mis en place permettent de masquer la coopération, transformant ainsi les système de relayage en un simple canal MIMO point-à-point liant la source à la destination, ce qui ouvre la voie pour réutiliser les algorithmes efficaces de détection conjointe MIMO côté destination.

– La perte de débit engendrée par la contrainte half-duplex a été réduite en introduisant une stratégie de multiplexage spatial niveau-signal basée sur PF qui, contrairement à AF, présente un débit qui augmente quand le relais se rapproche de la destination.

– L'amélioration notable du gain de diversité et du débit pour les relais MIMO half-duplex via une conception conjointe du relayage PF et du HARQ ; une architecture qui traduit la diversité temporelle du protocole ARQ en une diversité spatiale à travers le concept de projection orthogonale.

ANNEXE

```
function out = Bivariate_Meijer_G(am1, ap1, bn1, bq1, cm2, cp2, dn2, dq2, em3, ep3, fn3, fq3, x, y)
%************************************************* Integrand definition ***************************************************
F = @(s,t)(GammaProd(am1,s+t).* GammaProd(1-cm2,s).* GammaProd(dn2,-s).* GammaProd(1-em3,t).* GammaProd(fn3,-t)...
.* (x.^s) .* (y.^t)) ./(GammaProd(1-ap1,-(s+t)).* GammaProd(bq1,s+t).* GammaProd(cp2,-s).* Gam  maProd(1-dq2,s)...
.* GammaProd(ep3,-t).* GammaProd(1-fq3,t));
%*********************************************** Contour definition ******************************************************
Sups = min(dn2); Infs = -max(1-cm2); cs = (Sups + Infs)/2;% s is chosen between Sups and Infs
Supt = min(fn3); Inft = max([-am1-cs em3-1]); ct = Supt - ((Supt - Inft)/10);% t is chosen between Supt and Inft
W = 10; % W
%********************************* Bivariate Meijer G, Increase MaxFunEvals for higher W *********************************
out = (-1/(2*pi)^2)*quad2d(F,cs-j*W,cs+j*W,ct-j*W,ct+j*W,'AbsTol',10^-5,'RelTol',10^-5,'MaxFunEvals',2000,'Singular',true);
%************************************************* GammaProd subfunction *************************************************
    function output = GammaProd(p,z)
    [pp zz] = meshgrid(p,z);
        if (isempty(p)) output = ones(size(z));
        else output = reshape(prod(gamma(pp+zz),2),size(z));
        end
    end
% The gamma function here is the complex gamma, available in www.mathworks.com/matlabcentral/fileexchange/3572-gamma
end
```

RÉFÉRENCES

[1] S. Yang and J.-C. Belfiore, "Diversity of MIMO multihop relay channels-part I : Amplify-and-forward," submitted to *IEEE Trans. Inform. Theory,* available in http ://arxiv.org/abs/0708.0386.

[2] D. Chizhik, G. Foschini, M. Gans, and R. Valenzuela, "Keyholes, correlations, and capacities of multielement transmit and receive antennas," *IEEE Transactions on Wireless Communications*, vol. 1, no. 2, pp. 361–368, Apr. 2002.

[3] S. Loyka and A. Kouki, "On MIMO channel capacity, correlations, and keyholes : analysis of degenerate channels," *IEEE Transactions on Communications*, vol. 50, no. 12, pp. 1886–1888, Dec. 2002.

[4] H. Shin and J. H. Lee, "Capacity of multiple-antenna fading channels : spatial fading correlation, double scattering, and keyhole," *IEEE Transactions on Information Theory*, vol. 49, no. 10, pp. 2636–2647, Oct. 2003.

[5] D. Gesbert, H. Bolcskei, D. GORE, and A. Paulraj, "Outdoor MIMO wireless channels : Models and performance prediction," *IEEE Transactions on Communications*, vol. 50, no. 12, pp. 1926–1934, Dec. 2002.

[6] I. Emre Telatar, "Capacity of multi-antenna Gaussian channels," *European Transactions on Telecommunications*, vol. 10, pp. 585–595, 1999.

[7] Y. Sambo, M. Shakir, K. Qaraqe, E. Serpedin, and M. Imran, "Expanding cellular coverage via cell-edge deployment in heterogeneous networks : Spectral efficiency and backhaul power consumption perspectives," *IEEE Communications Magazine*, vol. 52, no. 6, pp. 140–149, Jun. 2014.

[8] H. T. Nguyen, J. B. Andersen, and G. F. Pedersen, "Characterization of the indoor outdoor to indoor MIMO radio channel at 2.140 ghz," *Wireless Personal Communications*, vol. 35, no. 3, pp. 289–309, 2005.

[9] B. L. Sharma and R. F. A. Abiodun, "Generating function for generalized function of two variables," *American Mathematical Society*, vol. 46, no. 1, pp. 69–72, Oct. 1974.

[10] I. Ansari, S. Al-Ahmadi, F. Yilmaz, M. Alouini, and H. Yanikomeroglu, "A new formula for the BER of binary modulations with dual-branch selection over generalized-k composite fading channels," *IEEE Transactions on Communications*, vol. 59, no. 10, pp. 2654–2658, Oct. 2011.

[11] H. Chergui, T. Ait-Idir, M. Benjillali, and S. Saoudi, "Joint-over-transmissions project and forward relaying for single carrier broadband MIMO ARQ systems," in *IEEE 73rd Vehicular Technology Conference (VTC Spring) 2011*, May 2011, pp. 1–5.

[12] K. J. Kim, T. Duong, and X.-N. Tran, "Performance analysis of cognitive spectrum-sharing single-carrier systems with relay selection," *IEEE Transactions on Signal Processing*, vol. 60, no. 12, pp. 6435–6449, 2012.

[13] D. T. E. M. Lifeng Wang, Kyeong Jin Kim and H. Poor, "Security enhancement of cooperative single carrier systems," *IEEE Transactions on Information Forensics and Security*, vol. 10, no. 1, pp. 90–103, 2015.

[14] L. Wang, "Physical layer security in wireless networks : Design and enhancement." Ph.D. dissertation, Queen Mary University of London, 2015.

Résumé

Le relayage coopératif, multiple-input multiple-output (MIMO) et hybrid-ARQ sont des techniques primordiales pour améliorer le débit et la qualité des transmissions sans-fil sur les canaux large-bande. L'analyse de performance permet d'en évaluer les gains conséquents, mais également dévoile les compromis qu'elles impliquent: la diversité spatiale des relais est obtenue aux dépens de la capacité suite à la contrainte half-duplex; la déficience de rang du canal multi-antennes aux bordures de la cellule, où les relais sont généralement déployés, entrave l'activation du multiplexage spatio-temporel; la diversité temporelle du hybrid-ARQ se trouve rapidement dégradée par la nature quasi-statique et long-terme des environnements à évanouissement lent. Cette thèse essaie de surmonter ces enjeux inhérents en proposant une conception conjointe des trois techniques pour les communications sur les canaux MIMO-ARQ limités par les interférences entre symboles (IES). Dans une approche niveau-signal, nous exploitons la déficience de rang du canal source-relai---découlant de la distribution des réflecteurs et/ou du nombre d'antennes---en s'appuyant sur un relayage de type project-and-forward (PF). Le concept de projection est premièrement validé à travers l'analyse de sa performance sur un canal mixte MIMO-pinhole/Rayleigh à évanouissement plat, et ce en utilisant des fonctions mathématiques généralisées. En invoquant la théorie des résidus, nous étudions le comportement asymptotique du système, ce qui mène à des recommandations sur la conception des schémas de relayage basés sur PF. Nous appliquons ensuite le concept de projection orthogonale aux canaux MIMO à IES pour alléger la contrainte half-duplex. Ainsi, nous introduisons une architecture de multiplexage spatial coopératif à base de PF pour réduire la durée de la phase de relayage, sans toutefois recourir à la détection ou la remodulation au niveau du relais. Le modèle de communication mis en place permet d'assimiler le système de relayage à une transmission point à point MIMO, ce qui permet d'adopter les techniques de détection et de combinaison conjointes côté destination. Finalement, nous introduisons une conception inter-couches, où la projection est effectuée conjointement sur des transmissions MIMO-ARQ multiples, augmentant ainsi le gain de diversité et l'efficacité spectrale.

Mots-clés : Analyse de performance, ARQ, comportement asymptotique, conception inter-couches, déficience de rang, degrés de liberté, MIMO large-bande, fonctions généralisées, project-and-forward, relayage coopératif, théorie des résidus, traitement conjoint.

Abstract

Cooperative relaying, multiple-input multiple-output (MIMO), and hybrid-automatic repeat request (ARQ) are paramount techniques to enhance the transmission throughput and quality over the wireless broadband channel. The performance analysis reveals their gain, but also unveils the practical trade-offs they encompass: the spatial diversity of relays comes at the expense of the spectral-efficiency due to the half-duplex constraint; the multi-antenna channel rank deficiency at cell-edge---where a relay is supposed to be deployed---does not allow for the space-time multiplexing mode; the temporal diversity of a pure hybrid-ARQ process is quickly degraded by the long-term quasi-static nature of slow fading environments. The present thesis attempts to overcome these inherent challenges by proposing a joint design of the three techniques for communications over the MIMO-intersymbol interference (ISI) ARQ channel. In a pure signal-level approach, we exploit the rank-deficiency of the source-relay channel---stemming from either the scatterers distribution or the number of antennas at both sides---by adopting project-and-forward (PF)-type relaying. The projection concept is first validated by analyzing its performance over the realistic mixed MIMO-pinhole and Rayleigh flat fading relay channel---using a wide set of generalized mathematical functions. Invoking the residue theory, we study the system asymptotic behavior and infer practical design recommendations. We then apply the orthogonal projection concept to the MIMO-ISI relay channel to alleviate the half-duplex constraint. Hence, we introduce a PF-based signal-level cooperative spatial multiplexing (CM) architecture that allows for the shortening of the relaying phase without resorting to any symbol detection or re-mapping at the relay side. The end-to-end communication model is derived in a seamless fashion; as though the destination is receiving multiple transmissions from the source, which maintains the possibility to use advanced joint detection and combining algorithms at the destination side. The final step of this thesis consists on introducing a cross-layer design, where the projection is performed jointly over multiple MIMO-ARQ transmissions to increase both the diversity gain and the spectral efficiency.

Keywords : ARQ, asymptotic behavior, broadband MIMO, cooperative relaying, cross-layer design, degrees of freedom, generalized functions, joint processing, performance analysis, project-and-forward, rank-deficiency, residue theory.

n° d'ordre : 2015telb0386

Télécom Bretagne

Technopôle Brest-Iroise - CS 83818 - 29238 Brest Cedex 3

Tél : + 33(0) 29 00 11 11 - Fax : + 33(0) 29 00 10 00